STRESS ANALYSIS OF METAL/CFRP ADHESIVE JOINTS SUBJECTED TO THE EFFECTS OF THERMAL STRESS

by

VISHAL MALLICK

A dissertation submitted for the Degree of Doctor of Philosophy at the University of Bristol, Department of Mechanical Engineering, September 1989

Abstract

Despite its benefits, the uptake of adhesive joint technology has been slow. One reason is expensive, or inadequate, joint stress analysis systems. These are necessary for the interpretation of joint test results and hence the development of design criteria and desirable adhesive properties. In this dissertation, an analysis for one of the most common joint tests, the lap shear, is presented.

Several methods of joint stress analysis already exist. These are based either on numerical techniques such as the finite element method, or on closed form solutions. The finite element method is capable of accurate analysis but remains expensive and requires specialist knowledge. It is therefore not suitable for the general adhesive technologist. Conversely, closed form methods may be easy-to-use but are less accurate. The main aim of the present analysis is to bridge the gap between the two, offering an accessible yet accurate stress analysis.

An analysis has been developed to cater for a general configuration such as the Aluminium to CFRP joint. Therefore, consideration of adherend anisotropy and thermal mismatch between adherends was necessary. The influences of adhesive plasticity and thermal deformation and joint rotation were also incorporated. Stress functions were used to describe the stresses throughout the joint. These were solved numerically by invoking the principal of minimum complementary energy. The solution procedure has been successfully implemented on a desktop computer.

The predicted stress distributions have been validated by a comparison with finite element results for a variety of joint configurations. The study revealed that the present analysis was accurate except at the very edge of the joint overlap.

Finally, the stress analysis has been used, in conjunction with various failure criteria, to predict the strength of Aluminium to CFRP single lap joints at both room and low (-55°C) temperatures. The predictions were in agreement with experimental measurements for three mechanically contrasting adhesives. The results suggested that the analysis was capable of providing an understanding of joint performance for a variety of adhesives.

Contents

List of Tables

List of Plates

List of Figures

Memorandum

The accompanying dissertation entitled "Stress analysis of metal/CFRP adhesive joints subjected to the effects of thermal stress" is submitted in support of an application for the degree of Doctor of Philosophy in Engineering at the University of Bristol.

The dissertation is based on independent work by the candidate - all contributions from others have been acknowledged fully within the dissertation. The supervisor's contribution was that normally made in a British University.

None of the work described has been, or is being, submitted for any other degree or diploma to this or any other University. A part of the work has formed the basis of two conference papers.

I hereby declare that the above statements are true

V. Mallick

September 1989

Acknowledgements

I would like to thank Prof. R.D. Adams for his supervision throughout this investigation. I am grateful to the other academic and technical staff of the Department of Mechanical Enginnering who provided advice and assistance, particularily Mr. J. Skinner for producing the adhesive and joint specimen. I also wish to thank Mr. X. Zhao for his general interest and for many helpful discussions. Thanks are also due to Dr. R.G.C. Arridge of the Department of Physics for the use of the Dartec hydraulic testing machine.

I would like to acknowledge the assistance offered by the staff at the Computer Centre, especially Mr. P. Buttner.

Thanks are due to the Department of Trade and Industry who, through the Royal Aircraft Establishment at Farnborough, financed the work. In particular, Mr. M.H. Stone for his help in the development of the software. Thanks are also due to Ciba Geigy and Permabond for the supply of adhesives.

Notation

E	-	Young's Modulus
G	-	Shear Modulus
ν	-	Poisson ratio
α	-	Coefficient of thermal expansion
l	-	Adherend overhang
t	-	Adhesive thickness
c	-	Joint overlap semi-length
c_i, k_i	-	Constants
P	-	Tensile load
M	-	Bending moment
Q,V	-	Shear force
D	-	Flexural rigidity
ζ	-	$\sqrt{(P/D)}$
k	-	Bending moment factor
ΔT	-	Temperature change
h	-	Adherend sheet thickness
ϕ	-	Stress function of x co-ordinate
w	-	Displacement normal to joint loading plane
σ	-	Tensile Stress tensor
τ	-	Shear Stress tensor
ε	-	Normal Strain tensor
γ	-	Shear Strain tensor
f	-	Modified von Mises yield function
λ	-	Plastic strain incremental constant
A	-	Strain hardening parameter
[B]	-	Shape function array

[K]	-	Displacement finite element method stiffness matix
[f]	-	Displacement finite element method load array matix
[δ]	-	Displacment array
[D]	-	Modulus array
[σ]	-	Stress array
[ε]	-	Strain array
[F]	-	Formulation stiffness matrix
[ϕ]	-	Nodal stress function values array
[H]	-	Formulation load matrix
U	-	Strain energy
U^*	-	Shear strain energy

SUBSCRIPTS

1	-	Upper adherend sheet
2	-	Lower adherend sheet
a	-	Adhesive
i,o	-	Initial value
e	-	Elastic value
ep	-	Elasto-Plastic value
eff	-	Effective value
p	-	Plastic value
t	-	Thermal value
max	-	Maximum value
x	-	Parallel direction to joint loading plane
y	-	Transverse direction to jont loading plane

Chapter 1

INTRODUCTION

Modern adhesives are usually synthetic organic materials based on epoxies and acrylics. These materials, when correctly used, produce bonds of such strength that the adhesive can be designed to bear much of the structural load. There are many advantages in using such adhesive joints in structures. Foremost is their ability to transfer load through the whole bonded area rather than a few discrete points as found with mechanical methods such as bolting or riveting. This inherent efficiency, combined with their naturally low weight, make adhesive joints an attractive choice for lightweight structural applications particularly in the aerospace industry. Other advantages of adhesives include their capacity to join almost any two materials and to accommodate various geometries and space limitations.

Recognition of these merits has lead to an ever increasing amount of interest in adhesive bonding. Consequently, adhesion science is an extremely active area of research today. The subject is truly multi-disciplinary involving aspects of surface chemistry and physics, polymer chemistry and stress and fracture analysis. A general review of the subject and recent advances is given by Kinloch, (1980,1982) and Adams and Wake (1984).

1.1 Definition of problem

Despite its benefits, the uptake of adhesive technology beyond the aerospace industry has been slow. Often this is due to its unsuitability. Adhesive joints are susceptible to long term environmental attack and are difficult to inspect non-destructively. Moreover, they can be difficult to manufacture. Nevertheless, there are many situations where the advantages far outweigh the disadvantages. In such cases it becomes the responsibility of the designer or engineer concerned whether or not to use adhesives. Therein lies the problem. There is a prevalent lack of confidence in designing with adhesive systems compared with conventional techniques. The main cause is poor test information and expensive, or inadequate, joint analysis systems.

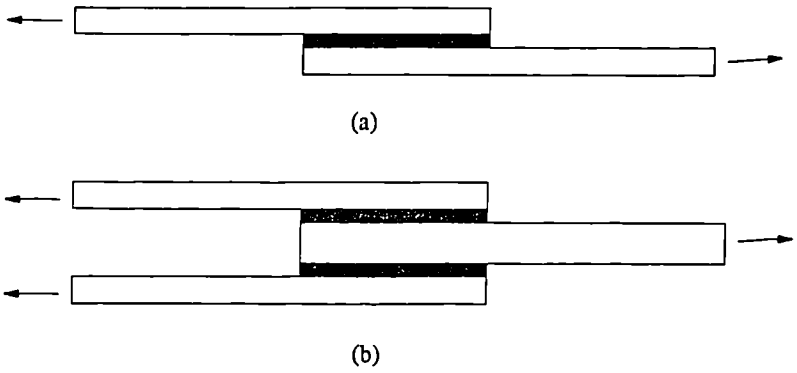

Fig. 1.1 *(a) Single lap and (b) double lap adhesive joint*

The lap shear test is one of the most common methods, used by adhesive technologists, to measure the performance of an adhesive joint. In this test (Fig. 1.1) an adhesive joint is formed between adherends and pulled to destruction. The ultimate load measured is taken as an indication of adhesive strength. However, this is a gross simplification of reality. The stress state within single and double lap joints is complex and adhesives with widely contrasting mechanical properties can give similar joint strengths. Thus, to interpret the measured joint strength, a parallel stress analysis is vital.

Many reports and papers have been published on the stresses in joints and these have fallen into two broad areas. First, there are the closed-form algebraic analyses in which exact solutions are given. Unfortunately, it is difficult to model properly the stresses at realistic discontinuities, or in the spew fillet, or when the adhesive and adherend behave plastically. The alternative has been to use finite element techniques so that the discontinuities and material non-linearities can be accommodated. The main disadvantage of finite elements is that the solution is expensive and is for a single configuration, so a parametric investigation is costly.

Unfortunately, none of the available methods is suitable for the adhesive technologist in general. The closed form methods are too simple while the finite element method is costly and requires specialist knowledge. So, there is a need for a method which bridges the gap between the two, offering an accessible yet accurate analysis. This is the background to the present objective of developing a stress analysis that is accessible by the widest possible audience.

1.2 Outline of the work

The first step, towards, was to identify the inadequacies in current methods through a literature survey. This review also revealed the most suitable way forward for a new stress analysis.

Stress analyses were then developed for single and double lap joints assuming elastic material properties. In order to be of general use, the analyses are intended to cater for a general joint. This means that the adherends can be of unequal thickness and be made of dissimilar materials. One common example of such a joint is the single lap CFRP to Aluminium joint used in aircraft structures. This is one of the most difficult types of joint to analyse since the adherends not only have different stiffness but one is anisotropic. Moreover, the difference in the adherends' coefficients of thermal expansion will introduce significant stresses into the adhesive when the joint is subjected to a temperature change. If the analysis is valid for this joint then it is applicable to almost any configuration. Therefore, particular emphasis was placed on incorporating thermal effects and adherend anisotropy into the solution. In this study, consideration of anisotropy has been limited to unidirectional laminates.

The other variable in an adhesive joint is the adhesive itself. Many modern adhesives can exhibit a large amount of plastic deformation before failure. Since the adhesive is often less stiff than the adherends it is very likely to yield. Consequently, the elastic solution was extended to model adhesive plasticity.

The accuracy of the solution has been established by comparing stress predictions with FEM results. For further validation, strengths of CFRP to Aluminium joints were predicted and then compared with experimental measurements.

Chapter 2

METHODS OF LAP JOINT STRESS ANALYSIS

Knowledge of the stresses and strains in an adhesive joint is necessary to an understanding of joint strength, and hence the development of appropriate design criteria and desirable adhesive properties. Stress distributions are determined either experimentally or theoretically in many structures. Experimental measurements in real adhesively bonded joints are extremely difficult, particularly when the adhesive layer is thin. A simple solution is to analyse large rubber (Adams *et al*, 1973) or photoelastic (McLaren and MacInnes, 1958) models of joints. Recently, through techniques of Moiré Interferometry pioneered by Post (1987), strains within the joint have been *directly* measured (Leichti *et al*, 1987). Even so, experimental methods are an inefficient and uneconomical method of analysis. Furthermore, they cannot give accurate results at the edges of the joint where the stresses are at a peak and where failure will occur. Much effort has therefore been devoted to the development of theoretical methods of stress analysis.

Broadly speaking, there have been two approaches to the problem. The first is the analytical, or closed form, approach in which an exact mathematical solution for the stress condition is attempted. A real joint consists of dissimilar materials and may be subjected to a combination of effects, including temperature, moisture, creep, fatigue, impact, material plasticity, tapering adherends and glue line thickness. In addition a single lap joint changes its geometry as it rotates under loading. Incorporating all these effects into a set of governing equations gives rise to serious mathematical difficulty. A closed form solution is very difficult if not impossible unless some simplifications are made.

The other approach is to use numerical methods. One such method, the finite element method (FEM), has gained universal acceptance since it facilitates more complete analyses than are otherwise possible. But there is a price to pay. FEM is not generally accessible since it requires powerful computers and specialist knowledge. As a result, there remains a demand for the simpler solutions offered by the closed form methods.

Reviews of both, closed form and numerical methods have been conducted amd published in the literature by Sneddon (1961), Kutscha (1964), Grant *et al* (1983) and Adams and Wake (1984). In the present study, particular emphasis has been placed on methods relevant to the objective of modelling joints consisting of one or more adherends; for example, the CFRP to Aluminium single lap joint, under tensile load and subjected to thermal stress.

2.1 ANALYSIS OF AN ADHESIVE JOINT: THE PROBLEM

A joint may be defined as a region where loads are transferred by shear across an interface. The basic principles of analysis apply to any type of joint, whether it is bolted, riveted or bonded. In fact, the analysis of bonded joints finds its roots in the analyses developed for bolted joints.

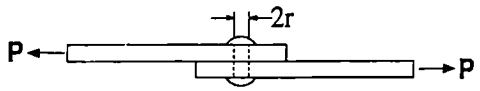

Fig. 2.1 *A bolted joint*

In the simplest form of the bolted joint (Fig. 2.1) the maximum shear stress in the pin is given by

$$\tau_{max} = \frac{P}{2\pi r^2} \qquad (2.1)$$

If the number of bolts, or rivets, is increased then the distribution of shear in each bolt becomes more complex. Consider the case of rigid sheets joined by a series of elastic bolts. Any relative displacement between the sheets would cause an equal displacement between each pair of holes resulting in equal shear stress in each bolt (Fig. 2.2a).

If on the other hand, the bolts were rigid and the sheets elastic, the displacement of the sheets would be resisted entirely by the end bolts, leaving the mid sheet and bolts unloaded (Fig. 2.2b).

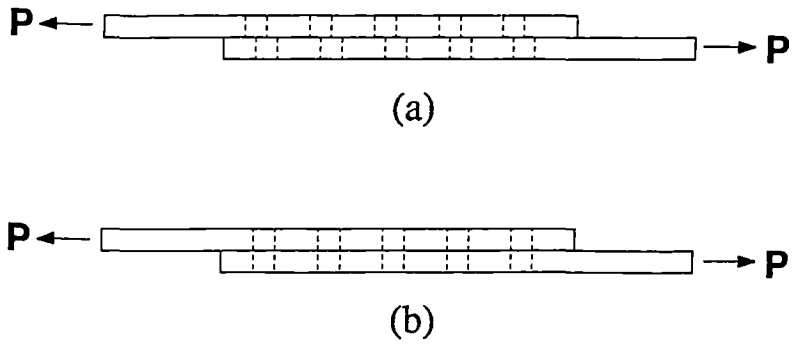

Fig. 2.2 *Deflections in a bolted joint with (a) rigid sheets and (b) rigid bolts*

In reality, both the adherends and bolts deflect and the situation is similar to that shown in Fig. 2.3a where the end bolts offer the greatest resistance but allow load transfer to occur to the middle region.

The end result is "differential" straining of the adherends culminating in the bolt stress distribution shown in Fig. 2.3b. It is interesting to note that if either the sheets or bolts (or both) suffer sufficient plastic deformation, then the loading situation will tend toward the case shown in Fig. 2.2a.

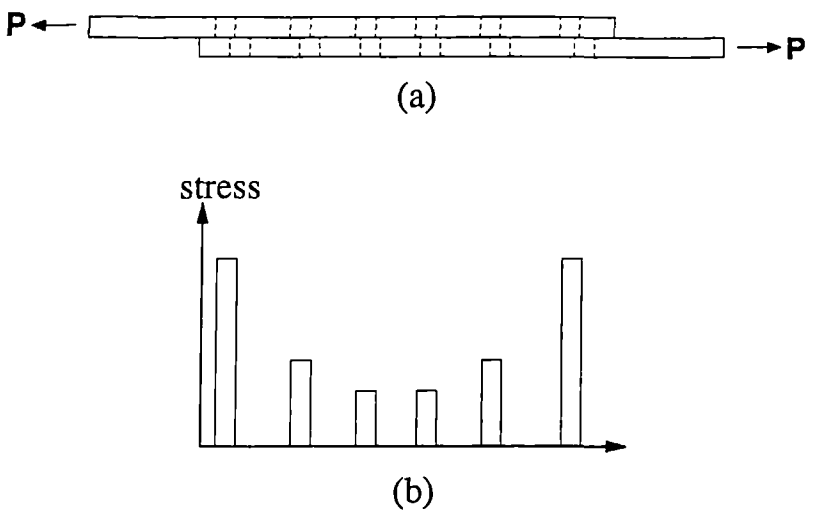

Fig. 2.3 *(a) Deflections and (b) elastic stresses in bolted joint.*

2.2 PAST SOLUTIONS

In its simplest form, the bonded joint may be considered to be a joint with an infinite number of elastic bolts. If these bolts do not offer any direct resistance either normal to or along the loading plane, they may be termed shear springs. This was the approach adopted by the earliest workers in the field such as Volkersen (1938).

2.2.1 Volkersen's solution

Owing to the continuous mutual support of the layers along its length, the joint is a *statically indeterminate* structure. It is therefore necessary to satisfy continuity as well as static equilibrium to obtain a solution.

To achieve this, Volkersen (1938) employed a continuum mechanics, or displacement field, approach. His differentially strained lap joint is illustrated in Fig. 2.4. The configuration is termed *balanced* or *antisymmetric* since the adherends are identical.

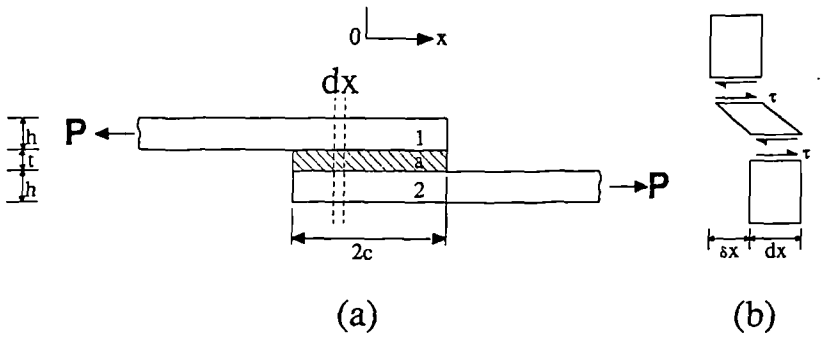

Fig. 2.4 *(a) Single-lap joint as analysed by Volkersen and (b) a deformed section.*

Consider the deformed section of the joint shown in Fig. 2.4b. The relative displacements between the two adherends (δ_x) is related to the adhesive shear strain (γ) by

$$\gamma t = \delta_x = \delta_0 + \int_{-c}^{x} \varepsilon_1 \, dx - \int_{-c}^{x} \varepsilon_2 \, dx \qquad (2.2)$$

Where ε_1, ε_2 are the strains in the adherends, δ_0 is the relative displacement at x = -c and t is the adhesive thickness. But

$$\gamma = \frac{\tau}{G_a} \tag{2.3a}$$

$$\varepsilon_1 = \frac{1}{Eh}\left[P - \int_{-c}^{x} \tau \, dx \right] \tag{2.3b}$$

$$\varepsilon_2 = \frac{1}{Eh}\left[\int_{-c}^{x} \tau \, dx \right] \tag{2.3c}$$

where G_a is the adhesive shear modulus, E the adherend Young's modulus and h the adherend thickness.

Substituting eqns (2.3) into eqn (2.2) and then differentiating twice gives

$$\frac{d^2\tau}{dx^2} = \frac{2G_a}{Eht} \tau \tag{2.4}$$

On solving eqn (2.4) it is found that the maximum shear stress occurs at the overlap *ends* and in a symmetrical joint is, for reasonable values of length, proportional to

$$\frac{G_a}{2Eth} \tag{2.5}$$

This is an entirely different result to eqn (2.1), suggesting that maximum shear stress is *not* dependent on joint width or length but on the sheet thicknesses and moduli.

Volkersen's analysis fails to incorporate several important effects. First, the shearing of the adherends, especially important in composites but also in metals, is not considered. Second, Volkersen does not satisfy the zero shear stress condition that must exist, due to complementary shear, at the joint edge where there is a free surface. On the contrary, shear stresses are predicted to be maximum at this point. Another serious omission is the failure to consider the bending moments which are generated at the joint edges due to the eccentricity of the load path (Fig. 2.5a).

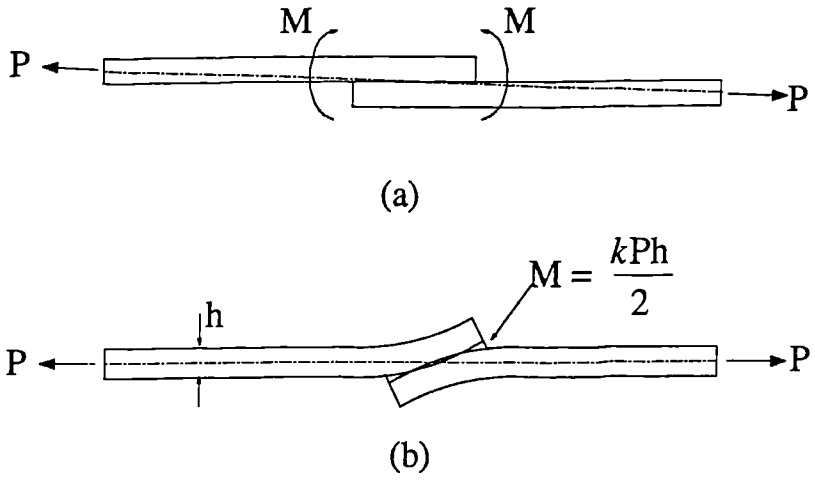

Fig. 2.5 *Load path in (a) undeformed and (b) deformed joint*

These moments are important since they cause joint rotation (Fig. 2.5b) thus introducing transverse normal, or peel, stresses into the adhesive layer. In joints where the bending effect is not significant, such as the double lap, the use of Volkersen's theory is justified.

2.2.2 **Goland and Reissner**

The next major step forward was the analysis of Goland and Reissner (1944) in which the effect of bending moments and joint rotation was considered. They argued that the net effect of the rotation was to relieve the bending moment, M, at the joint edges. In order to calculate M, a bending moment factor k, was introduced such that

$$M = \frac{kPh}{2} \tag{2.6}$$

where P is the joint tensile load (see Fig. 2.5a). In deriving k the joint and adherends were considered to be cylindrically bent plates in plane strain

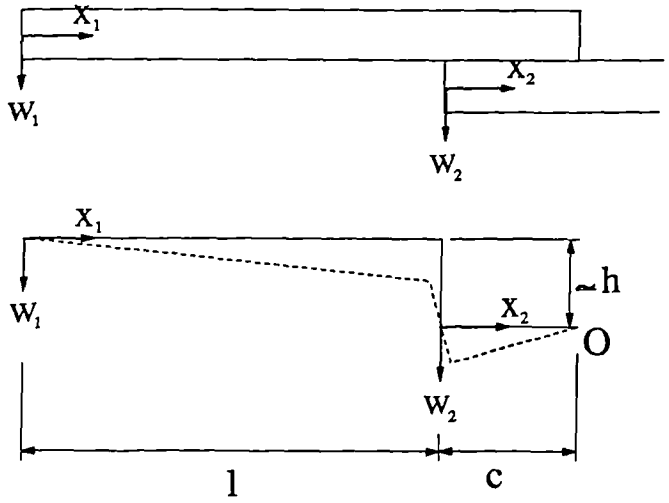

Fig. 2.6 *Analysis of joint rotation by Goland and Reissner*

Fig. 2.6 shows the neutral axis of the joint before (solid line) and after (dashed) loading. Due to antisymmetry about the mid-point of the joint, only half the joint is shown.

If the deflected coordinates for the adherend and overlap are (x_1,w_1) and (x_2,w_2) respectively then their respective bending moments are given by

$$M_1 = P\,[\beta x_1 - w_1] \qquad \text{for } 0 \le x_1 \le l \qquad (2.7a)$$

$$M_2 = P\,[\beta(l+x_2) - w_2 - h/2] \qquad \text{for } 0 \le x_2 \le c \qquad (2.7b)$$

where β is the angle between the x coordinates and the line of action of the applied loads:

$$\beta = h/2(l+c)$$

The transverse deflections of the sheets are related to their bending moments, eqn (2.7), by the equation

$$\frac{d^2w_1}{dx_1^2} = -\frac{M_1}{D_1} = -\frac{P}{D_1}\,[\beta x_1 - w_1] \qquad \text{for } 0 \le x_1 \le l \qquad (2.8a)$$

$$\frac{d^2w_2}{dx_2^2} = -\frac{M_2}{D_2} = -\frac{P}{D_2}\,[\beta(l+x_1) - w_2 - h/2] \qquad \text{for } 0 \le x_1 \le c \qquad (2.8b)$$

D_1 and D_2 are the flexural rigidities of the adherend and overlap respectively. Eqn (2.8) can be solved together with the four boundary conditions

at $x_1 = 0$	$w_1 = 0$
at $x_1 = l$, $x_2 = 0$	$w_1 = w_2$
at $x_1 = l$, $x_2 = 0$	$\frac{dw_1}{dx_1} = \frac{dw_2}{dx_2}$
at $x_2 = c$	$w_2 = 0$

to give the transverse deflection functions of w_1 and w_2. Then, according to the condition

$$M = M_1 \Big|_{x_1=l} = -D_1 \frac{d^2w_1}{dx_1^2} \Big|_{x_1=l}$$

the bending moment is

$$M = \frac{Ph}{2} \frac{1}{1+2\sqrt{2}\tanh(\zeta c/2\sqrt{2})} \tag{2.9}$$

where $\zeta = \sqrt{(P/D_1)}$. Comparing eqn (2.9) with eqn (2.6) it can be seen that the bending moment factor k is

$$k = \frac{1}{1+2\sqrt{2}\tanh(\zeta c/2\sqrt{2})} \tag{2.10}$$

Therefore, for small loads, very little joint rotation takes place, $k \approx 1.0$, thus $M \approx Ph/2$. As the load increases, the joint rotates and the bending moment factor decreases. The relationship between the bending moment and joint load for a typical joint is illustrated in Fig. 2.7.

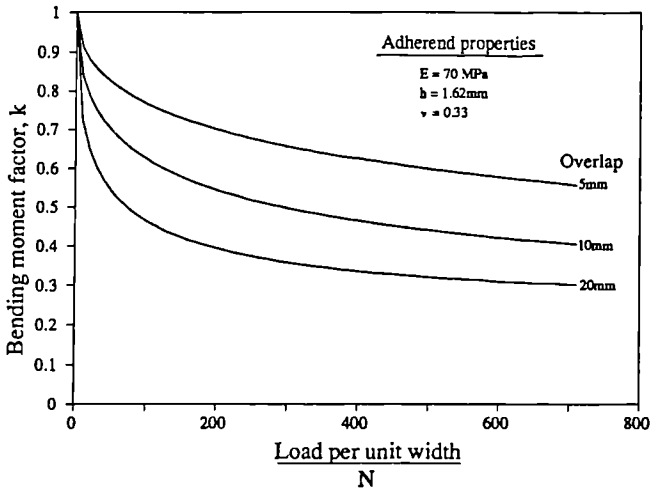

Fig. 2.7 *Bending moment factor versus joint load per unit width for various overlaps according to Goland and Reissner*

Having established the joint edge loading conditions, Goland and Reissner addressed the problem of determining the stress distribution. They considered two cases and developed an analysis for each. The first analysis neglected the flexibility of the adhesive layer. This is considered to be the case when criterion (2.11a) is satisfied.

$$\frac{tE}{hE_a} \leq 0.1, \qquad \frac{tG}{hG_a} \leq 0.1 \tag{2.11a}$$

$$\frac{hE_a}{tE} \leq 0.1, \qquad \frac{hG_a}{tG} \leq 0.1 \tag{2.11b}$$

The second analysis treats the adhesive as a series of shear and tension springs and is applicable to joints satisfying the second Goland and Reissner criterion (2.11b). Generally, the first analysis is applicable to wooden joints while metal joints, of interest here, are best analysed by the second theory.

The solution for the shear and normal stresses in the adhesive layer is found through solving differential equations which satisfy compatibility and equilibrium throughout the joint. To facilitate a solution, Goland and Reissner ignored the shear and normal deformations in the adherend. The differential equations are derived by considering relative displacements in a manner similar to that employed by Volkersen (eqns (2.2)-(2.4)). The main advance is that the relative displacement in the y direction is also considered. The resulting shear (τ) and peel (σ) stress distributions are found to be of the form:

$$\tau = c_1\{c_2(1+c_3k)\cosh(c_4x) + 3(1-k)\} \tag{2.12}$$

$$\begin{aligned}\sigma = \; & c_5\{(c_6k+c_7k')\cosh(c_8x)\cos(c_8x) \\ & +((c_9k+c_{10}k')\sinh(c_8x)\sin(c_8x)\}\end{aligned} \tag{2.13}$$

where c_i are material and geometric constants, k is the bending moment factor and k' is defined as Qc/Pt_a^2, where Q is the shear force at the overlap edges. It can be seen that the stresses are assumed to vary with x only and are therefore constant through the adhesive thickness.

For a typical metal joint with a glue line of 0.15mm, the parameters

$$\frac{hE_a}{tE} = 0.457, \qquad \frac{hG_a}{tG} = 0.492 \tag{2.14}$$

are outside the bounds (2.11b) suggested by Goland and Reissner. Lubkin and Reissner (1956) have suggested that the bounds (2.11b) are too conservative. Later work by Peppiat (1974) has shown that Goland and Reissner's second theory does in fact give reasonable results for joints satisfying criterion (2.14). Thus the bounds are a rough guide but nevertheless apply to any theory which similarly neglects the shear and normal stresses in the adherends.

In spite of its deficiencies, Goland and Reissner's work served to illustrate the importance of the bending moments and therefore the need to consider normal (or peel) stresses.

2.3 CURRENT THEORIES

In later work, Volkersen (1965) attempted to model the ends of the single lap joint, where a shear stress free surface exists, by satisfying the stress equilibrium relationship

$$\frac{\partial \sigma_y}{\partial y} + \frac{\partial \tau_{xy}}{\partial x} = 0$$

As explained by Peppiat (1974) there were a number of errors in the paper, particularly in the assumed boundary conditions, and a solution is not possible.

Despite their limitations, the early solutions became the classical method of joint analysis and were part of the early strength of materials texts (Shanley, 1957). Later workers made modifications to analyse tapered, scarfed (Wah, 1973) and stepped joints (Hart-Smith, 1973a, Grant and Taig, 1976 and Reddy and Sinha 1975) . The increasing use of adhesives to bond dissimilar materials gave rise to thermal mismatch considerations (Chen and Cheng, 1982, Sinha and Reddy, 1976 and Chen and Nelson, 1979). There has also been much work to understand creep and viscoelastic behaviour, by Weitsman (1977,1980,1981) in particular. But it was the advent of composite materials that brought about a resurgence of interest in developing analyses. The earliest work in accounting for anisotropic adherends was by Wah (1973) and Srinivas (1975). Since then several other analyses have been presented, notably by Renton and Vinson (1977), Allman (1977) and Delale *et al* (1981).

2.3.1 **Renton and Vinson**

Renton and Vinson (1977) have produced a solution for a single lap joint between orthotropic sheets by including adherend shear and bending. The adherends can be unbalanced and deform thermally but cannot be general laminates since it is assumed that there is no coupling between bending, stretching or shearing. The adhesive is modelled as a series of shear/tension springs, so the shear and peel stresses are not allowed to vary through the thickness. Since the shear and normal stresses within the adherends are included in the formulation, Renton and Vinson's solution can be applied to joints which are outside the bounds of Goland and Reissner's second parameter, eqn (2.11b). However, the complexity of the solution in comparison with eqns (2.5), (2.12) and (2.13) is such that it is necessary to resort to digital computers to ease the burden of calculations.

2.3.2 **Delale *et al***

Probably the most thorough continuum mechanics analysis of lap joints is that presented by Delale et al (1981). Their approach takes the adhesive beyond the shear/tension spring model by incorporating the longitudinal (x direction in Fig. 2.8a) strain. However, they ignore variations through the adhesive thickness and fail to satisfy the stress free boundary conditions at the overlap ends. Moreover, like Renton and Vinson, Delale *et al* ignore the coupling terms so the degree of anisotropy that can be modelled is similarly limited.

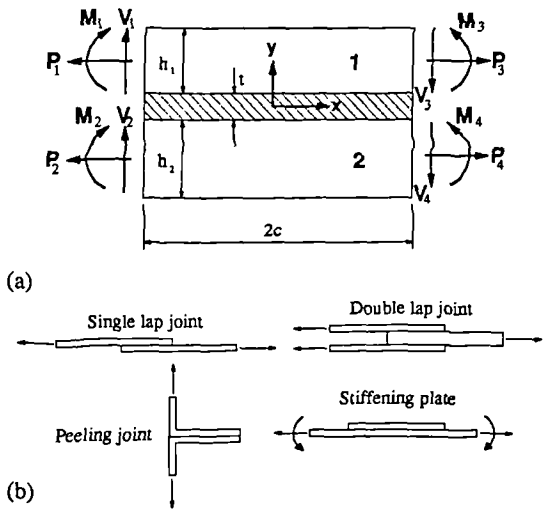

Fig. 2.8 *(a) A general joint and (b) joint configurations*

The power of the analysis lies in the fact that it has been developed for a general joint. A general joint, illustrated in Fig. 2.8a, is a joint which can have dissimilar adherends, while the loading consists of any combination of shear, bending and tension on each of its four faces. Consequently, any of the joint configurations shown in Fig. 2.8b can be analysed.

The first step in their solution was to relate the relative adherend displacements to the adhesive stress resultants in both in-plane and normal directions. Then kinematic relations were used to determine an adhesive strain field from the displacements. Finally, through use of an adhesive stress-strain relationship, differential equations for the adhesive stresses are obtained and solved. As was the case with Renton and Vinson's analysis, the solution is unwieldy and has to be implemented on computer.

In their paper, Delale *et al* suggest a method for introducing adhesive non linearity. By representing the adhesive stress-strain relationship in the Ramberg-Osgood form, an alternative system of differential equations is derived. However, Delale *et al* encountered mathematical difficulty in solving the equations analytically. Recently, Bigwood (1989) has produced a numerical solution to a similar system of differential equations.

2.3.3 **Weitsman**

Until the work of Weitsman (1977), the study of hygrothermal effects in joints was limited to the analysis of thermal expansion in the adherends. However, adhesives often have a much larger coefficient of expansion than adherend materials and are notoriously susceptible to swelling due to moisture. The net result of both these effects is large adhesive strains, particularly in the x direction, and failure might occur *without any load* being applied. For a loaded joint, Coppendale (1977) has shown that adhesive thermal deformation has a direct influence on the stresses in the end region. But closed form formulations often ignore the strain (and therefore stress) in the x-direction and thus fail to consider the full effect of adhesive hygrothermal behaviour.

In his analysis, Weitsman assumed a fully two-dimensional state of stress in the adhesive. But in order to realise a closed form solution, the adherends are treated as rigid bodies. Loading other than hygrothermal has not been considered.

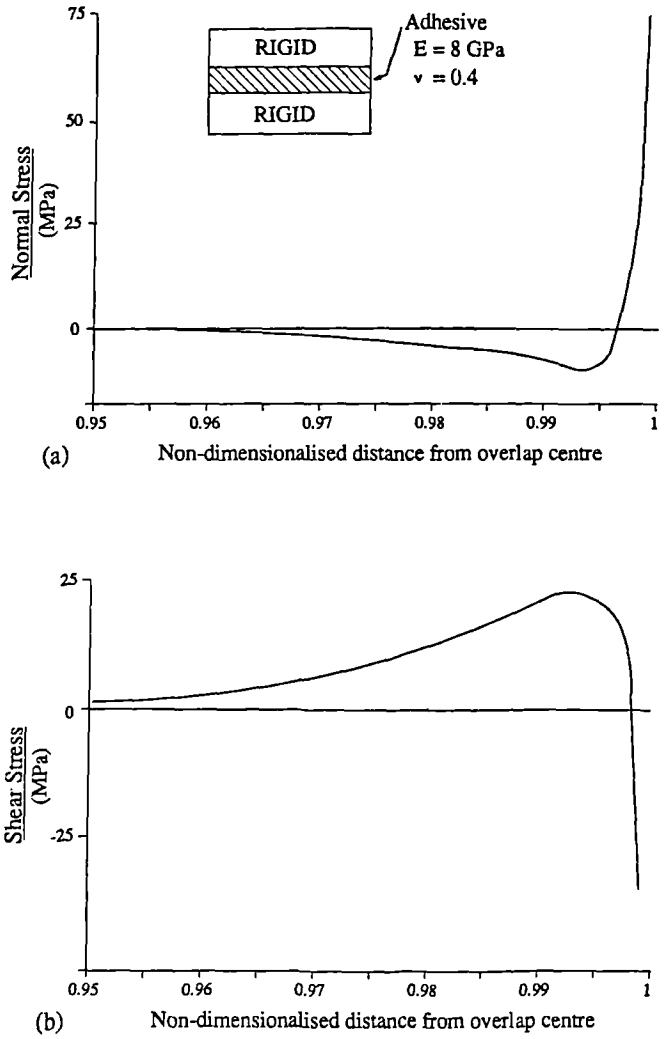

Fig 2.9 *Hygrothermal (a) Peel and (b) Shear stresses at a joint interface for a fully saturated epoxy adhesive, Epoxy 3501 (from Weitsman, 1977)*

Results from the analysis suggest that stresses are significant in both shear and peel. Fig. 2.9 shows the stresses at the adhesive/adherend interface for a fully saturated epoxy adhesive. The stresses appear to be concentrated entirely at the joint edge region. In fact there appears to be a singularity at the edge, where there is a tri-interface between the adhesive, adherend and free-surface.

2.3.4 **Allman**

The alternative to continuum mechanics for the solution of a statically indeterminate problem is to use energy methods. This is the approach adopted by Allman (1977) (and independently by Chen and Cheng, 1983). The

analysis includes the effect of bending, stretching and shearing of the adherends and accounts for the shearing and peeling of the adhesive. The stress distribution throughout the joint is defined in terms of two unknown functions $\phi_1(x)$ and $\phi_2(x)$ which satisfy the equations of equilibrium (2.15) and the stress boundary conditions including the stress free surfaces.

$$\frac{\partial \sigma_x}{\partial x} + \frac{\partial \tau_{xy}}{\partial y} = 0 \qquad (2.15a)$$

$$\frac{\partial \sigma_y}{\partial y} + \frac{\partial \tau_{xy}}{\partial x} = 0 \qquad (2.15b)$$

A complementary energy function for the joint is derived in terms of the two unknown stress functions and their derivatives. The function is then minimised, using the Euler-Lagrange equations of variational calculus, to yield two fourth order differential equations for the stress functions. For an unbalanced joint, the equations are coupled and a closed form solution is not possible. Instead, Allman suggests an approximate numerical method. For a balanced joint, the equations uncouple and can be analytically solved to give the stress functions.

The solution compares favourably with other closed form methods. Not only does it account for the shear stress free edges, but it allows a linear variation of peel stress through the adhesive thickness. The solution published by Allman is capable of analysing unidirectional adherends and could, with a modification to the energy function, analyse adherend thermal deformation.

2.3.5 **Hart-Smith**

All the closed form analyses discussed above assume that the joint materials are elastic. However, it is well known that certain adhesives are very ductile and can withstand large plastic deformation. In addition, the strength of some adhesives is such that the adherends may yield. Hart-Smith (1973b) provided a step forward in the modeling of material non-linearities by using a simple elasto-plastic adhesive model. The basic solution itself is similar to Goland and Reissner's except for the introduction of an iterative procedure to model plasticity.

There are several deficiencies in Hart-Smith's plastic solution. First, consideration of non-linearity is restricted to the adhesive. Through an elasto-plastic finite element analysis, Adams and Harris (1984) demonstrated that large amounts of adherend yield can increase the stress concentration at the adhesive edge and thus induce premature failure. In any case, much of the adherend yield occurs just outside the overlap so closed form analyses can never consider the full effect. Secondly, Hart-Smith considers plasticity to arise from the shear stress only. Although peel stresses are predicted by the solution, he argues that joint design should minimise their influence. Finally, for the sake mathematical simplicity, the adhesive is characterised as a bilinear curve, with the same strain energy as the true stress strain curve (Fig. 2.10). Hart-Smith justifies this by stipulating that the strength of an adhesive is defined not by the shape of the curve but by the shear strain energy described.

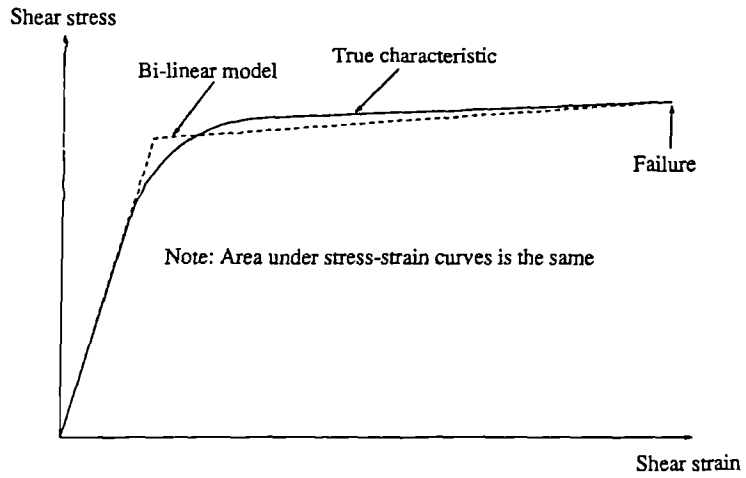

Fig. 2.10 *Bi-linear characterisation of a adhesive*

Apart from plasticity, Hart-Smith has made another contribution in the analysis of lap joints. For the single lap joint, he states that the bending moment factor developed by Goland and Reissner is based on erroneous boundary conditions. Goland and Reissner neglected the flexibility of the adhesive layer and assumed the joint to be a plate of twice the adherend thickness.

In developing his expression for the bending moment factor, k, Hart-Smith assumed the bending moment to be applied only at edge AB (see Fig. 2.11). In comparison, Goland and Reissner assume the bending moment to be applied along the complete edge AC which is clearly wrong since edge BC is a free surface.

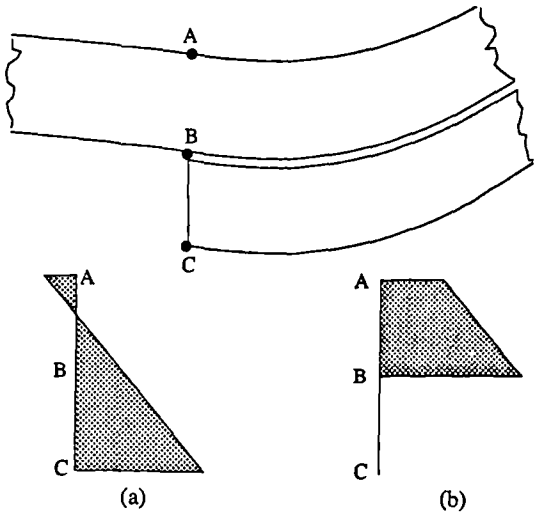

Fig 2.11 *Longitudinal stress distributions assumed by (a) Goland and Reissner and (b) Hart-Smith*

The bending moment factor, k, according to Hart-Smith is given by the equation

$$k = \frac{1}{1+\zeta c+(\zeta^2 c^2/6)} \tag{2.16}$$

The difference between eqns (2.10) and (2.16) is illustrated in Fig. 2.12. It can be seen that Hart-Smith predicts lower bending moments than Goland and Reissner for large overlaps.

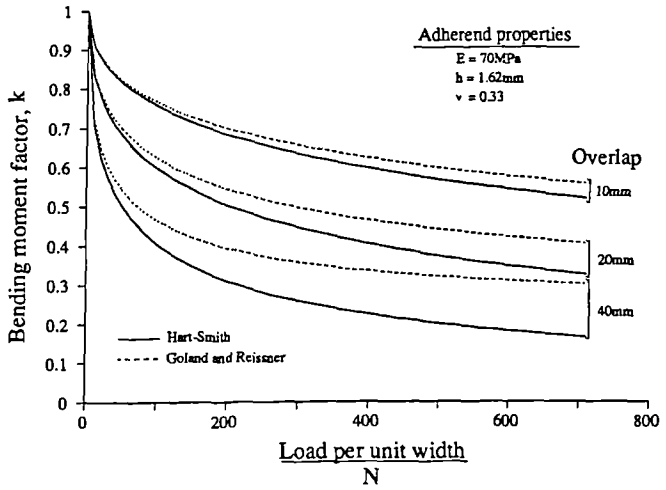

Fig 2.12 *Comparison of the bending moment factors given by Hart-Smith with Goland and Reissner's.*

2.3.6 Other

Grant and Taig (1976) have extended Goland and Reissner's theory to the analysis of stepped lap joints. More important, however, has been their work in modelling adhesive plasticity. They have developed Volkersen's equations in a manner not unlike Hart-Smith. The solution employs an iterative procedure for the analysis of a mulitstep lap joint which can have dissimilar adherends. Being a shear analysis, the peel stresses are ignored and the plasticity is therefore due to shear only.

The Engineering Sciences Data Unit (ESDU) have implemented this work into two commercial software package; one for elastic stresses in joints subjected to bending moments (Item 80039, 1980) and the other for the non-linear shear lag analysis (Item 79016, 1979). The latter applies to double lap joints and can predict strength according to a maximum shear strain criterion. The evidence presented by ESDU, reproduced in Fig. 2.13, suggests that the predictions are accurate.

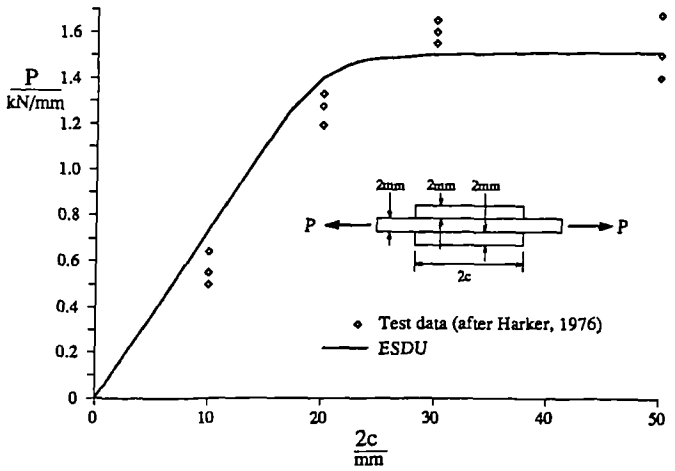

Fig 2.13 *Predicted strengths for double lap joints with a non-linear adhesive by ESDU's computer program (from ESDU Item 79016)*

Another commercial program for the plastic analysis of joints has been produced at Harwell (1986). This analysis goes beyond Hart-Smith's, since it allows both shear and peel to contribute to plasticity.

Like the plastic solutions of Hart-Smith and Grant, Harwell's is not strictly a closed form solution since an iterative procedure is used. The solution's capabilities are somewhat similar to that of Delale *et al* (1981) in

that general joints may be analysed. In addition the adherends may be orthotropic. Unfortunately, the adhesive is modelled as shear/tension springs. Therefore thickness variations are ignored and the x (in plane) stress is neglected. Although thermal deformation is included, this is limited to the adherends. Nevertheless, the analysis remains one of the most advanced available.

2.4 NUMERICAL METHODS

From a review of the theories it is clear that, while it may be possible to model a joint *realistically*, *difficulties* arise when a *closed form* solution to the ensuing differential equations is attempted. Solving the equations numerically, using finite differences, leads to a heavy reliance on computers. Until the early 1970's, the computing power required was in the form of large, expensive mainframe machines. It is only recently, with the advent of personal computers and workstations, that stress analysts have had readily available computing power. This has led to a concentration of effort in developing numerical methods.

2.4.1 Finite Difference Method (FDM)

In developing a three dimensional stress analysis for a lap joint, Adams and Peppiat (1973) used finite differences to obtain a solution to their governing differential equations. Despite the fact that bending was ignored, the analysis enabled them to reveal stresses across the *width* of the joint.

Kline (1982) has produced an analysis in which the adhesive stresses can vary linearly through the thickness. The adherends deform as thin plates in cylindrical bending, thus accounting for bending, shearing and stretching in the adherend. To solve the resulting system, a finite difference scheme was employed.

The greatest advantage offered by finite differences is that they enable solutions to be obtained for otherwise redundant closed form analyses. For instance, the uncoupled differential equations produced by Allman could conceivably be solved by finite differences.

In order to take full advantage of the accuracy available with a finite difference solution, the amount of computational effort will approach that required for a simple finite element analysis. Cooper and Sawyer (1979) obtained solutions using both methods and concluded that there is good agreement. However, the FDM

requires a system of governing differential equations to be set up for each type of problem, whereas the FEM can model any geometry under any boundary conditions. This flexibility has made the latter method the more popular numerical method for stress analysis.

2.4.2 Finite Element Method (FEM)

The FEM is a general method for the stress analysis of structures. A brief summary of the finite element method is given briefly in the next chapter. Here, the capabilities it offers for the modelling of adhesive joints are outlined.

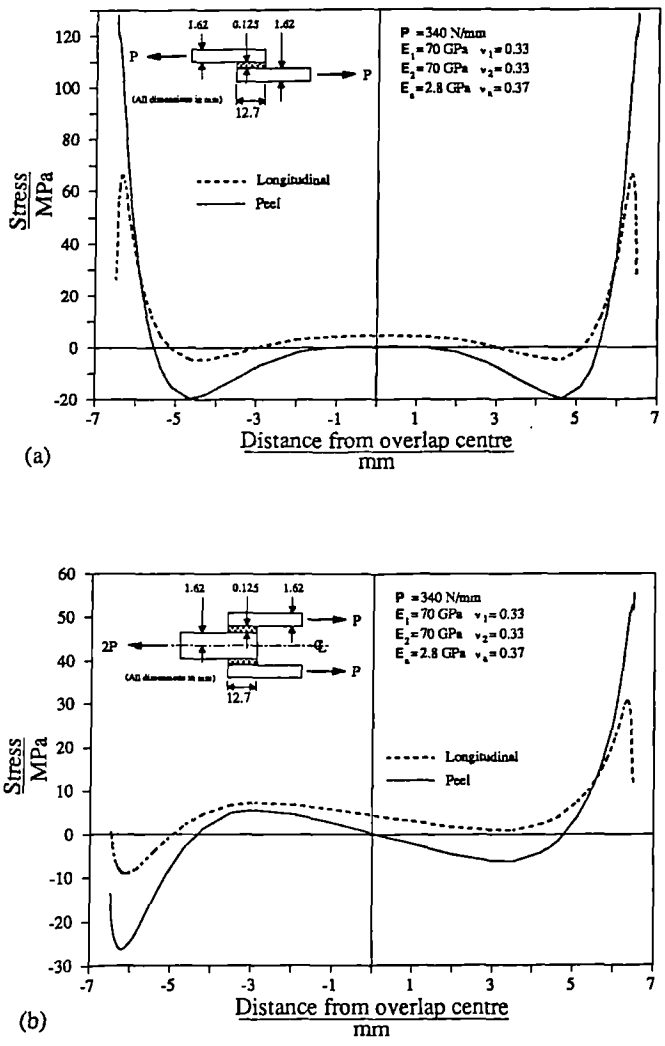

Fig. 2.14 *Average peel and longitudinal stresses, within the adhesive, predicted by FEM for (a) single and (b) double lap joints.*

With FEM the adhesive can be treated as an elastic continuum. This means that no component of stress or strain is neglected. Closed form analyses often ignore the adhesive stress in the x direction. A simple finite element analysis has been conducted to illustrate the significant of this stress. The results in Fig. 2.14 show that the longitudinal stress can be as much as 50% of the peel stress for both single and double lap joints. Thus σ_x will have a significant influence on the principal stress condition and therefore the yield criterion.

In addition, FEM's make no assumptions about the variation of stresses across the adhesive thickness. In closed form analyses, stresses are often assumed to be constant through the adhesive thickness. This assumption, possibly true in the mid regions, is clearly wrong at the edges as suggested by the FEM results in Fig. 2.15 and limits closed form analyses to joints with a very thin adhesive.

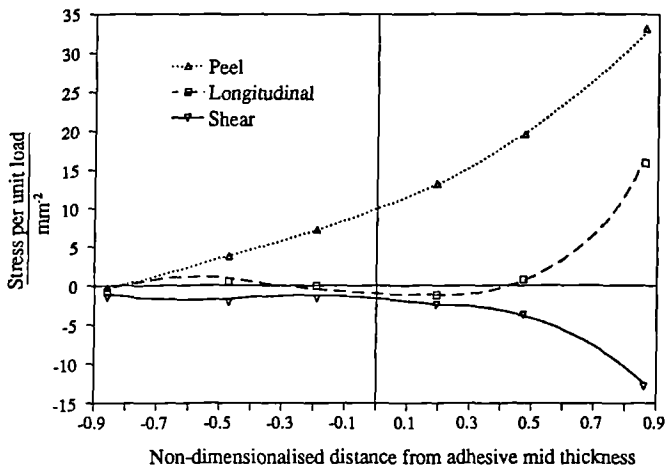

Fig. 2.15 *Through thickness variations of adhesive stresses at the edge of a joint with a square edge.*

As there is no such constraint on FEM, Crocombe and Adams (1981) were able to investigate the influence of adhesive thickness. Furthermore, extra layers can be relatively easily included into a model thus enabling Crocombe and Evans (1987) to consider another thickness effect; the cladding on Aluminium adherends.

The joint rotation that occurs in single lap joints can be modelled if a *large displacement* FEM is employed. After carrying out a large displacement finite element analysis, Cooper and Sawyer (1979) concluded that in comparison with small displacement analyses, the maximum peel stresses were 35% lower. Maximum shear was reduced by 28%.

Closed form analyses have shown that the ends of the overlap are critical regions in terms of joint strength since this is where maximum values of stress occur. The stresses in this region can be studied in greater detail using FEM. Taking advantage of this FEM capability, Adams and Peppiat (1974) illustrated the significance of the spew fillet. The spew is a region of excess adhesive at the edge of the joint, usually created at the manufacturing stage as the adhesive is squeezed out. The fillet geometry is very difficult to model mathematically and is therefore ignored by closed form methods, but FEM shows that it is responsible for a 30% reduction and complete re-orientation of stresses (Adams and Peppiat, 1974).

Perhaps the greatest advantage of the finite element method is its ability to model material non-linearity. Most joint materials are elasto-plastic and without a non-linear analysis the full potential of such joints cannot be understood. Recently, Adams and Harris (1984) have analysed joints allowing both the adhesive and the adherend to behave non-linearly. They discovered that a small amount of plastic deformation at the overlap edges, rather than being detrimental to joint strength, was advantageous since it enhanced further rotation, thus reducing the harmful bending moments. Large amounts of deformation, however, were found to increase stress concentrations in the adhesive. Plasticity in the adhesive was found to redistribute the stresses along the overlap, thus increasing the load bearing capacity of the joint. These insights into joint behaviour are only available through finite element analysis and explains why workers using this approach have been able successfully to predict the strength and mode of failure for a variety of configurations and material properties.

2.5 CONCLUSIONS

If joint behaviour is to be understood, then it is imperative that the stresses (and strains) at the ends are known. The FEM provides the only reliable technique of stress evaluation in this region. Although analytical solutions are limited in their accuracy by the assumptions made during the formulation, they are often easier to use.

Several analytical solutions exist and their relative merits can be assessed by ranking them on the basis of assumptions made and the accuracy of the solution. Such an exercise, for the analyses reviewed above, leads to Table 2.1.

RANK	METHOD	Spew fillet	Stresses in adhesive	Stresses in adherend	Thermal deformation	Non-linear materials
1	FEM	Yes	$\sigma_x,\sigma_y,\tau_{xy}$	$\sigma_x,\sigma_y,\tau_{xy}$	All sheets	All sheets
2	Allman	No[1]	σ_y,τ_{xy}	$\sigma_x,\sigma_y,\tau_{xy}$	Adherends[2]	All sheets[2]
3	Delale et al	No	$\sigma_x,\sigma_y,\tau_{xy}$[3]	$\sigma_x,\sigma_y,\tau_{xy}$	No	Adhesive[2]
4	Harwell	No	σ_y,τ_{xy}[3]	$\sigma_x,\sigma_y,\tau_{xy}$	Adherends	Adhesive
4	Hart-Smith	No	σ_y,τ_{xy}[3]	$\sigma_x,\sigma_y,\tau_{xy}$	No	Adhesive
5	Renton Vinson	No	σ_y,τ_{xy}[3]	σ_x,σ_y,τ_x	Adherends	No
6	Goland Reissner	No	σ_y,τ_{xy}[3]	σ_x	No	No
7	Volkersen	No	τ_{xy}[3]	σ_x	No	No

[1]The end condition of a shear stress free surface is satisfied

[2]Although the capability is not included in the solution published, the author suggests how it may be incorporated

[3]The stresses remain constant across the adhesive thickness

Table 2.1 *Joint analyses ranked on the basis of inherent assumptions and accuracy of predictions.*

Chapter 3

A METHOD FOR THERMAL ANALYSIS OF LAP JOINTS

The main objective of the present work is to provide for the widest possible user base, a method of predicting the stresses in axially loaded lap joints subjected to a thermal environment. To achieve this, the method should not only be rigourous enough to satisfy the requirements of a specialist stress analyst but also be in an accessible form to cater for the non-specialist.

From the literature review, it is patently clear that the ability of the FEM to model almost any aspect of joint behaviour will enable it to analyse the type of joint considered here. However, FEM requires expert knowledge for data preparation and result interpretation. In addition, a thorough finite element analysis needs mainframe computing power. This is not widely available and therefore conventional FEMs cannot meet the basic aim of the method required. However, the need for some form of computing power is inescapable since, as discovered during the literature review, the better closed form solutions are more efficient when programmed. Today, computing power is widely available in the form of desktop Personal Computers (PC) and workstations. Therefore, the main aim of the present work can be met if the method developed can be implemented on such machines.

Although it is possible to implement the FEM on a PC, limitations are imposed on the number of elements which can be used and this limits the accuracy of the solution. It would be more productive to develop a method of solution which is as accurate as possible within the confines of a PC. This was the philosophy behind the approach adopted for the present work.

To aid the development of the analysis, finite element analysis of joints has been performed. The aim was to identify the important aspects of the thermal response of a joint for inclusion within the analysis. Later, the FEM results were used to check the accuracy of the solution.

In the next section the principles of elastic FEM theory are outlined, fuller details are given by Zienckiewicz and Taylor (1989). This is followed by a study of lap joint thermal behaviour from which an *elastic* theoretical model is developed and then solved.

3.1 FINITE ELEMENT METHOD

Zienckiewicz describes the finite element method as *"a general discretization procedure of continuum problems posed by mathematically defined statements"*. For stress analysis, the structure is divided into discrete *elements* interconnected at *nodes*. The elements are mathematical representations of a *basic variable*, usually displacements, in terms of its nodal values. Variational principles are then used to find these nodal values by minimising energy while ensuring force and displacement continuity between adjacent elements.

While a displacement based approach is the most common, it is possible to work with stress as the basic variable. Such approaches are termed force or equilibrium methods. Latterly, there has been much work, pioneered by Pian (1973), to develop hybrid elements in which stresses are the unknown with prescribed displacement boundary conditions. Although more difficult to formulate, the hybrid element offers greater accuracy, especially for plate bending problems.

In the present work, a plane strain displacement method has been employed. If $\{\delta\}$ is a vector of elemental nodal displacements and $\{\varepsilon\}$ the strains throughout the element then

$$\{\varepsilon\} = [\mathbf{B}]\{\delta\} \tag{3.1}$$

where the [B] matrix is the strain-displacement relationship and is determined from the shape function array, which relates displacements at any point within the element to the nodal displacements. Stresses are related to strains through the elastic modulus matrix [D] by eqn (3.2).

$$\{\varepsilon\} = [\mathbf{D}]\{\sigma\} \tag{3.2}$$

Then, the total potential energy, expressed as the functional Π, is

$$\Pi = \frac{1}{2} \{\delta\}^T[\mathbf{K}]\{\delta\} + \{\delta\}^T[\mathbf{f}]$$

where [f] is a vector of applied and initial forces and [K] is the stiffness matrix given by eqn (3.3).

$$[K] = \int_V [B]^T[D][B]\, dv \tag{3.3}$$

Considering a variation $\Delta\Pi$ in the potential energy,

$$\Delta\Pi = \frac{1}{2}\Delta\{\delta\}^T[K]\{\delta\} + \frac{1}{2}\{\delta\}^T[K]\Delta\{\delta\} + \Delta\{\delta\}^T\{f\})$$

so

$$\{f\} = [K]\{\delta\} \tag{3.4}$$

This is the basic equation of the finite element method. The next stage in the procedure is to assemble the global stiffness matrix $[\underline{K}]$ and load vector $[\underline{f}]$ from the elemental contributions. The displacements, for the complete structure, are then given by

$$\{\underline{\delta}\} = [\underline{K}]^{-1}\{\underline{f}\} \tag{3.5}$$

Once displacements are known, the stresses and strains can be calculated from eqns (3.1) and (3.2).

3.1.1 **Thermal FEM**

A computer program implementing the finite element method expounded above was used for the present work. The program, FELDEP, was developed by Crocombe (1981), and employs eight noded isoparametric elements. It is capable of performing a two-dimensional, large displacement analysis. However, FELDEP did not have thermal capability. Inclusion of thermal effects in a linear system is easily achieved by modifying the left hand side of eqn (3.4). Substituting eqn (3.3) into eqn (3.4) gives

$$\{f\} = \int_V [B]^T\{\sigma\}\, dv \tag{3.6}$$

If thermal strains are present

$$\{\sigma\} = [D]^{-1}\{\varepsilon - \varepsilon_t\} \tag{3.7}$$

where $\{\varepsilon_t\}$ is the thermal strain vector. After substituting eqn (3.7) into eqn (3.6) and re-arranging, we have the new system equation

$$\{f\} \; - \int_V [B]^T\{\sigma_o\}\, dv = [K]\{\delta\}$$

where $\{\sigma_o\} = [D]^{-1}\{\varepsilon_t\}$. Appendix Ia explains how this was implemented in FELDEP.

3.2 THERMAL ANALYSIS

A typical single lap joint has been analysed to investigate the influence of temperature. The finite element mesh for this geometry was generated with the aid of an automatic mesh generator, GMESH, developed at Bristol University by Chen (1983). The boundary conditions imposed allow free expansion and are shown, together with the mesh, in Fig. 3.1. Throughout the study it was assumed that the joint had reached a steady state of temperature.

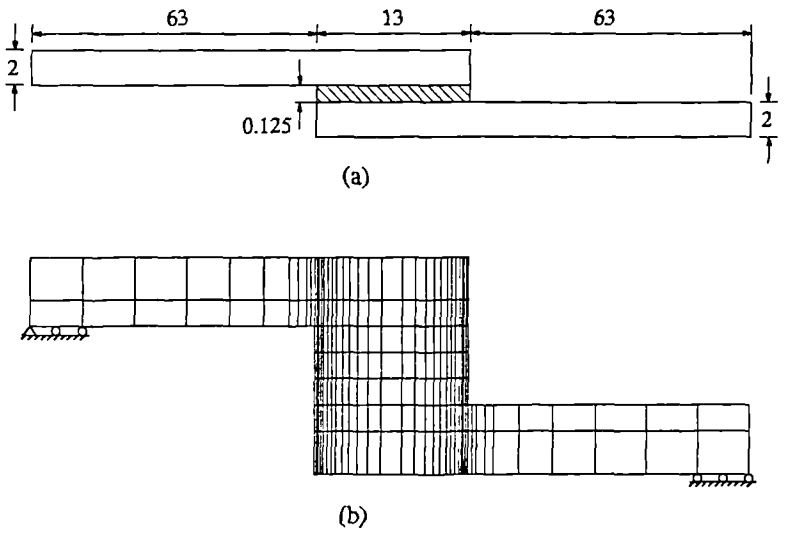

Fig. 3.1 *(a) Joint geometry (in mm) and (b) the finite element mesh and boundary conditions.*

To gain overall insight of the response of the adhesive, the following two cases were investigated:

(1) Only one adherend deforms. This is equivalent to the effect of thermal mismatch.

(2) Adhesive thermal deformation. Often neglected, this effect may be significant, especially in joints where the adhesive coefficient of expansion is greater than that of the adherends. It can also be caused by either cure shrinkage or contraction of the adhesive when joints cool from cure to operating temperatures.

For the purpose of the investigation, the joint sheet materials have been given idealised values. The moduli are representative of aluminium alloy and epoxy adhesives. Arbitrary values of thermal coefficients have been chosen to ease the comparison. The modelling data for each type of joint is listed in Table 3.1.

	JOINT	
	1	**2**
E_1 (GPa)	70	70
E_2 (GPa)	70	70
E_a (GPa)	3	3
ν_1	0.33	0.33
ν_2	0.33	0.33
ν_a	0.37	0.37
α_1 (10^{-6}/°C)	10	0
α_2 (10^{-6}/°C)	0	0
α_a (10^{-6}/°C)	0	10
t_1 (mm)	2.0	2.0
t_2 (mm)	2.0	2.0
t_a (mm)	0.125	0.125
c (mm)	6.5	6.5

For each joint, $\Delta T = +100°$

Table 3.1 *Joint data used in the finite element analysis.*

3.2.1 **Thermal mismatch**

To study thermal mismatch, a joint has been given properties, listed under JOINT-1 in Table 3.1, such that only sheet 1 is allowed to expand. The result is a bimetallic strip effect between sheets 1 and 2. Sheet 1 expands while sheet 2 resists, and the joint deforms in the manner shown in Fig. 3.2.

The finite element analysis output gives stress and strain values at gauss points. From the mesh used, it is possible to plot the stress variations along the adhesive at the cross sections AA, BB and CC shown in Fig. 3.3.

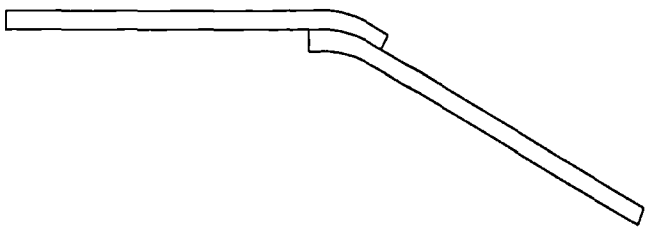

Fig. 3.2 *Joint deformation for JOINT-1*

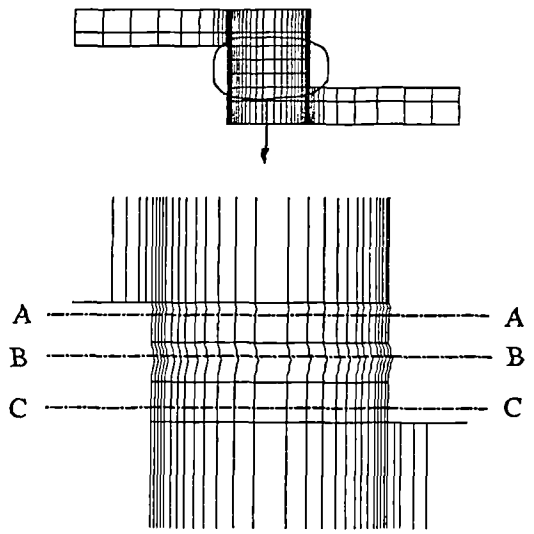

Fig. 3.3 *Position of Gauss point sections, in adhesive mesh, at which results are plotted.*

The shear stress distribution, plotted in Fig. 3.4a, is almost constant throughout the adhesive thickness. Peel stresses (Fig. 3.4b), however, vary considerably through the adhesive thickness, with maximum values occurring at the interface. Also plotted in Fig. 3.4b is the *average* peel stress. This gives the misleading impression of a lightly stressed adhesive in peel.

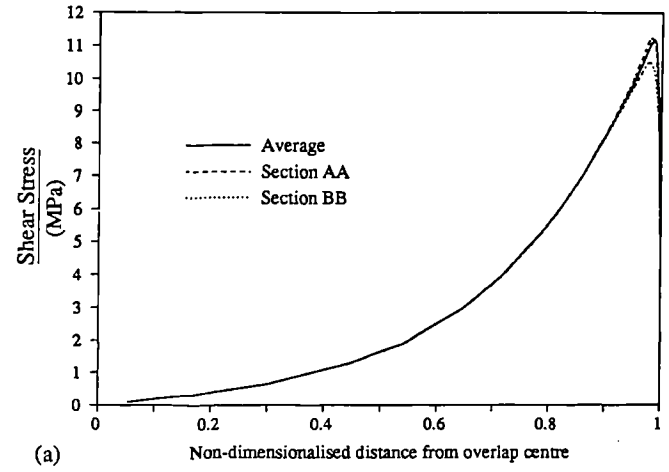

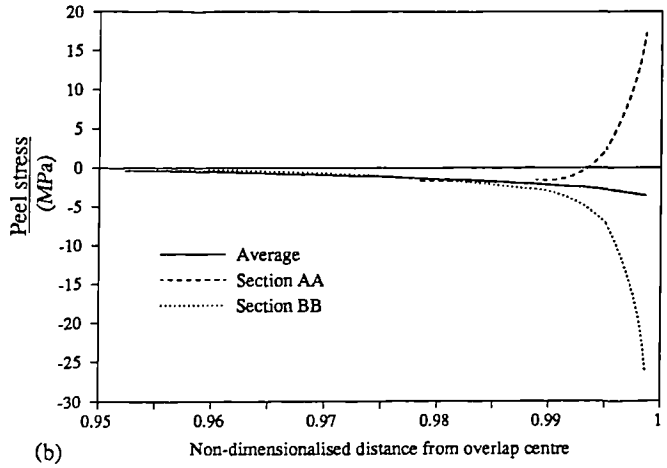

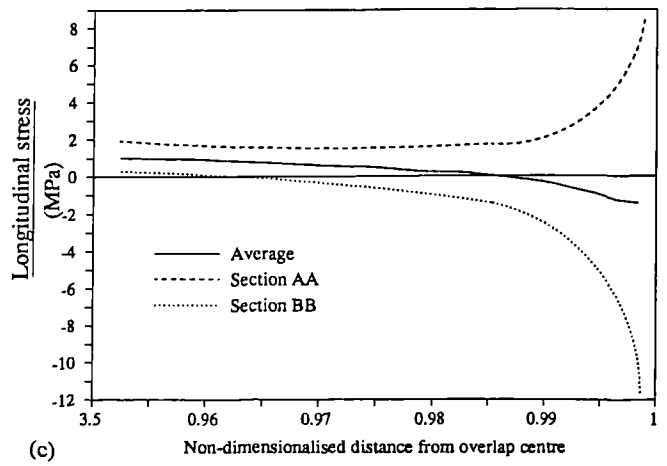

Fig 3.4 *(a) Shear, (b) Peel and (c) Longitudinal stress distributions in JOINT-1 (Table 3.1).*

Since several closed form solutions do not allow through thickness variations, they can only predict an average peel stress and would therefore underestimate the debonding stresses at the interface. Finally, the maximum longitudinal stress is similar in magnitude to the maximum shear stress and approximately half the peel stress. So longitudinal stresses are definitely not negligible as is assumed by many closed form solutions for thermal mismatch (eg. Hart-Smith 1973 and Chen and Nelson 1979).

3.2.2 Adhesive deformation

Closed form theories which incorporate the thermal behaviour of joints usually disregard adhesive deformation. The adhesive often has a larger coefficient of expansion than the adherends. Weitsman (1977) has shown that this effect alone can lead to debonding.

In order to concentrate on adhesive deformation, the adherends were not allowed to expand in the finite element analysis (JOINT-2, Table 3.1). The results are plotted in Fig. 3.5. It can be seen that the peel stresses (Fig. 3.5a) are promoting a disbond, particularly at the ends where the shear (Fig. 3.5b) is also maximum. While the shear stresses tend to zero at the joint ends in the mid region, closer to the tri-interface, between adherend/adhesive/free-surface, there appears to be a singularity.

As in the mismatch case above, the longitudinal stresses (Fig. 3.5c) are similar in magnitude to the peel and shear stresses and should therefore be incorporated in any analysis which attempts to model adhesive deformation.

3.3 CHOOSING A METHOD OF ANALYSIS

From the thermal FE analysis, it can be concluded that there are two aspects of joint thermal behaviour which ought to be considered in any theoretical model. One is the thermal deformation of the adhesive and the other is the variation of stresses through the adhesive thickness. Proper consideration of the former means that longitudinal stresses in the adhesive cannot be ignored. Therefore, a realistic mathematical analysis for a lap joint subjected to a tensile load and thermal stress should include all three stresses, shear, peel and longitudinal, in both adherend and adhesive.

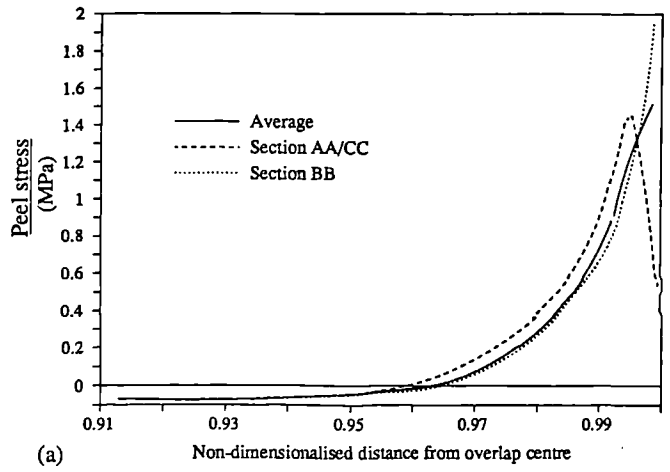

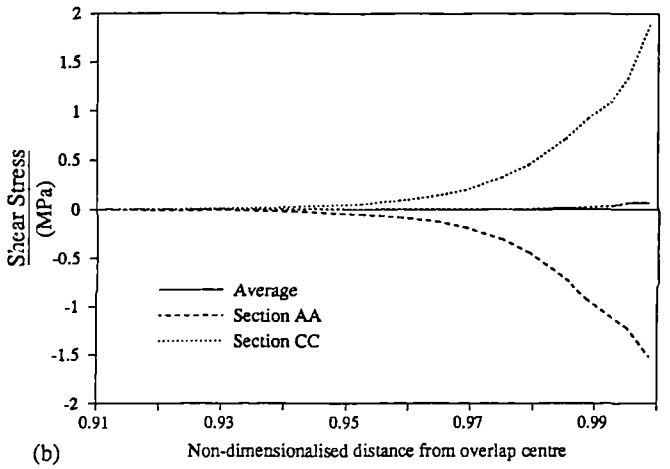

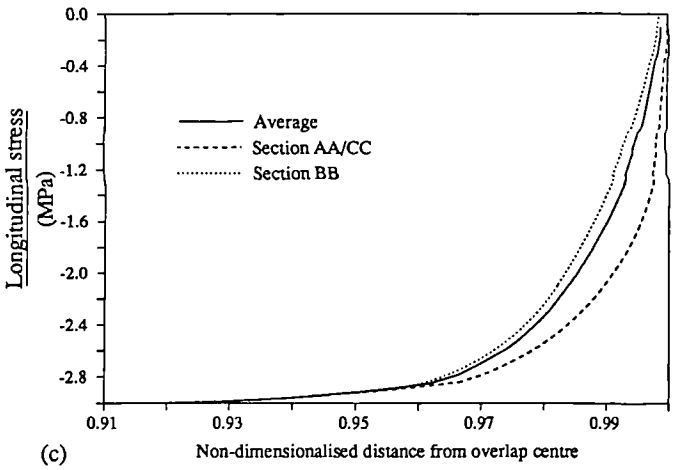

Fig 3.5 *(a) Peel, (b) Shear and (c) Longitudinal stress distributions in JOINT-2 (Table 3.1).*

The question of which method to develop for such an analysis now arises. The method ranked highest in Table 2.1, displacement FEM, has already been rejected since it requires specialist knowledge and expensive computing power The next best method was felt to be that proposed by Allman (1977) which is based on minimising complementary energy while satisfying equilibrium.

The equilibrium formulations offer certain advantages over the displacement methods such as those proposed by Renton and Vinson (1977) and Delale *et al* (1981). Boundary conditions, particularly at the joint ends, are easier to satisfy. Higher order solutions can be achieved with fewer variables or functions. This reduces the amount of computing power required. Another benefit, of major importance here, is that thermal stresses are easily included. For these reasons, it was decided to adopt a similar approach for the present work.

3.4 ENERGY METHODS

Detailed explanations of complementary energy methods may be found in Tauchert (1974) and Washizu (1982); only a brief overview is given here.

The stress condition in a body is found by making use of the principle of minimum complementary energy.

> The Principle of minimum complementary energy states that "*Of all states of stress which satisfy the equations of equilibrium, the correct state is that which makes the total complementary energy of the structure a minimum*"

Strain energy density, U, is usually defined as the work stored, per unit volume, in the body when a stress causes a strain. This quantity is given by

$$U = \int_0^{\varepsilon} \sigma \, d\varepsilon \qquad (3.8)$$

The *complementary energy density*, U^*, may be determined from

$$U^* = \int_0^{\sigma} \varepsilon \, d\sigma \qquad (3.9)$$

In order to extend the energy definitions to include thermoelastic strain, it is necessary to generalise equations (3.8) and (3.9). Strain energy is defined as the energy associated with stressing only. Thus, if ε'' is the strain induced by a temperature change, ε' the strain due to stress σ and ε is the total strain then eqn (3.8) becomes

$$U = \int_0^{\varepsilon} \sigma \, d\varepsilon' - \int_0^{\varepsilon} \sigma \, d\varepsilon'' \tag{3.10}$$

and the corresponding complementary energy is defined by

$$U^* = \int_0^{\sigma} \varepsilon' \, d\sigma + \int_0^{\sigma} \varepsilon'' \, d\sigma \tag{3.10}$$

These quantities are shown in diagramatic form in Fig. 3.6.

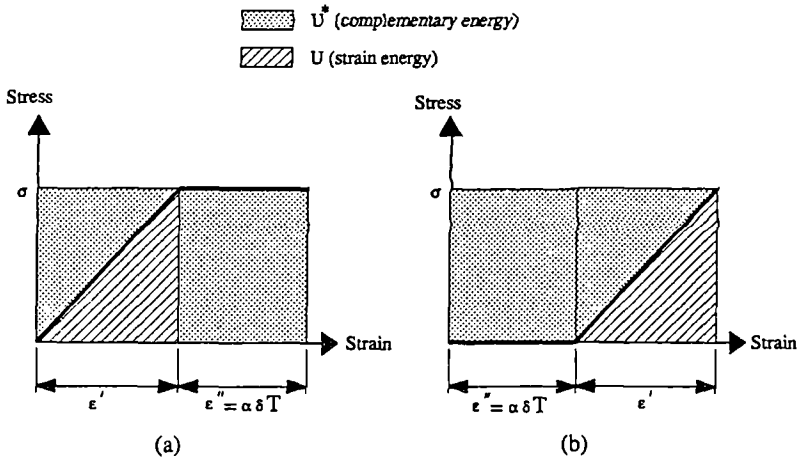

Fig. 3.6 *Stress strain curve for a body subjected to (a) a load followed by temperature rise and (b) temperature rise then load.*

In the present work, it is necessary to determine some unknown stress functions for a joint. This is achieved by developing an expression for the complementary energy of the joint in terms of the unknown stress functions. Then, applying the principal of minimum complementary energy yields the stress functions.

3.4.1 Model: Basic considerations

The single lap joint (SLJ) is assumed to be in equilibrium with the edge loadings as shown in Fig. 3.7. Since the joint width is large it is reasonable to assume conditions of plane strain.

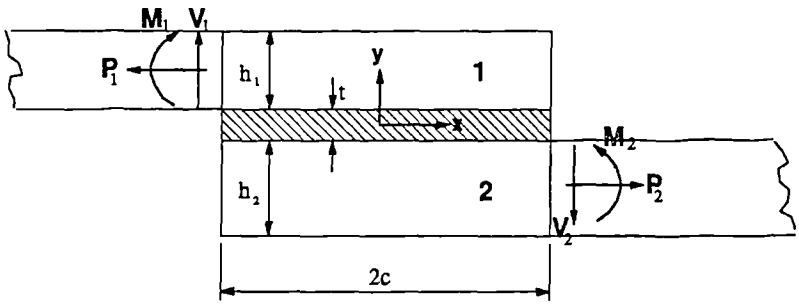

Fig. 3.7 *Loads at the overlap edges of a single lap joint.*

Therefore, the problem is reduced to one of two dimensional elasticity where the distributions of longitudinal (σ_x), peel (σ_y) and shear (τ_{xy}) stresses need to be determined for each layer. The main simplification to be made is that σ_x in the adherends varies linearly in the transverse coordinate y. This is consistent with the classical beam-plate theory of bending and allows the stress field in an adherend to be described by two independent functions of x. The same cannot be said for σ_x in the adhesive. Through thickness variations of the three stresses at the joint edge were shown earlier in Fig. 2.15. Since the edge region is critical, it is vital that the distributions assumed are accurate there. Thus, the lowest order of variations one could assume would be quadratic shear, quadratic peel and cubic longitudinal stresses. These assumptions can be satisfied by using at least three stress functions in the adhesive.

Therefore, a minimum of seven independent functions (two for each adherend and three for adhesive) are needed to describe the stress field in the joint. It can be shown that this reduces to five functions by satisfying adhesive/adherend interface conditions. Since it was not possible to find a solution for these functions using known closed form methods, a numerical solution had to be attempted. In formulating the numerical scheme it soon became evident that it could not be solved on a desktop computer. However, a solution based on four functions could be solved. In order to have a four function solution it is necessary to make a simplification regarding the stresses in the adhesive layer. If one of the adhesive stresses (σ_{xa}, σ_{ya} or τ_{xya}) is assumed to vary linearly across the thickness, then a four function solution is possible. It was decided to assume linear

longitudinal stress, even though its variation is of the highest order, because it is the shear and peel stresses which have the largest influence on joint strength.

Having made the basic assumption that variation of the longitudinal stress in all three layers of the joint is linear in the y direction, the stress distributions were found in the manner described below.

3.4.2 Formulation

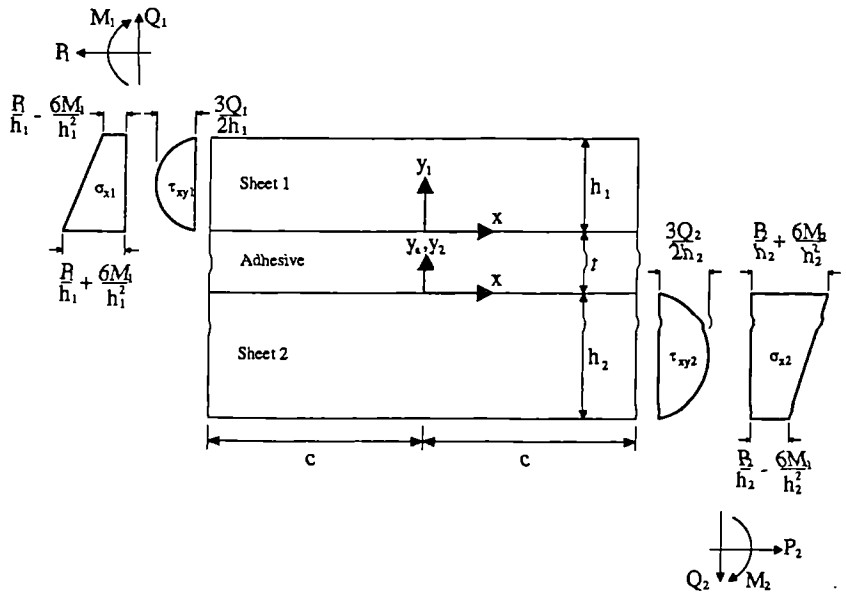

Fig. 3.8 *Mathematical representation of a single lap joint and its boundary conditions*

The joint geometry and boundary conditions are shown in Fig. 3.8. The x origin is located at the centre of the joint and is common for all layers. P, Q and M are the tensile load, shear load and bending moment per unit applied load respectively. The coordinates y_1, y_2, y_a and stress components (σ_{x1}, σ_{y1}, τ_{xy1}), (σ_{x2}, σ_{y2}, τ_{xy2}), (σ_{xa}, σ_{ya}, τ_{xya}) refer to the upper adherend, lower adherend and adhesive respectively. According to the theory of two dimensional elasticity the stress distributions must satisfy the equations of equilibrium (2.15), repeated here:

$$\frac{\partial \sigma_x}{\partial x} + \frac{\partial \tau_{xy}}{\partial y} = 0 \qquad (3.11a)$$

$$\frac{\partial \sigma_y}{\partial y} + \frac{\partial \tau_{xy}}{\partial x} = 0 \qquad (3.11b)$$

Let us consider the upper adherend first. If the longitudinal stress, σ_{x1}, varies linearly in the y direction then it can be expressed as

$$\sigma_{x1} = \phi_{11}(x) + \phi_{21}(x) \frac{y_1}{h_1} \tag{3.12}$$

h_1 is introduced in order to reduce numerical error. Since $\phi_{11}(x)$ and $\phi_{21}(x)$ are functions of the x coordinate only, notation will be made more concise by dropping the (x) and writing ϕ_{11} and ϕ_{21} instead. Substituting the boundary condition, for all y,

$$\sigma_{x1} \Big|_{x=c} = 0$$

into eqn (3.12) gives the following boundary values for the stress functions ϕ_{11} and ϕ_{21}:

$$\phi_{11} \Big|_{x=c} = 0 \tag{3.13a}$$

$$\phi_{21} \Big|_{x=c} = 0 \tag{3.13b}$$

At the opposite end of the joint, the boundary conditions

$$\sigma_{x1} \Big|_{\substack{y=0 \\ x=-c}} = \frac{P_1}{h_1} + \frac{6M_1}{h_1^2}$$

$$\sigma_{x1} \Big|_{\substack{y=h_1 \\ x=-c}} = \frac{P_1}{h_1} - \frac{6M_1}{h_1^2}$$

when substituted into eqn (3.12) gives

$$\phi_{11} \Big|_{x=-c} = \frac{P_1}{h_1} + \frac{6M_1}{h_1^2} \tag{3.13c}$$

$$\phi_{21} \Big|_{x=-c} = \frac{-12M_1}{h_1^2} \tag{3.13d}$$

Differentiating eqn (3.12) with respect to x and substituting the result into eqn (3.11a) we get

$$\frac{\partial \tau_{xy1}}{\partial y_1} = -\phi'_{11} - \phi'_{21} \frac{y_1}{h_1}$$

Integrating this and using the boundary condition, for all x,

$$\tau_{xy1}\Big|^{y_1=h_1} = 0$$

gives the following expression for the shear stress in the upper adherend:

$$\tau_{xy1} = \phi'_{11}(h_1-y_1) + \phi'_{21}\left[\frac{h_1}{2} - \frac{y_1^2}{2h_1}\right] \tag{3.14}$$

When the shear stress boundary conditions

$$\tau_{xy1}\Big|_{x=c} = 0$$

$$\tau_{xy1}\Big|_{x=-c}^{y=0} = 0$$

$$\tau_{xy1}\Big|_{x=-c}^{y=h_1/2} = \frac{-3Q_1}{2h_1}$$

are substituted into eqn (3.14), the boundary values for the first derivatives of the stress functions are found to be, for all y:

$$\phi'_{11}\Big|_{x=c} = 0 \tag{3.15a}$$

$$\phi'_{21}\Big|_{x=c} = 0 \tag{3.15b}$$

$$\phi'_{11}\Big|_{x=-c} = \frac{6Q_1}{h_1^2} \tag{3.15c}$$

$$\phi'_{21}\Big|_{x=-c} = \frac{-12Q_1}{h_1^2} \tag{3.15d}$$

By substituting eqn (3.14) into the second equilibrium eqn (3.11b), then integrating and using the boundary condition, for all x

$$\sigma_{y1}\Big|^{y_1=h_1} = 0$$

the peel stress is obtained as:

$$\sigma_{y1} = \phi''_{11}\left[\frac{y_1^2}{2} - h_1y_1 + \frac{h_1^2}{2}\right] + \phi''_{21}\left[\frac{y_1^3}{6h_1} - \frac{h_1y_1}{2} + \frac{h_1^2}{3}\right] \tag{3.16}$$

Similarly, for the lower adherend the stresses are

$$\sigma_{x2} = \phi_{12} + \phi_{22} \frac{y_2}{h_2} \tag{3.17}$$

$$\sigma_{y2} = \phi''_{12} \left[\frac{y_2^2}{2} + h_2 y_2 + \frac{h_2^2}{2} \right] + \phi''_{22} \left[\frac{y_2^3}{6h_2} - \frac{h_2 y_2}{2} + \frac{h_2^2}{3} \right] \tag{3.18}$$

$$\tau_{xy2} = \phi'_{12}(-h_2 - y_2) + \phi'_{22} \left[\frac{h_2}{2} - \frac{y_2^2}{2h_2} \right] \tag{3.19}$$

The boundary values of the stress functions ϕ_{12} and ϕ_{22} are

$$\phi_{12}\Big|_{x=-c} = 0 \tag{3.20a}$$

$$\phi_{22}\Big|_{x=-c} = 0 \tag{3.20b}$$

$$\phi_{12}\Big|_{x=c} = \frac{P_2}{h_2} + \frac{6M_2}{h_2^2} \tag{3.20c}$$

$$\phi_{22}\Big|_{x=c} = \frac{12M_2}{h_2^2} \tag{3.20d}$$

and for the first derivatives

$$\phi'_{12}\Big|_{x=c} = \frac{-6Q_2}{h_2^2} \tag{3.21a}$$

$$\phi'_{22}\Big|_{x=c} = \frac{-12Q_2}{h_2^2} \tag{3.21b}$$

$$\phi'_{12}\Big|_{x=-c} = 0 \tag{3.21c}$$

$$\phi'_{22}\Big|_{x=-c} = 0 \tag{3.21d}$$

In the adhesive, for reasons given in section 3.4.1, the longitudinal stress is assumed to vary linearly with y giving

$$\sigma_{xa} = \phi_{1a} + \phi_{2a} \frac{y_a}{t} \tag{3.22}$$

Now, for all y,

$$\sigma_{xa}\Big|_{x=\pm c} = 0$$

therefore

$$\phi_{1a}\Big|_{x=\pm c} = 0 \tag{3.23a}$$

$$\phi_{2a}\Big|_{x=\pm c} = 0 \tag{3.23b}$$

Substituting eqn (3.22) into equilibrium eqn (3.11a) and integrating with respect to y we get

$$\tau_{xya} = -\phi'_{1a} y_a + \phi'_{2a} \frac{y_a^2}{2t} + f_1 \tag{3.24}$$

where f_1 is a function of x arising from the integration. The shear stress in the upper adherend and adhesive must be equal at the interface, for all x:

$$\tau_{xya}\Big|_{y_a=t} = \tau_{xy1}\Big|_{y_1=0}$$

Therefore we can set $y_a=t$ in eqn (3.24) and $y_1=0$ in eqn (3.14) and equate the resulting expressions to give

$$f_1 = \phi'_{11} h_1 + \frac{\phi'_{21} h_1}{2} + \phi'_{1a} t + \frac{\phi'_{2a} t}{2} \tag{3.25}$$

Alternatively, we could have equated the shear stresses at the other interface:

$$\tau_{xya}\Big|_{y_a=0} = \tau_{xy2}\Big|_{y_2=0}$$

This results in the following expression for f_1:

$$f_1 = -\phi'_{12} h_2 + \phi'_{22} \frac{h_2}{2} \tag{3.26}$$

Equating the right hand sides of eqns (3.25) and (3.26) then integrating, we have

$$-\frac{\phi_{22} h_2}{2} + \phi_{12} h_2 + \phi_{11} h_1 + \frac{\phi_{21} h_1}{2} + \phi_{1a} t + \frac{\phi_{2a} t}{2} = k_1 \tag{3.27}$$

where k_1 is a constant of integration. Substituting the boundary values at x = c, (3.13a & b), (3.20a & b) and (3.23a & b), into eqn (3.27) gives $k_1 = P_1$ while substitution of conditions at x = -c, (3.13c & d), (3.20c & d) and (3.23a & b), gives $k_1 = P_2$. Therefore the constraint

$$k_1 = P_1 = P_2 \tag{3.28}$$

is imposed on the system. In other words the x forces should be in equilibrium. Therefore we can write P for both P_1 and P_2.

Substituting eqn (3.24) into equilibrium eqn (3.11b) and integrating with respect to y, we get

$$\sigma_{ya} = \phi_{1a}'' \frac{y_a^2}{2} + \phi_{2a}'' \frac{y_a^3}{6t} - f_1' y_a + f_2 \tag{3.29}$$

where f_2 is a function of x arising from the integration. Analogous to the shear stress, the peel stress at the adherend-adhesive interfaces must be equal, therefore, for all x,

$$\sigma_{ya}\Big|^{y_a=t} = \sigma_{y1}\Big|^{y_1=0}$$

$$\sigma_{ya}\Big|^{y_a=0} = \sigma_{y2}\Big|^{y_2=h_2}$$

From these conditions the following two expressions for f_2 may be derived:

$$f_2 = \frac{\phi''_{12}h_2^2}{2} - \frac{\phi''_{22}h_2^2}{2} \tag{3.30}$$

$$f_2 = \frac{\phi''_{11}h_1^2}{2} + \frac{\phi''_{21}h_1^2}{3} - \frac{\phi''_{1a}t^2}{2} - \frac{\phi''_{2a}t^2}{6} + f_3' t \tag{3.31}$$

Substituting eqn (3.30) into eqn (3.31) and then integrating gives

$$\frac{\phi'_{11}h_1^2}{2} + \frac{\phi'_{21}h_1^2}{3} - \frac{\phi'_{1a}t^2}{2} - \frac{\phi'_{2a}t^2}{6} + f_1 t - \frac{\phi'_{12}h_2^2}{2} + \frac{\phi'_{22}h_2^2}{3} = k_2 \tag{3.32}$$

where k_2 is a constant of integration. Using the boundary conditions at $x = \pm c$, (3.15) and (3.21), and the fact that τ_{xya} in eqn (3.24) is equal to zero at these points we find that

$$k_2 = Q_1 = Q_2 \tag{3.33}$$

This constraint imposes equilibrium in the y direction, and we can replace Q_1 and Q_2 with Q.

Integrating eqn (3.32) gives

$$\frac{\phi_{11}h_1^2}{2} + \frac{\phi_{21}h_1^2}{3} - \frac{\phi_{1a}t^2}{2} - \frac{\phi_{2a}t^2}{6} - \phi_{21}h_2t + \frac{\phi_{12}h_2}{2} - \frac{\phi_{21}h_2^2}{2} + \frac{\phi_{12}h_2^2}{3} = Qx + k_3 \tag{3.35}$$

The constant of integration, k_3, is determined by considering the boundary values of the stress functions at $x = \pm c$ in a manner similar to that employed in finding k_1 and k_2. The value k_3 is then found to be:

$$k_3 = \frac{Ph_1}{2} - M_1 - Qc$$

or $$k_3 = \frac{-Ph_2}{2} + M_2 - Pt - Qc$$

If the right hand sides of the two expressions for k_3 are equated, then we have the following condition which ensures moment equilibrium:

$$Q = \frac{P}{4c}(h_1+h_2+2t) - \frac{1}{2c}(M_1+M_2) \tag{3.36}$$

This, together with constraints (3.28) and (3.33), ensures that the joint is in a state of static equilibrium.

Eqns (3.27) and (3.35) can be viewed as two simultaneous equations of ϕ_{1a} and ϕ_{2a} in terms of the other stress functions. Solving for ϕ_{1a} and ϕ_{2a} we get

$$\phi_{1a} = [A_1]^T\{\Phi\} \tag{3.37a}$$

and $$\phi_{2a} = [A_2]^T\{\Phi\} \tag{3.37b}$$

where $\{\Phi\} = \{\phi_{11}\ \phi_{21}\ \phi_{12}\ \phi_{22}\ x\ 1\}^T$,

$$[A_1] = \frac{1}{t^2}\begin{bmatrix} 2h_1t + 3h_1^2 \\ h_1t + 2h_1^2 \\ -4h_2t - 3h_2^2 \\ 2h_2t + 2h_2^2 \\ -6P \\ -2Qt - 6k_3 \end{bmatrix} \qquad [A_2] = \frac{1}{t^2}\begin{bmatrix} -6h_1t - 6h_1^2 \\ -3h_1t - 4h_1^2 \\ 6h_2t + 6h_1^2 \\ -3h_2t - 4h_2^2 \\ 12P \\ 6Qt + 12k_3 \end{bmatrix}$$

The formulation is now complete. The joint stresses have been defined in terms of four independent functions (ϕ_{11}, ϕ_{21}, ϕ_{12} and ϕ_{22}) as opposed to the two functions used by Allman (1977) and Chen and Cheng (1983). The next, and final stage, of the solution procedure is to determine these functions. This can be achieved by defining the complementary energy in terms of the stress functions. Then minimisation of the energy function will yield the stress functions. Unfortunately, a closed form solution is very difficult, if not impossible, since four coupled fourth order differential equations need to be solved. Therefore a numerical solution has been sought.

3.4.3 **Numerical solution**

As advocated by Allman (1977), the present formulation is well suited to a finite element solution. Allman has suggested a solution procedure based on an equilibrium FEM. A similar approach has been adopted here.

For a body in plane strain,

$$\{\sigma\} = [D]\ \{\varepsilon - \varepsilon_t\} \tag{3.38}$$

where

$$\{\sigma\} = \begin{Bmatrix} \sigma_x \\ \sigma_y \\ \tau_{xy} \end{Bmatrix} \qquad \{\varepsilon\} = \begin{Bmatrix} \varepsilon_x \\ \varepsilon_y \\ \gamma_{xy} \end{Bmatrix}$$

and $\{\varepsilon_t\}$ is the thermal strain array:

$$\begin{Bmatrix} (1+\nu)\alpha\Delta T \\ (1+\nu)\alpha\Delta T \\ 0 \end{Bmatrix}$$

If the material is *linearly elastic* then [D] is the plane strain modulus array.

Substituting eqn (3.38) into eqn (3.9) gives the complementary energy as

$$U^* = \frac{1}{2} \int_v \{\sigma\}^T [D]^{-1} \{\sigma\} \, dv + \int_v \{\sigma\}^T \{\varepsilon_t\} \, dv \tag{3.39}$$

Remembering that for the joint $\{\sigma\} = \{\sigma_{x1} \; \sigma_{y1} \; \tau_{xy1} \; \sigma_{xa} \; \sigma_{ya} \; \tau_{xya} \; \sigma_{x2} \; \sigma_{y2} \; \tau_{xy2}\}^T$, we can use eqns (3.12), (3.14), (3.16) to find arrays [N] and $\{C(x)\}$ such that

$$\{\sigma\} = [N]\{\Phi\} + \{C(x)\} + \{k\} \tag{3.40}$$

where

$\{\Phi\} = \{\phi_{11} \; \phi'_{11} \; \phi''_{11} \; \phi_{21} \; \phi'_{21} \; \phi''_{21} \; \phi_{12} \; \phi'_{12} \; \phi''_{12} \; \phi_{22} \; \phi'_{22} \; \phi''_{22}\}^T$,

$\{C(x)\}$ is an [9×1] array of functions of x which are known,

and $\{k\}$ is an array of constants derived from the joint geometry and loading. Now consider the joint divided into a number of finite elements of the type shown Fig. 3.9.

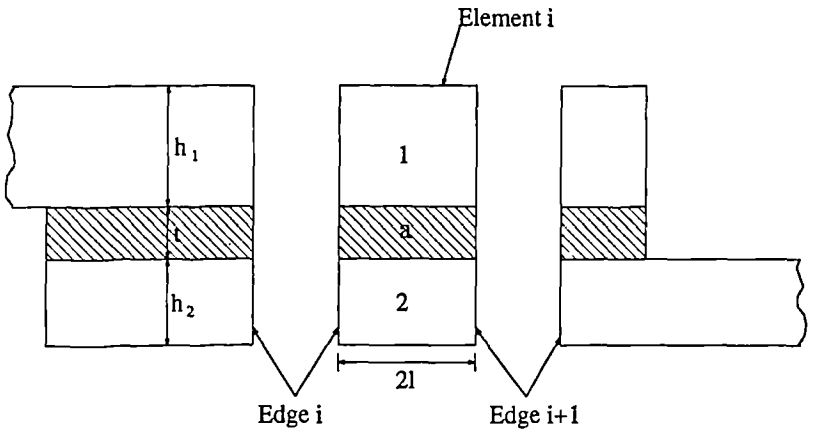

Fig. 3.9 *A finite element*

In this element, the edges can be viewed as a nodes and the degrees of freedom are the stress functions and their first derivatives. Thus each element consists of two nodes and sixteen degrees of freedom. If $\{\phi\}$ is the array of the stress functions and their first derivatives for an element with end nodes (i) and (i+1) then:

$$\{\phi\} = \{\phi_{11}^{(i)} \; \phi'_{11}^{(i)} \; \phi_{21}^{(i)} \; \phi'_{21}^{(i)} \ldots\ldots \phi_{22}^{(i+1)} \; \phi'_{22}^{(i+1)}\}_{16\times1}$$

Then we can define a shape function array [B] (see Appendix II) such that

$$\{\Phi\} = [\mathbf{B}]\{\phi\} \tag{3.41}$$

Substitution of eqns (3.40) and (3.41) into eqn (3.39) results in the following expression for the complementary energy for an element:

$$U^{*(e)} = \frac{1}{2} \{\phi\}^T[\mathbf{F}]\{\phi\} - \{\phi\}^T[\mathbf{H}] + \text{constant}$$

If the joint is assumed to have unit width, then for each element

$$[\mathbf{F}] = \int\int \frac{1}{2}([\mathbf{B}]^T[\mathbf{N}]^T[\mathbf{D}]^{-1}[\mathbf{N}][\mathbf{B}])\, dxdy$$

$$[\mathbf{H}] = \int\int -([\mathbf{B}]^T[\mathbf{N}]^T[\mathbf{D}]^{-1}\{\mathbf{C}(x)\} + [\mathbf{B}]^T[\mathbf{N}]^T\{\varepsilon_t\})\, dxdy$$

Here [D] is a [9x9] matrix and is the elastic modulus for the whole joint. The integration is taken over the whole are of the element. Appendix III details matrices [D], [F] and [H] for the general case of a single lap joint with transversely isotropic adherends.

The total joint complementary energy is obtained by summing elemental contributions according to well known structural analysis matrix methods. Thus, the joint complementary energy is

$$U^* = \frac{1}{2} \{\underline{\phi}\}^T[\underline{\mathbf{F}}]\{\underline{\phi}\} + \{\underline{\phi}\}^T[\underline{\mathbf{H}}] + \text{constant} \tag{3.42}$$

where $\{\underline{\phi}\}$, $[\underline{\mathbf{F}}]$, and $[\underline{\mathbf{H}}]$ are global matrices. The complementary energy, U^*, is minimised when

$$[\underline{\mathbf{F}}]\{\underline{\phi}\} = [\underline{\mathbf{H}}] \tag{3.43}$$

This is a set of linear equations which can be solved, using standard matrix methods (Bathe and Wilson, 1976), to give the $\{\underline{\phi}\}$ vector. For a solution to exist, $[\underline{\mathbf{F}}]$ must be a positive definite matrix. This is achieved by applying the boundary conditions (3.13), (3.15), (3.20) and (3.21) to eqn (3.43). Once $\{\underline{\phi}\}$ has been obtained, the stress function at any point in the joint is determined from eqn (3.41). Finally, the stress distribution is calculated from eqns (3.12), (3.14), (3.16-3.19), (3.22), (3.24) and (3.29).

3.4.4 The Double lap joint

A double lap joint (DLJ) is illustrated in Fig. 3.10. In the present work, mid-plane symmetry will be assumed, so we need only consider one half of the joint. The DLJ differs from the SLJ in two fundamental ways. First of all, there is no *external* bending moment in the DLJ since it does not rotate like the SLJ. Secondly, due to symmetry, there is no net shear or peel force in the mid-adherend.

The formulation is similar to the SLJ case. Once again we place the x origin at the centre of the joint (Fig. 3.10). The coordinates y_1, y_2, y_a and stress components (σ_{x1}, σ_{y1}, τ_{xy1}), (σ_{x2}, σ_{y2}, τ_{xy2}), (σ_{xa}, σ_{ya}, τ_{xya}) refer to the upper adherend, lower adherend and adhesive respectively.

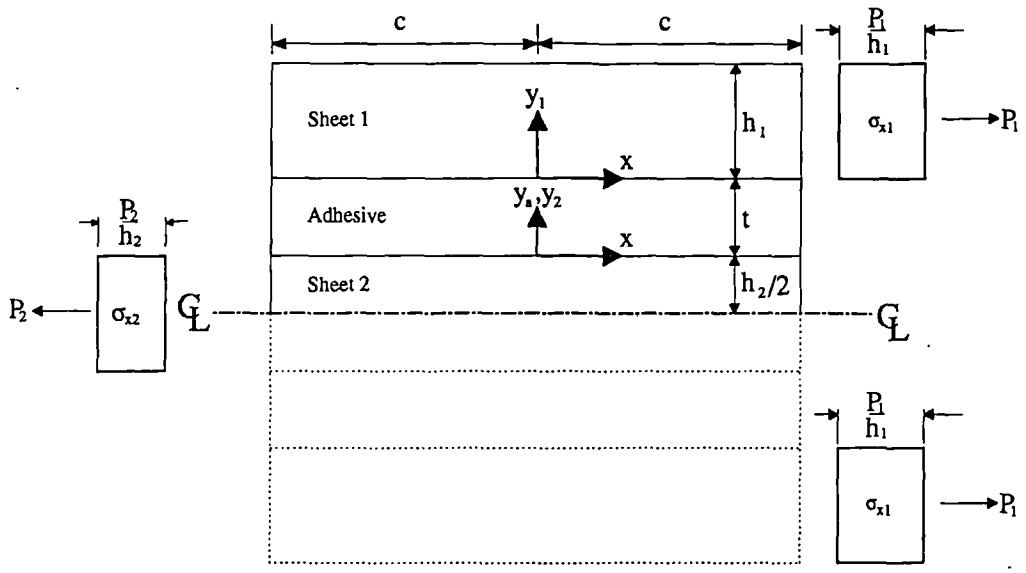

Fig. 3.10 *Mathematical representation of a double lap joint and its boundary conditions*

Employing the same arguments as we did for the SLJ, we find that the stress distribution in the upper adherend in the DLJ are given by

$$\sigma_{x1} = \phi_{11}(x) + \phi_{21}(x)\,\frac{y_1}{h_1} \tag{3.44}$$

$$\tau_{xy1} = \phi'_{11}(h_1 - y_1) + \phi'_{21}\left[\frac{h_1}{2} - \frac{y_1^2}{2h_1}\right] \tag{3.45}$$

$$\sigma_{y1} = \phi''_{11}\left[\frac{y_1^2}{2} - h_1 y_1 + \frac{h_1^2}{2}\right] + \phi''_{21}\left[\frac{y_1^3}{6h_1} - \frac{h_1 y_1}{2} + \frac{h_1^2}{3}\right] \tag{3.46}$$

and the edge boundary conditions are

$$\begin{bmatrix} \phi_{11} \\ \phi'_{11} \\ \phi_{21} \\ \phi'_{21} \end{bmatrix}_{x=c} = \begin{bmatrix} T_1/h_1 \\ 0 \\ 0 \\ 0 \end{bmatrix} \tag{3.47a}$$

$$\begin{bmatrix} \phi_{11} \\ \phi'_{11} \\ \phi_{21} \\ \phi'_{21} \end{bmatrix}_{x=-c} = \begin{bmatrix} 0 \\ 0 \\ 0 \\ 0 \end{bmatrix} \tag{3.47b}$$

Turning our attention to the lower adherend, let us begin with the usual assumption that the longitudinal stress is

$$\sigma_{x2} = \phi_{12} + \phi_{22}\frac{y_2}{h_2} \tag{3.48}$$

In this sheet there is no net applied bending moment, thus

$$\int_{-h_2/2}^{h_2/2} \sigma_{x2}\, y_2\, dy_2 = 0$$

Substituting eqn (3.48) into this condition we find that

$$\phi_{22} = 0$$

Therefore

$$\sigma_{x2} = \phi_{12}\frac{y_2}{h_2} \tag{3.49}$$

Substituting eqn (3.49) into the first equilibrium eqn (3.11a) and then integrating we have

$$\tau_{xy2} = -\phi_{12}' y_2 + g_1$$

where g_1 is a function of x. However, $g_1 = 0$ if there is no net shear force in the y direction. So, we have

$$\tau_{xy2} = - \phi'_{12}\, y_2 \tag{3.50}$$

Substituting eqn (3.50) into the second equilibrium eqn (3.11b) gives

$$\sigma_{y2} = \phi''_{12} \frac{y_2^2}{2} + g_2 \tag{3.51}$$

where g_2 is a function of x.

In the adhesive,

$$\sigma_{xa} = \phi_{1a} + \phi_{2a} \frac{y_a}{t} \tag{3.52}$$

When eqn (3.52) is substituted into equilibrium eqn (3.11a), we get the following expression for the shear stress:

$$\tau_{xya} = - \phi'_{1a} y_a - \phi'_{2a} \frac{y_a^2}{2t} + g_3 \tag{3.53}$$

Substitution of eqn (3.53) into equilibrium eqn (3.11b) gives

$$\sigma_{ya} = \phi''_{1a} \frac{y_a^2}{2} + \phi''_{2a} \frac{y_a^3}{6t} - g_3' y_a + g_4 \tag{3.54}$$

where g_3 and g_4 are functions of x.

In order to satisfy the edge conditions, the values of the stress functions, at these points must be:

$$\begin{bmatrix} \phi_{12} \\ \phi'_{12} \\ \phi_{1a} \\ \phi'_{1a} \\ \phi_{2a} \\ \phi'_{2a} \end{bmatrix}_{x=c} = \begin{bmatrix} 0 \\ 0 \\ 0 \\ 0 \\ 0 \\ 0 \end{bmatrix} \tag{3.55a}$$

$$\begin{bmatrix} \phi_{12} \\ \phi'_{12} \\ \phi_{1a} \\ \phi'_{1a} \\ \phi_{2a} \\ \phi'_{2a} \end{bmatrix}_{x=-c} = \begin{bmatrix} P_2/h_2 \\ 0 \\ 0 \\ 0 \\ 0 \\ 0 \end{bmatrix} \qquad (3.55b)$$

From the two interface conditions, for all x,

$$\tau_{ya}\Big|_{y_a=t} = \tau_{y1}\Big|_{y_1=0}$$

$$\tau_{ya}\Big|_{y_a=0} = \tau_{y2}\Big|_{y_2=h_2/2}$$

we have the following expressions for g_3:

$$g_3 = -\phi'_{12}h_2/2$$

$$g_3 = \phi'_{11}h_1 + \frac{\phi'_{21}h_1}{2} + \phi'_{1a}t + \frac{\phi'_{2a}t}{2}$$

Equating the right hand sides of these expressions and then integrating we get

$$\phi_{11}h_1 + \frac{\phi_{21}h_1}{2} + \phi_{1a}t + \frac{\phi_{2a}t}{2} + \frac{\phi_{12}h_2}{2} - k = 0 \qquad (3.56)$$

Applying the stress function boundary values (3.47) we get $k = P_1$ while (3.55) gives $k = P_2/2$. Therefore $2P_1 = P_2$, and static equilibrium is satisfied. We can re-arrange eqn (3.56) to express ϕ_{12} in terms of the other functions. This means that the entire stress condition can now be described in terms of four independent stress functions: ϕ_{11}, ϕ_{21}, ϕ_{1a}, ϕ_{2a}.

These can be solved numerically employing an identical procedure to that outlined in the previous section (3.4.3). The [F] and [H] matrices for the double lap joint are given in Appendix III.

3.5 DETAILS OF COMPUTER PROGRAM

A computer program for a desktop PC, JOINT, has been developed to implement the numerical solution described above. The program has been written in MODULA-2 and the main subroutine is listed below.

```
BEGIN
   DataIn; (* Reads joint data and generates coarse mesh *)
   SetLoad; (* Shear forces and bending moment calculated for a SLJ *)
   UpdateSystem; (* Global arrays [F] and [H] calculated and b.c.'s applied *)
   Solve; (* System equation {φ^e} = [F]^-1[H] is solved by Gaussian elimination *)

   NewMesh; (* A better mesh is generated from the solution *)
   UpdateSystem; (* [F] and [H] re-calulated and b.c.'s applied *)
   Solve;

   CalcFields; (* The stresses are found according to {σ} = [B][N]{φ^e} + {C(x)} *)
   Output; (* Results are output *)
END.
```

One objective of the present theory was to provide an easily accessible means of stress analysis. This feature is evident in JOINT, where the only requirement of the user is a knowledge of the joint geometry and material properties. Unlike FEM, there is no need for the user to consider mesh refinement. The element here is one dimensional and the joint mesh can therefore be automatically generated. Initially, the joint is divided into elements of equal size and a coarse analysis is performed. The mesh is then refined by concentrating elements at regions of maximum work. The implementation allows a maximum of fifty elements although thirty elements were found to be sufficient for most analyses.

Chapter 4

ELASTIC ANALYSIS OF LAP JOINTS SUBJECTED TO THERMAL STRESS

A theory for the elastic stresses in lap joints, introduced in the last chapter, is validated here by comparison with the FEM. Both methods are then used to assess the influence of thermal stresses in load bearing lap joints. The FEM is used to study, in detail, stresses at joint ends while the present theory is used to perform a parametric investigation.

4.1 COMPARISON OF SOLUTION WITH THE FEM

The present theory is applicable for a variety of joint configurations: balanced or unbalanced single or double lap joints. A joint representative of each type of configuration has been analysed. The material and geometric details of these joint are given in Table 4.1. The programs JOINT and FELDEP were used to perform stress analysis according to the theory and the FEM respectively. For the FEM work the mesh shown in Fig. 3.1 has been used.

	JOINT		
	1	**2**	**3**
E_{1x},E_{1y} (GPa)	70,70	70,70	70,70
E_{2x},E_{2y} (GPa)	70,70	200,200	205,7.58
E_a (GPa)	2.8	2.8	2.8
G_1 (GPa)	26.3	26.3	26.3
G_2 (GPa)	26.3	75.2	5.05
ν_{1x},ν_{1y}	0.33,0.33	0.33,0.33	0.33,0.33
ν_{2x},ν_{2y}	0.33,0.33	0.33,0.33	0.03,0.01
ν_a	0.37,0.37	0.37,0.37	0.37
α_1 (10^{-6}/°C)	0	23	23
α_2 (10^{-6}/°C)	0	15	10
α_a (10^{-6}/°C)	0	0	60
t_1 (mm)	1.62	1.62	1.62
t_2 (mm)	1.62	1.62	1.62
t_a (mm)	0.125	0.125	0.125
c (mm)	6.5	6.5	6.5

Table 4.1 *Material and geometric properties of joints analysed.*

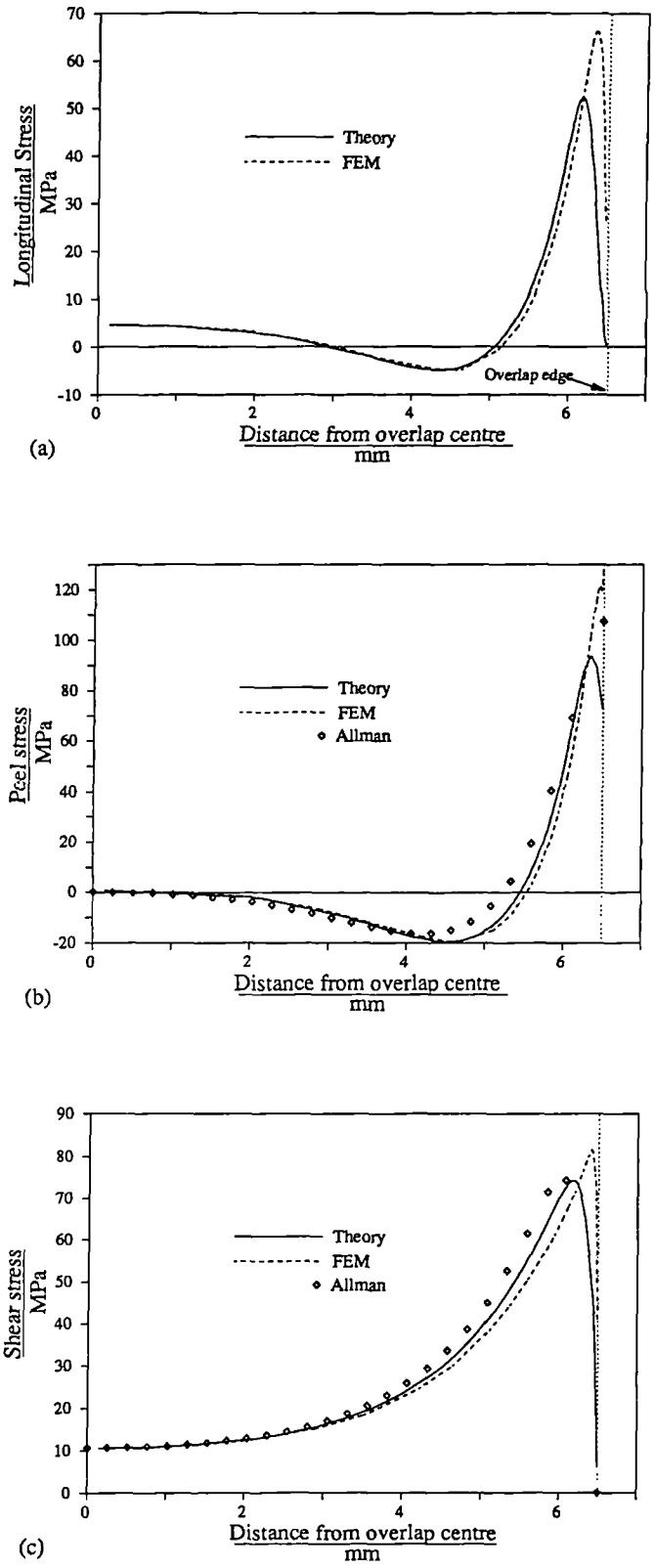

Fig. 4.1 *The (a) longitudinal, (b) peel and (c) shear stress distributions in an Al-Al balanced joint subjected to a load of 8.5 kN.*

4.1.1 Balanced single lap joint

The properties of the balanced single lap joint analysed are listed in Table 4.1 under JOINT-1. For the theoretical solution, edge bending moments were calculated according to Hart-Smith's bending moment factor (eqn 2.21). The corresponding shear forces were calculated according to eqn (3.36).

The theoretical and FEM stress predictions are plotted in Fig 4.1. To allow comparison, the distributions have been averaged across the adhesive thickness. Also included are results from a program implementing Allman's solution. The present theory agrees well with the FEM except at the very ends where the FEM shear and longitudinal stress peaks are higher and closer to the edges. The difference is because, in the theoretical model, constraints were imposed on the variation of stresses in the transverse direction (section 3.4.1). Further constraints occur at the edge of the overlap where the boundary conditions were also imposed. The net effect of these constraints seems to be a prevention of the high stresses which are found at the corners of the adhesive with FEM.

In comparison with Allman's solution, the present method is in better agreement with FEM distributions. This may be attributed to the thickness variations that are incorporated in the present work.

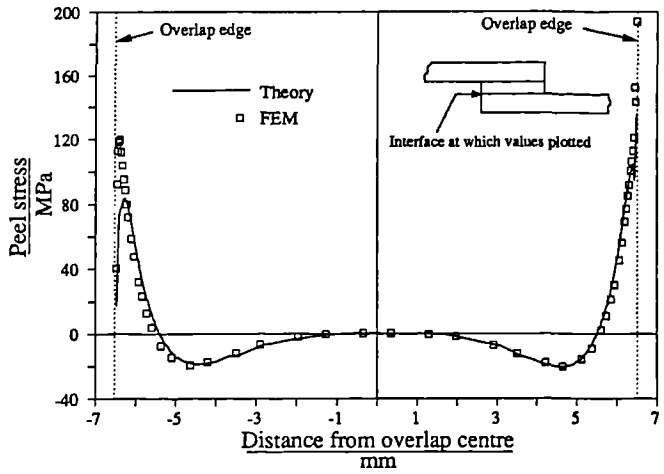

Fig 4.2 *Peel stress at the adherend/adhesive interface*

Contrary to finite element predictions, the theoretical peel stresses fall slightly at the ends. This is one of the dangers in plotting the averaged stresses. Fig. 4.2, a plot of the peel stress at the lower adherend/adhesive

interface, shows that both methods predict stresses falling at the unloaded end. At the other end, the presence of a corner between the adhesive and adherend gives rise to a singularity. FEM results are unreliable at singularity points since the stress peak is entirely dependent on the degree of mesh refinement. In other words, the finer the mesh, the higher the stresses that will be predicted. Therefore it is difficult to draw any conclusion from the difference between the two predictions at the loaded end.

One feature of the present solution is its ability to model through thickness variations. Comparison with FEM is conveniently achieved by plotting the principal stress vectors within the adhesive layer (Fig. 4.3). In this plot the two principal stresses intersect at the Gauss point where they act. Vectors drawn with bars at each end signify a compressive principal stress.

It can be seen that the stress directions predicted by the FEM are less vertical. This is because, close to the edges, the FEM predicts larger shear stresses (see Fig 4.1c). The effect of shear stress on the principal axis is to cause a rotation away from the vertical plane towards a plane at 45° to the x axis.

The theoretical longitudinal stresses, like the shear, are lower at the ends. This would explain why some theoretical principal vectors are compressive, contradicting the FEM. If FEM stresses are drawn ignoring longitudinal stress, then similar compressive vectors occur (Fig. 4.3c). Thus it seems that the theoretical predictions are inaccurate at the very edge. It must be remembered, however, that the plots show details of stresses within a distance, from the joint edge, which is in the order of a glue line thickness, from the edge. Nevertheless, the theoretical vectors suggest a through thickness *variation* similar to the FEM.

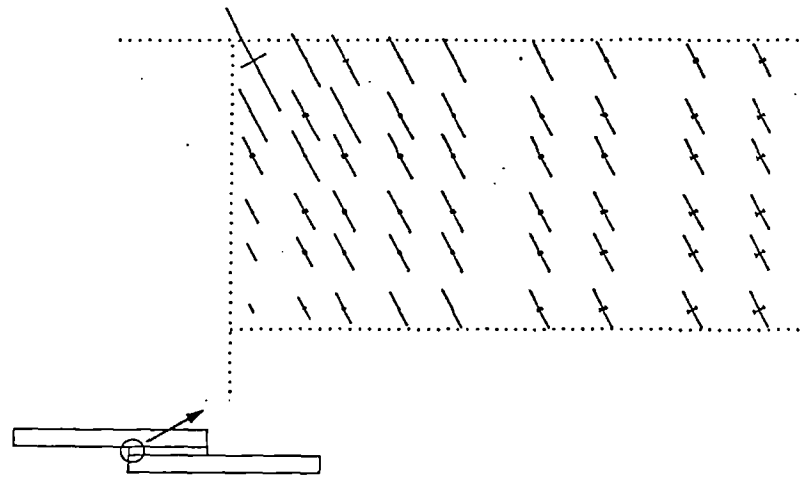

(a)

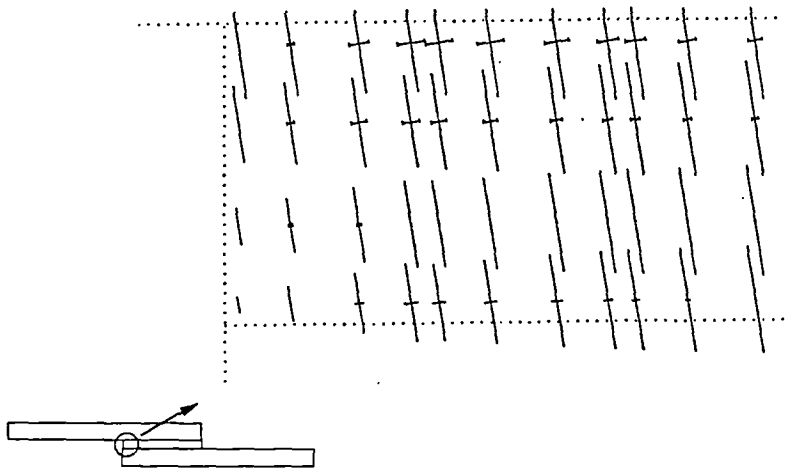

(b)

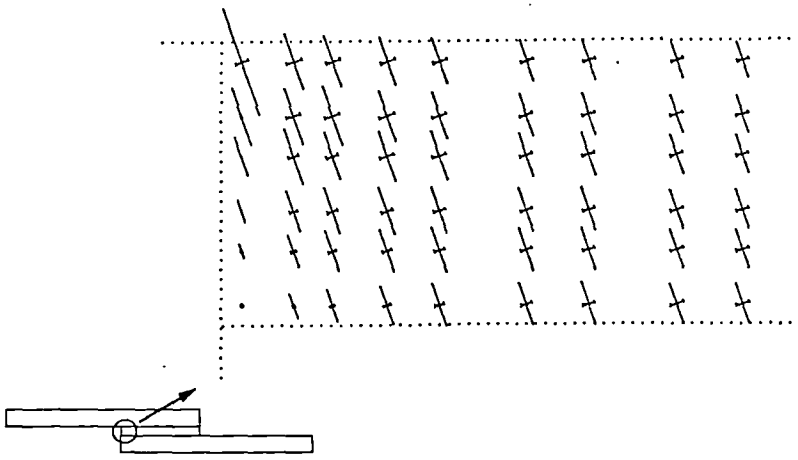

(c)

Fig 4.3 *(a) FEM and (b) theoretical principal stress vectors. (c) FEM vectors when longitudinal stress is ignored*

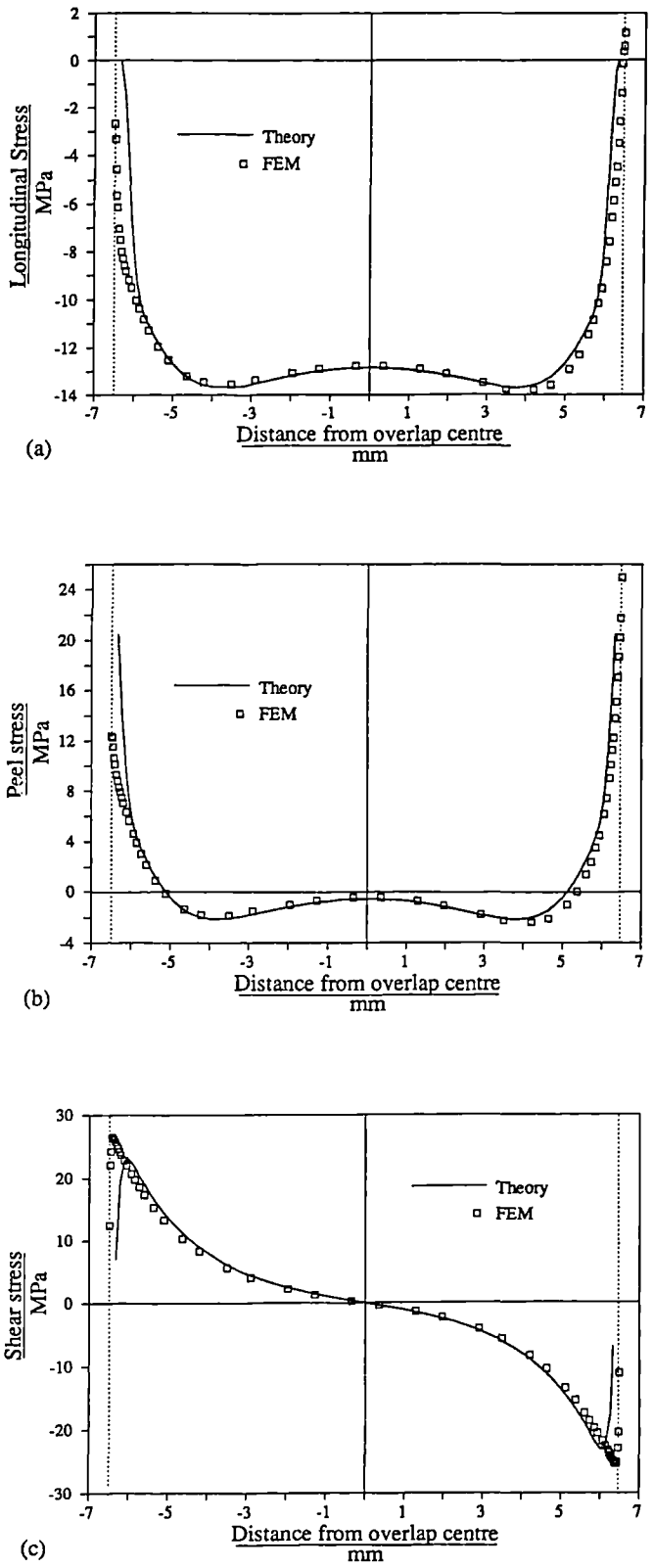

Fig. 4.4 *The (a) longitudinal, (b) peel and (c) shear stress distributions in an Al-Steel joint subjected to ΔT = -150 ℃.*

4.1.2 Thermal mismatch

To test its thermal stress capability, the present theory has been applied to an Aluminium-Steel joint (JOINT-2 in Table 4.1). The stresses due to a temperature drop of 150° are compared with FEM predictions in Fig. 4.4. Clearly, there is good agreement for each stress distribution. As with the balanced joint above, the FEM peaks are higher than the theoretical. Again, this is because the FEM stresses at the singularity points are large, thus distorting the average.

4.1.3 Unbalanced single lap joint

Before the theory can be applied to a load-bearing unbalanced joint, a new expression for the edge bending moment calculation is required. The expressions developed by Goland and Reissner (2.12) and Hart-Smith (2.21) apply to balanced lap joints only. In general, the unbalanced joint will be subjected to unequal bending moments at each end.

Hart-Smith did extend his bending moment factor theory to unbalanced joints. However the result was not an explicit expression but a non-linear equation requiring an iterative solution. The complexities in Hart-Smith's solution arise because the effect of each overlap layer on joint rotation is considered. In contrast, Goland and Reissner treated the overlap as a homogeneous plate. Brooker (1980) extended the latter work for unbalanced joints but did not produce a closed form solution.

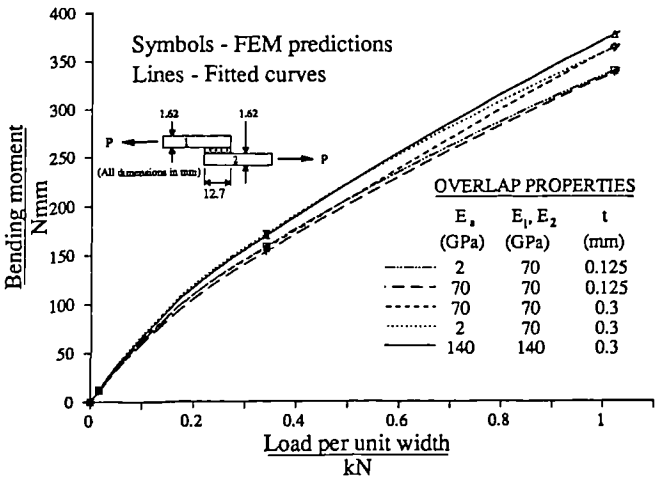

Fig. 4.5 *Bending moments in a balanced single lap joint.*

Fig. 4.5 plots the bending moments, obtained by the FEM, for various overlap properties in a balanced joint under tensile loading. The moments do not seem to be greatly influenced by the adhesive thickness or flexibility and nor does the stiffness of the adherend within the overlap have a significant effect. This suggests that it would be plausible to develop an expression for the bending moment based on the assumption that the overlap region remained rigid during rotation. Adopting this approach Zhao (1989) has obtained the following explicit relationship for the edge bending moments at the left hand side (M_1) and the right hand side (M_2) of the joint:

$$M_1 = \frac{u_2(t_1+t_2)}{2(u_2+u_1u_2l+u_1)} \tag{4.1a}$$

$$M_2 = \frac{u_1(t_1+t_2)}{2(u_2+u_1u_2l+u_1)} \tag{4.1b}$$

where l is the joint overlap, t_1 and t_2 the adherend thicknesses and u_1 and u_2 are the adherend flexural rigidities. Therefore $u_i=\sqrt{\{12P(1-\nu_i^2)/(E_it_i^2)\}}$ for i=1,2.

A comparison of the bending moments in Fig. 4.6 shows that Zhao's expression is in close agreement with the other theories. The results shown here are for an overlap of 12.7mm, but Zhao's results (1989) suggest that the theory is accurate for overlaps up to 50mm.

Consequently, the study of unbalanced joints has been limited to overlaps of less than 50mm. In any case, in long unbalanced joints, there will generally be initial curvature in the overlap due to thermal mismatch. This invalidates the bending moment expressions (4.1), not only because the overlap is now curved but because the adherend length will affect the edge bending moment, as illustrated in Fig. 4.7.

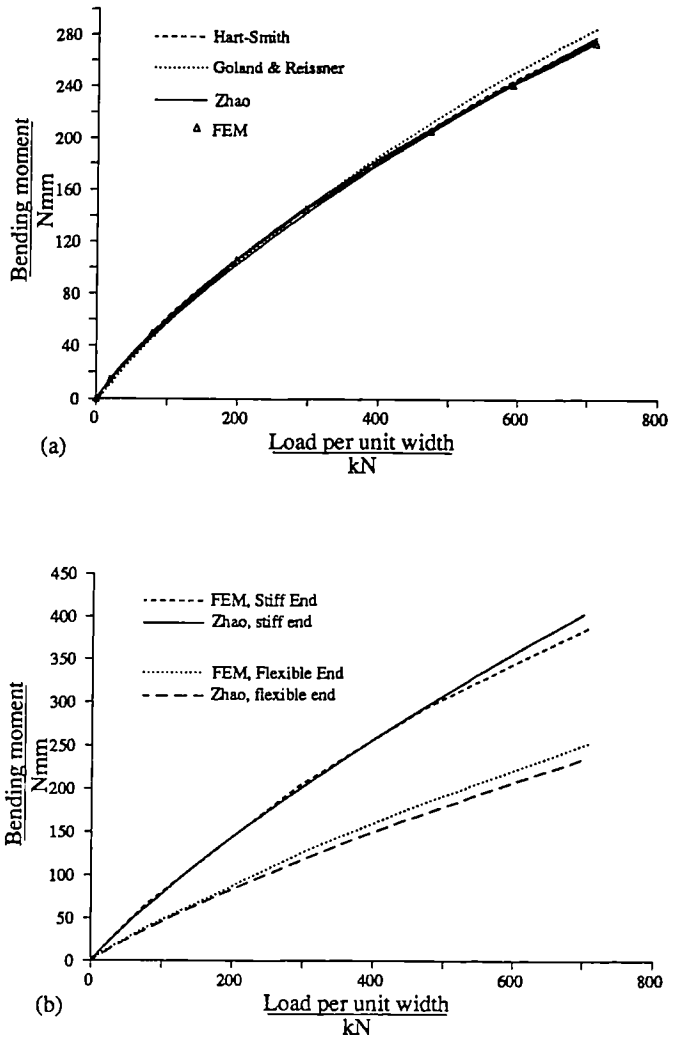

Fig. 4.6 *Bending moments in (a) balanced and (b) unbalanced single lap joint with a 12.7mm overlap.*

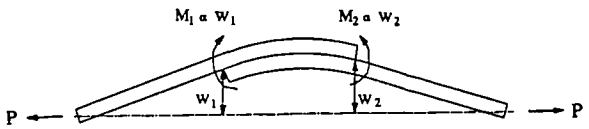

Fig. 4.7 *Effect of adherend free length on edge bending moments in a thermally mismatched joint.*

The results from the analysis of an Aluminium/CFRP joint (JOINT-3 in Table 4.1) are given in Fig. 4.8.

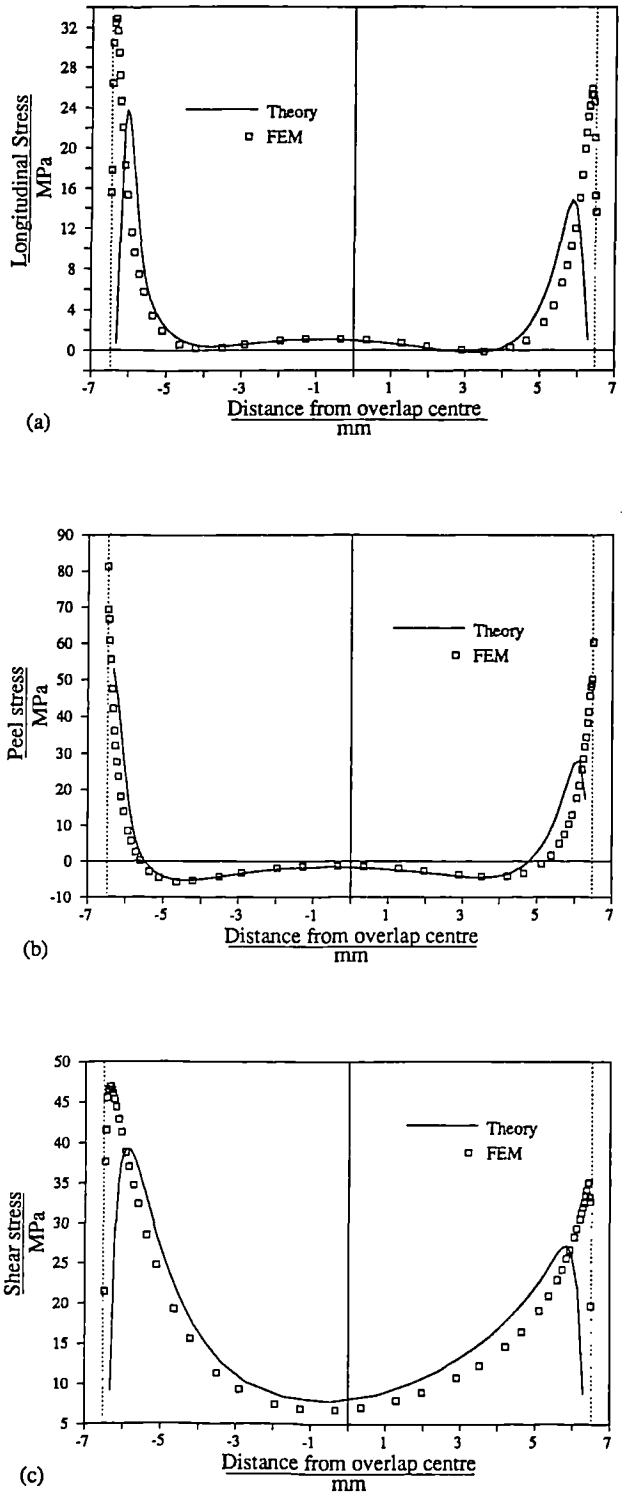

Fig. 4.8 *Averaged (a) longitudinal, (b) peel and (c) shear stress distributions in JOINT-3 (Table 4.1)*

The theoretical predictions agree well with the FEM in the mid-region, while at the ends the maximum stresses are lower. However, the error is greater than the 7% found in the balanced joint above (see Fig. 4.1). This cannot be due to errors in calculating the bending moments since these were within 3% of the FEM values.

On closer examination of the finite element results, it was found that the shear stress distribution across the adherend thickness was highly unsymmetrical, particularly at the loaded composite end. The peak was close to the adhesive (Fig. 4.9) rather than at the adherend centre as inferred by the parabolic assumption (section 3.4.2). This further illustrates the fact that the joint edge region can only be modelled accurately by using finite elements.

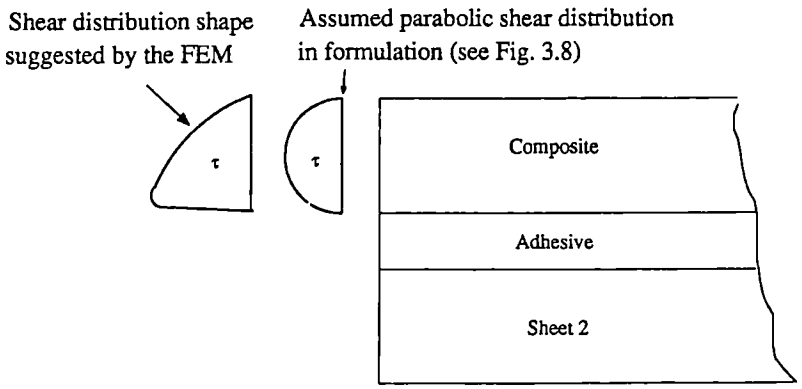

Fig. 4.9 *Theoretical and FE shear distribution at the loaded adherend edge*

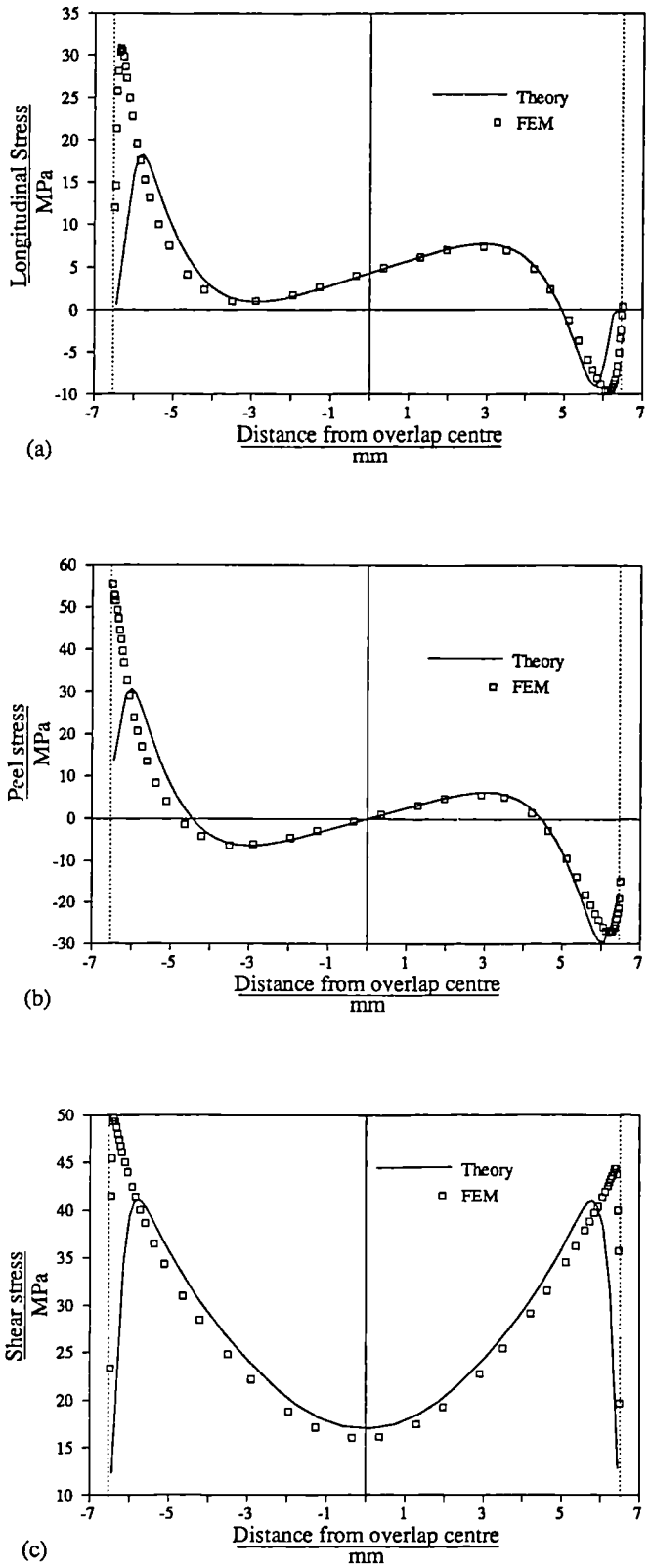

Fig. 4.10 *Stresses in a double lap joint (JOINT-1 in Table 4.1): (a) longitudinal, (b) peel and (c) shear*

4.1.4 Double lap joint

The theoretical and FEM stress predictions for a double lap joint are compared in Fig. 4.10. While the theoretical distributions are symmetrical, the FEM predicts higher stresses at the left hand side. This is because the large displacement FEM is able to account for the adherend deflections which occur due to internal bending (Fig. 4.11). These bending moments are due to internal shear forces arising from the stresses within the joint . The problem is therefore non-linear and cannot be modelled by the present theory.

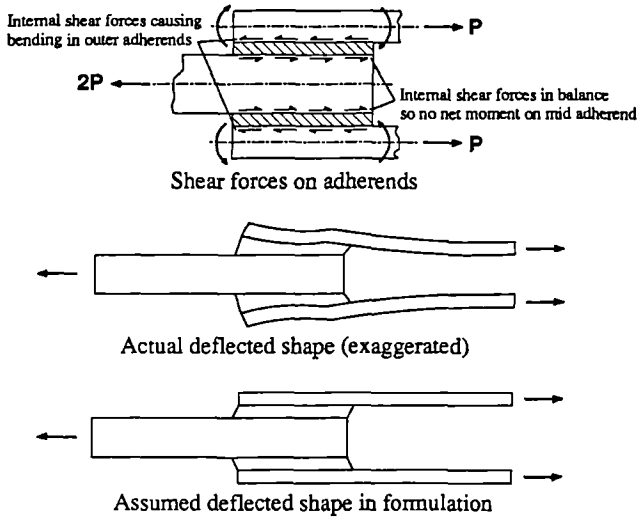

Fig. 4.11 *Internal bending moment and deflections in a double lap joint.*

4.1.5 Discussion

The present theoretical solution appears to predict stress distributions well, improving upon previous theories by treating the adhesive as a two-dimensional elastic continuum. In comparison with FEM, however, the stress peaks at the extreme edges of the overlap are lower. The FEM is able to predict higher stresses in this region because it is less constrained and thus allows singularities to occur at the loaded corner of the adhesive; refining the mesh in this region leads to higher stresses. In a mathematical model, such as the one developed here, singularities cannot occur; otherwise a solution would not be possible. In any case, the whole question of singularities is yet to be resolved. For instance, if a perfectly square edge existed then, theoretically, the glue should either crack or yield (or both). This has prompted some workers (Kinloch, 1981) to use fracture mechanics to try to understand the fracture behaviour. Others, notably Adams and his co-workers (1984), have

argued that a square edge cannot exist and local geometry effects such as spew fillet and corner rounding influence the stress field. It may be that these end effects reduce the maximum stresses to levels predicted by the present solution.

Whatever the case, the present theory offers an economic method of lap joint analysis for elastic adhesives. It provides a viable alternative to the FEM and thus enables the non-specialiest to calculate stresses for a variety of joint configurations.

4.2 INFLUENCE OF TEMPERATURE

The distributions of stresses in joints due to temperature were discussed earlier (section 3.2). It was seen that the stresses were concentrated at the overlap edges. In this section, these stresses are studied, using the FEM, in greater detail in order to establish their significance, if any, in a loaded joint.

The joint to be analysed is the Aluminium/CFRP joint listed as JOINT-3 in Table 4.1. The Aluminium and the adhesive were given thermal expansion coefficients values of 23×10^{-6}/°C and 60×10^{-6}/°C, while the CFRP coefficient was 10×10^{-6}/°C. The principal stress vectors at Gauss points for the three cases of (a) load, (b) thermal mismatch between adherends and (c) adhesive thermal deformation are plotted in Fig 4.12. In case (b) the adhesive coefficient of expansion was set to zero while for case (c) the adherend coefficients were set to zero.

For case (a) a load of 5kN was applied while a temperature drop of 150°C was introduced for cases (b) and (c). All the vectors are scaled relative to the maximum principal stress vector in the load only case (Fig 4.12a).

Applying a tensile load to the lap joints creates an almost uniform field of predominantly tensile stress at the ends (Fig 4.12a), whereas thermal mismatch (Fig. 4.12b) introduces a state of shear. In case (c) where only adhesive thermal deformation is permitted there is compression at the joint edge, light shearing just inside and tension further inside (Fig. 4.12c). Even though these stresses are small compared to the loading stresses, they are for the most part the same order of magnitude as the mismatch stresses.

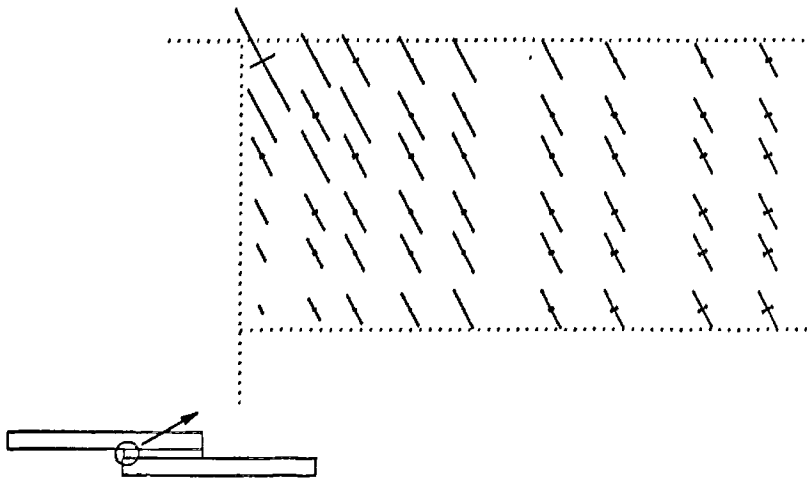

(a)

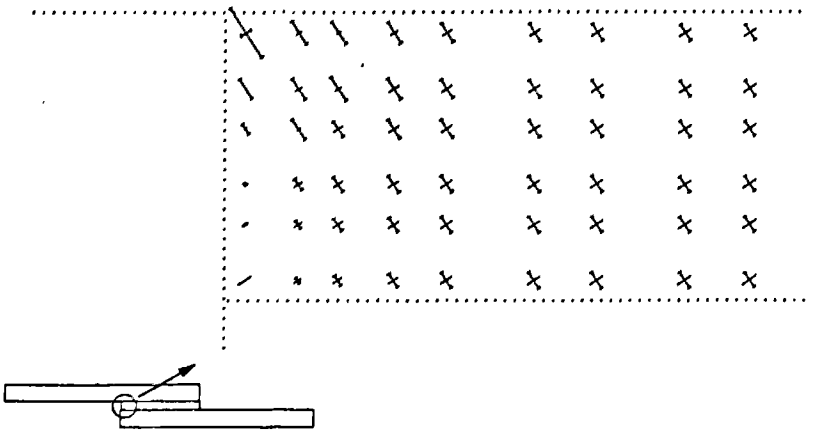

(b)

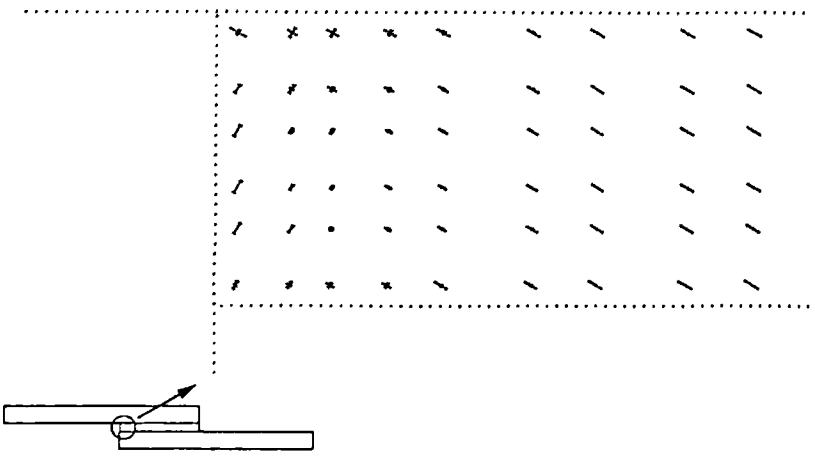

(c)

Fig. 4.12 *Principal stress vectors in JOINT-3 (Table 4.2) due to (a) load, (b) thermal mismatch (c) adhesive contraction.*

The vectors indicate that, while adhesive contraction augments the loading stresses, the mismatch stresses act in the opposite direction. For example, at the loaded corner of the adhesive, where the stresses are highest, the maximum principal stress is tensile for both load and adhesive contraction but compressive for thermal mismatch. If the mismatch and adhesive deformation vectors are superimposed, the resulting plot (Fig. 4.13a) looks similar to the mismatch case (Fig. 4.12b). This suggest that adhesive deformation has little impact in JOINT-3; it causes slight re-orientations and changes in magnitude.

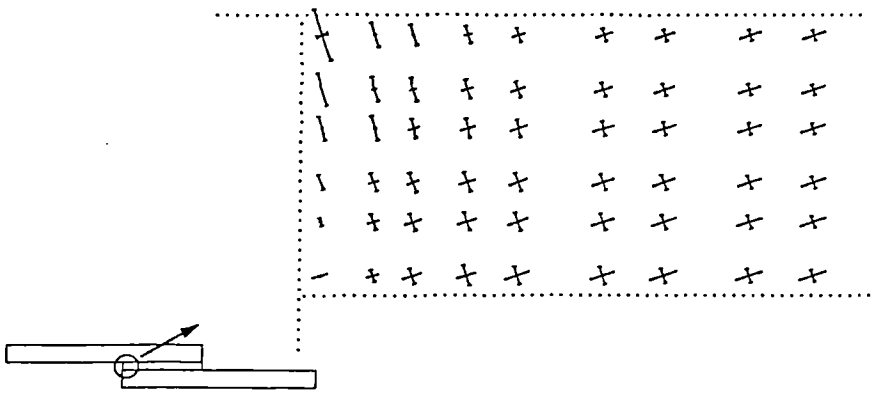

(a)

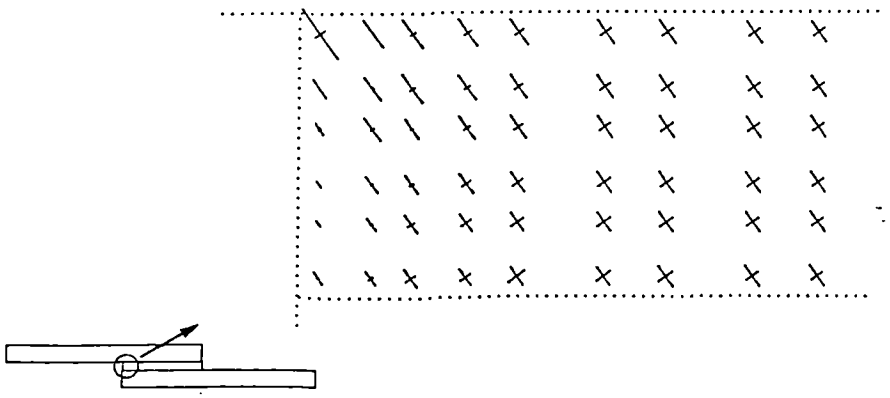

(b)

Fig. 4.13 *Principal stress vectors in JOINT-3 (Table 4.2) due to (a) temperature and (b) load and temperature.*

The thermal impact on the load vectors, shown in Fig. 4.13b, is to reduce the maximum principal stress. Furthermore, the temperature drop is suppressing yield since the principal stresses are now almost without

exception tensile thus producing a hydrostatic state of stress. The obvious conclusion is that the temperature drop is increasing the load bearing capacity of the joint. However, due to symmetry, thermal stresses have the reverse effect on the other side of the joint. When a load was applied, this was the less critical edge (Fig. 4.14a). The presence of thermal stress has significantly increased the maximum stress here (Fig. 4.14b). Not only is this the critical edge now, but the maximum stress is higher (cf. Fig. 4.12a). Therefore, the net effect of the thermal stress is to decrease the load bearing capacity.

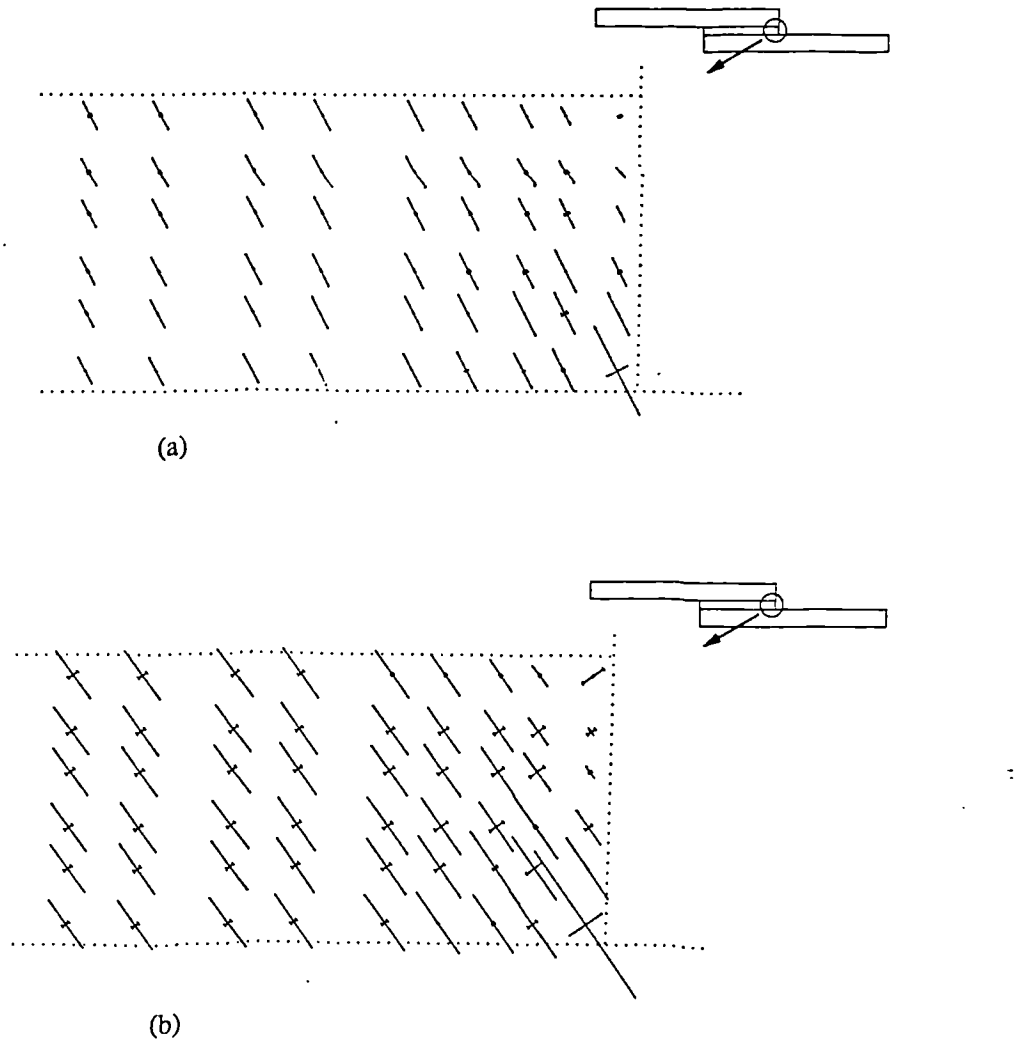

Fig. 4.14 *Principal stress vectors at the right edge of JOINT-3 (Table 4.2) due to (a) load and (b) load and temperature.*

4.2.1 **Parametric study of thermal stress**

In the previous section only one joint, albeit a representative one, was studied. An attempt is made here to determine the effect of parameters which might be intuitively expected to influence the magnitude of the thermal stresses. The investigation has been conducted using the present elastic theory.

4.2.2 **Joint overlap**

In a joint where thermal mismatch exists, stresses arise within the adhesive layer because it does work to prevent the two adherends from having a difference between their lengths. If the adherends were able to deform freely then this difference, δ, would be:

$$\delta = \alpha_d \Delta T(2c)$$

where α_d is the difference in their coefficients of expansion, ΔT the temperature change and 2c the overlap length. Therefore, the difference in expansion is directly proportional to the overlap. This suggests that increasing the overlap for a given joint would raise the stresses as the adhesive has to do more work to keep the adherends together. This is found not to be the case.

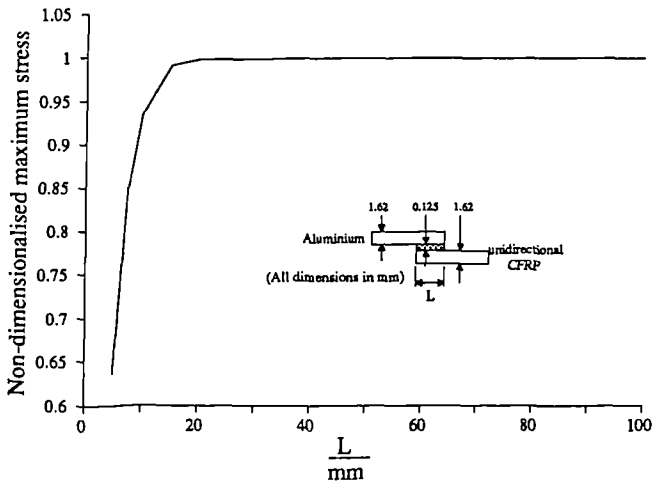

Fig. 4.15 *The effect of varying the overlap on the maximum principal stress*

Fig. 4.15 plots the maximum principal stresses within the adhesive of a Aluminium/CFRP joint (JOINT-3, Table 4.1) for a given overlap. The reason for the lack of stress increase is straightforward: not only does the

adhesive do work but the adherends themselves will stretch or contract in order to accommodate δ. Therefore, it is reasonable to speculate that it is the sheet stiffnesses that will determine the final stresses.

4.2.3 Adherend stiffness

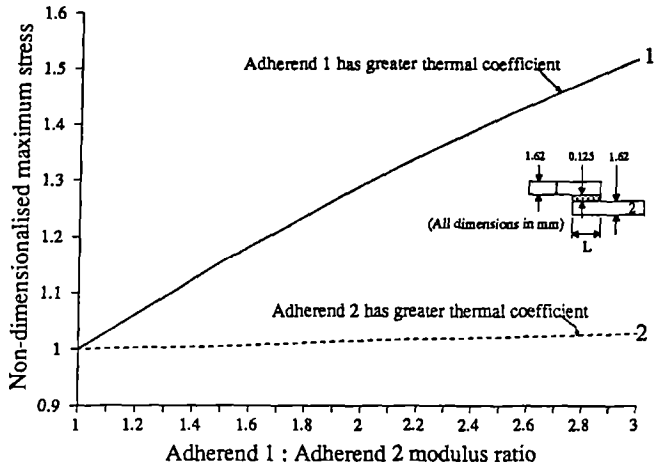

Fig. 4.16 *Effect of varying adherend stiffness ration on the maximum principal stress*

Fig. 4.16 is a plot of the variation of maximum thermal stress with the adherend modulus ratio. Curves 1 and 2 represents the cases where adherends 1 and 2 have the greater coefficient of expansion respectively. In order to concentrate on the influence of the adherend, adhesive thermal deformation was not permitted. The results imply that the adhesive stresses are only sensitive to the stiffness of the adherend which expands (or contracts) the most. Varying the stiffness of the other adherend has little effect.

4.2.4 Adhesive stiffness

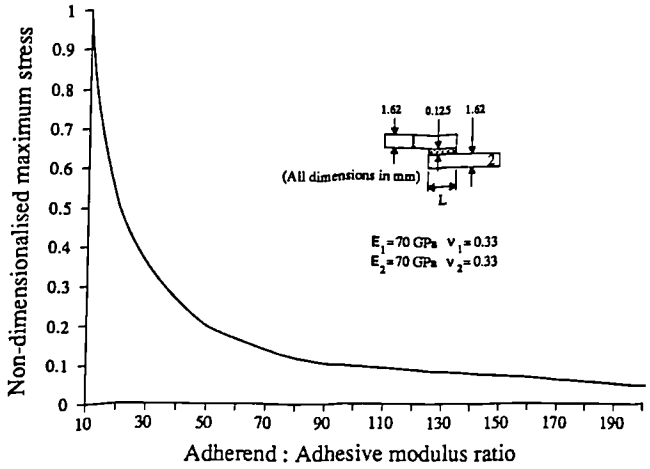

Fig. 4.17 *Effect of varying adhesive stiffness of the maximum principal stress*

In section 4.2 it was observed that the stresses due to adhesive thermal deformation were smaller than those due to mismatch. However, Fig. 4.17 suggests that the adhesive stiffness has a significant influence on the magnitude of these stresses. It is often the case that high modulus adhesives require a high curing temperature. Therefore there is a strong likelihood of significant thermal stress even in balanced lap joints as the joint cools from cure to operating temperature. Further stresses may arise from the adhesive shrinkage during cure (Chen, 1985 and Coppendale, 1983). These sources of residual stresses are often neglected but results here indicated that they may be significant.

The stiffness of polymer materials such as adhesives can vary with temperature. Consider MY 750/HY 956, for instance, which has a modulus of 3.18 GPa at +20°C, while at -55°C it is 5.62 GPa (see section 6.3.1). If the thermal principal stresses for a drop in temperature from +20°C to -55°C are calculated using the properties at +20°C, then the result is curve A in Fig. 4.18. If, however, the -55°C properties are used then the distribution B is obtained. Neither will be correct since the adhesive stiffness will have varied throughout the temperature drop. By making the assumption that the stiffness varies linearly with temperature, it was found that the stresses were given by curve C. These stresses lie in between A and B and show the importance of considering the variation of adhesive properties with temperature if stresses are to be predicted accurately.

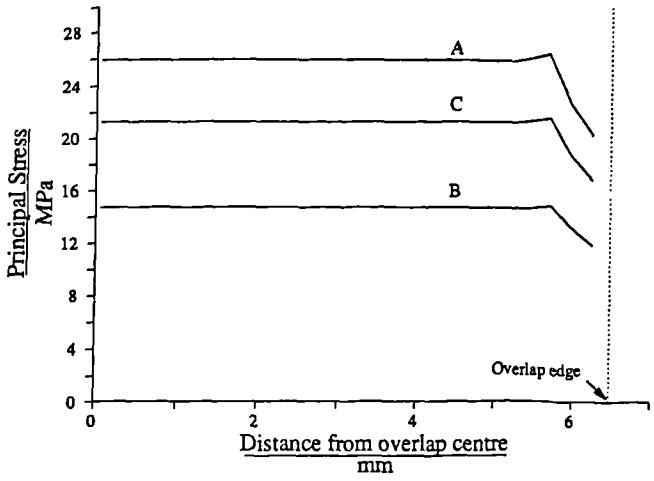

Fig. 4.18 *Thermal stress due to adhesive contraction in an Aluminium-Aluminium joint.*

4.3 COMMENT ON MOISTURE

The main difference between moisture and temperature induced stresses is the manner in which the initial strains arise. Mathematically, the analysis will be identical. In fact the above discussion on temperature will apply to joints subjected to moisture by substituting diffusion coefficient and moisture concentration for thermal expansion coefficient and temperature change.

There are, however, further complications peculiar to adhesive joints subjected to moisture. Apart from changing the adhesive properties significantly moisture will also affect adhesion itself, thus undermining the basis of strength prediction. The diffusion rate will be important since transient stresses due to moisture uptake will be significant (Weitsman, 1977). Furthermore, as Lefebvre *et al* (1989a,b) and Roy (1989) found, the diffusion of moisture may be dependant on the strain levels already present.

Chapter 5

ANALYSIS OF LAP JOINTS WITH ELASTO-PLASTIC ADHESIVE

Many modern adhesives undergo large plastic strains before failure. In joints, plastic deformations begin at the overlap ends and spread towards the middle, redistributing stress in the process. These effects can not be modelled by the theory in its present form since linearly elastic material behaviour was assumed (see chapter 3). In order to overcome this difficiency, the solution has been extended to model plastic deformation within the adhesive layer.

Prior to the description of the plastic analysis, fundamentals of plasticity theory are summarised. A more thorough explanation can be found in Johnson and Mellor (1973).

5.1 THEORY OF PLASTICITY AND THE ELASTO-PLASTIC MODULUS

The mathematical theory of plasticity provides a relationship between stress and strain for a material which exhibits an elasto-plastic response. A material is said to deform plastically when it suffers irreversible strains which are not time dependent. Here it is assumed that the material behaves in a *linear* elastic manner until it reaches a certain stress. This stress state, $\{\sigma\}$, is given by a yield criterion of the form

$$f(\{\sigma\}) = 0 \tag{5.1}$$

where f is some function, usually defined in terms of the hydrostatic stress, J_1, and the deviatoric stress, J_2, where

$$J_1 = \sigma_x + \sigma_y + \sigma_z$$

$$J_2 = {}^1/_2\{(\sigma_x - J_1/3)^2 + (\sigma_y - J_1/3)^2 + (\sigma_z - J_1/3)^2 + (\tau_{xy})^2 + (\tau_{xz})^2 + (\tau_{yz})^2\}$$

For ductile materials, the Von Mises yield function

$$f(\{\sigma\}) = \sqrt{(3J_2)} - Y_T = 0 \tag{5.2}$$

is often used. Y_T is the yield stress derived from a uniaxial tensile test on the material. For polymers, the yield in tension and compression are often different. This is accounted for in Raghava's criterion (1973) by including the hydrostatic stress, J_1:

$$\{J_1(S-1) + (J_1)^2(S-1)^2 + 12J_2S\}/2S = Y_T^2 \tag{5.3}$$

where S is the ratio of the yield stress in compression to the yield stress in tension.

Until initial yield, the strain $\{\varepsilon\}$ is related to the stress $\{\sigma\}$ according to the elastic law

$$\{\varepsilon\} = [D]^{-1}\{\sigma\} \tag{5.4}$$

where [D] is the modulus matrix. After yielding the total strain, $\{\varepsilon\}$, will be partly elastic, $\{\varepsilon_e\}$, and partly plastic $\{\varepsilon_p\}$:

$$\{\varepsilon\} = \{\varepsilon_e\} + \{\varepsilon_p\} \tag{5.5}$$

While the elastic part is given by eqn (5.4), the plastic strain is determined from the theory of plasticity. However, the theory provides a rule for the determination of plastic strain *increments*. This "flow" rule is of the form

$$d\{\varepsilon_p\} = \lambda(\partial f/\partial\{\sigma\}) \tag{5.6}$$

where $d\{\varepsilon_p\}$ is the vector of plastic strain increments and λ is an instantaneous constant that can vary throughout loading. The flow rule ensures that the plastic strain increment is normal to the yield surface defined by f and also that the stress remains within the surface ($f(\{\sigma\}) < 0$).

To accommodate the incremental nature of plasticity theory, increments of strain have to be considered. Re-writing eqn (5.5) in incremental form gives

$$d\{\varepsilon\} = d\{\varepsilon_e\} + d\{\varepsilon_p\} \tag{5.7}$$

Substituting eqns (5.5) and (5.6) into eqn (5.7) and re-arranging, we get

$$d\{\sigma\} = [D]d\{\varepsilon\} + [D]\{\alpha\}\lambda \tag{5.8}$$

where $\{\alpha\}=(\partial f/\partial\{\sigma\})$. It can be shown (Hinton and Owen, 1978) that

$$[D]\{\alpha\}\lambda = [D_p]\{\varepsilon\} \tag{5.9}$$

where

$$[D_p] = \frac{[D]\{\alpha\}\{\alpha\}^T[D]}{A + \{\alpha\}^T[D]\{\alpha\}} \tag{5.10}$$

and A is equal to the instantaneous gradient of the uniaxial stress-plastic strain curve. Therefore, we have the following relationship between stress and strain:

$$d\{\sigma\} = [D_{ep}]d\{\varepsilon\} \tag{5.11}$$

where $[D_{ep}] = [D] - [D_p]$ and is known as the elasto-plastic modulus.

If the material strain *softens* then A will be negative. This can lead to a situation where the stiffness matrix is not positive definite (Nayak and Zienkiewicz, 1972). Therefore, at this stage in the present work, only strain hardening has been considered.

5.2 PLASTICITY APPLIED TO THE PRESENT METHOD

For an elastic joint, it was shown (eqn (3.43) in section 3.4.3) that a solution is obtained by solving the equation

$$[\underline{F}]\{\underline{\phi}\} = [\underline{H}] \tag{5.12}$$

where $[\underline{F}]$ is a function of geometry and material constants and $[\underline{H}]$ is a function of applied loading. The arrays were derived by minimising the complementary energy function (3.42).

The problem with including material non-linearity is that an explicit constitutive law similar to eqn (3.38) is no longer available. Instead, the non-linear relationship

$$f(\{\sigma\}) < 0 \tag{5.13}$$

has to be satisfied which makes it extremely difficult to develop an energy function similar to (3.42). Fortunately, this is not necessary since it is possible, with slight modification, to solve eqn (5.12) iteratively such that eqn (5.13) is satisfied. There are basically three types of iterative procedures; initial stress (Gallagher,

1971), initial strain (Rybicki and Schmit, 1970) and direct iteration. To facilitate a thorough comparison, in terms of accuracy and computing requirements, each has been implemented.

5.2.1 Direct iteration

In direct iteration, a solution to the system

$$[\underline{F}(\{\underline{\phi}\})]\{\underline{\phi}\} - [\underline{H}(\{\underline{\phi}\})] = 0 \tag{5.14}$$

is sought. This is essentially the same as eqn (5.12) except the $[\underline{F}]$ $[\underline{H}]$ arrays are now functions of stress which ensure that the stresses lie on the yield surface. To solve the non-linear system (5.14), initial values of $[\underline{F}_0] = [\underline{F}(0)]$ and $[\underline{H}_0] = [\underline{H}(0)]$ are determined (see Fig. 5.1). Then a first approximation for $\{\underline{\phi}\}$ is (the subscript numbers refer to the iteration):

$$\{\underline{\phi}\}_1 = [\underline{F}]^{-1}{}_0[\underline{H}]_0$$

Successive approximations are made according to the iterative procedure

$$\{\underline{\phi}\}_j = [\underline{F}]^{-1}{}_{j-1}[\underline{H}]_{j-1}$$

where $[\underline{F}]_{j-1} = [\underline{F}(\{\underline{\phi}\}_{j-1})]$ and $[\underline{H}]_{j-1} = [\underline{H}(\{\underline{\phi}\}_{j-1})]$. A solution is achieved when the the difference $\{\underline{\phi}\}_{j-1} - \{\underline{\phi}\}_j$ is sufficiently small (see Fig. 5.1).

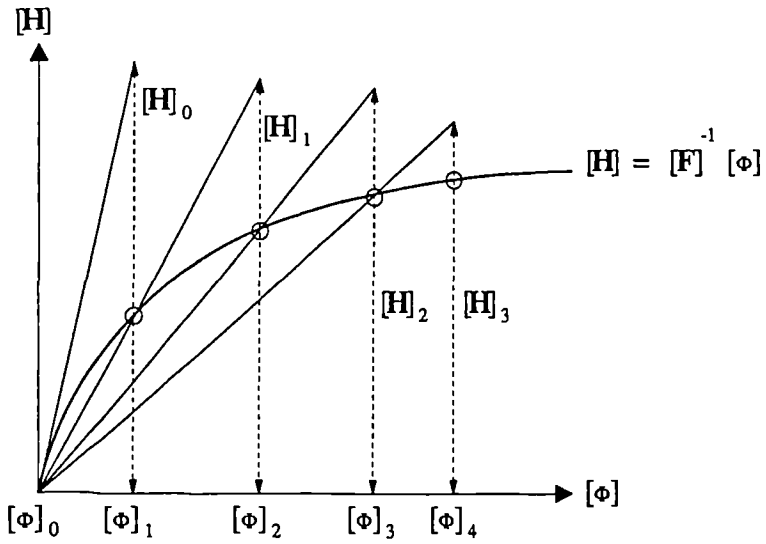

Fig. 5.1 *Direct iteration solution procedure*

As mentioned above, arrays [F] and [H] are required such that the adhesive stress-strain state obeys the constitutive law (5.13). In the elastic joint (section 3.4.3), the elemental arrays were

$$[F] = \int\int \frac{1}{2}([B]^T[N]^T[D]^{-1}[N][B])\,dxdy \tag{5.15}$$

$$[H] = \int\int -([B]^T[N]^T[D]^{-1}\{C(x)\} + [B]^T[N]^T\{\varepsilon_t\})\,dxdy \tag{5.16}$$

When the adhesive is plastic, [D] ceases to be constant throughout the element. In general, at any given point within the element:

$$\{\sigma\} = [D_t]^{-1}\{\varepsilon\}$$

where $[D_t]$ is an effective modulus array for the stress-strain state $(\{\sigma\},\{\varepsilon\})$ (see Fig. 5.1). Since $(\{\sigma\},\{\varepsilon\})$ will vary throughout the element, so will $[D_t]$. Including this variation in eqns (5.15) and (5.16) is fairly straightforward if [F] and [H] are integrated numerically using suitable Gaussian quadrature formulae. In which case, $[D_t]$ need only be determined at the Gauss points within the element. Now, [F] contains sixth order terms in both x and y (see Appendix II, III) while [H] contains third order terms only. So [F] will be more sensitive to the number of Gauss points used. For a sixth order polynomial, four Gauss points are needed. Therefore sixteen Gauss points were used per element; four each in the x and y directions.

The complete iterative procedure then is as follows:

(1) Initially, the $(\{\sigma\},\{\varepsilon\})$ field is not available, so the elemental [F] and [H] matrices (eqns (5.17) and (5.18)) are calculated with the elastic modulus $[D_t]$ set equal to the elastic matrix [D]. $[\underline{F}] = [\underline{F}]_0$ and $[\underline{H}] = [\underline{H}]_0$ are assembled and the solution $\{\underline{\phi}\}_1 = [\underline{F}]^{-1}_0[\underline{H}]_0$ is computed.

(2) From $\{\underline{\phi}_1\}$ the stresses, $\{\underline{\sigma}\}_1$, and strains, $\{\underline{\varepsilon}\}_1$, are computed.

(3) Then for each sampling (Gauss) point the equivalent stress strain state (σ_1,ε_1) is compared with the uniaxial curve. If the curve gives a stress σ_1' for the strain ε_1 such that $\sigma_1 \approx \sigma_1'$ then there is no need to compute a new modulus $[D_t]$.

If a new $[D_t]$ is required then the adhesive effective Young's modulus, E'_a, for the stress strain state $(\sigma_1', \varepsilon_1)$ is given by

$$E'_a = \sigma_1'/\varepsilon_1$$

The new $[D_t]$ is derived by simply substituting E'_a for E_a in the [D] matrix (see Appendix III).

(4) The elemental [F] and [H] are calculated and assembled to give the global arrays $[F_1]$ and $[H_1]$. The process

$$\{\underline{\phi}\}_j = [\underline{F}]^{-1}_{j-1}[\underline{H}]_{j-1}$$

is repeated until the difference $\{\underline{\phi}\}_{j-1} - \{\underline{\phi}\}_j$ is small.

(5) The converged $\{\underline{\phi}\}_n$ array is used to calculate the final stress and strain condition.

The main problem with direct iteration is that at each iteration, both arrays [F] and [H] have to be calculated. In the initial strain and stress methods only [H] is recalculated. Furthermore, since the [H] matrix is of third order in both x and y, only four Gauss points are per element are needed, so less core memory is required.

5.2.2 Initial strain

In the initial strain method the complementary energy function (3.9) is modified to include plastic strain. The load is applied incrementally allowing the plastic strains to be built up correctly.

The first step in developing the initial strain energy function is to rewrite eqn (3.38). The stress strain relationship at the the *n*th load increment is now defined as:

$$\{\sigma\} = [D](\{\varepsilon\} - \{\varepsilon_t^{(n)}\} - \{\varepsilon_p^{(n)}\}) \tag{5.19}$$

where $\{\varepsilon_t^{(n)}\}$ is the accumulated thermal strain vector and $\{\varepsilon_p^{(n)}\}$ is the accumulated plastic strain vector and can be viewed as the initial strain. So

$$\{\varepsilon_t^{(n)}\} = \sum_{j=1}^{n} \{\delta\varepsilon_t^{(j)}\}$$

and $$\{\varepsilon_p^{(n)}\} = \sum_{j=1}^{n-1} \{\delta\varepsilon_p^{(j)}\} + \delta\varepsilon_p$$

The plastic strain due to the nth load increment, $\delta\varepsilon_p$, is determined from the stress state according to eqn (5.11). This introduces non-linearity into eqn (5.19), so that iterations are required within each load increment.

Adopting eqn (5.19) as the stress strain relationship does not affect [**F**], but [**H**] now becomes

$$[\mathbf{H}] = \int_v ([\mathbf{B}]^T[\mathbf{N}]^T[\mathbf{D}]^{-1}\{\mathbf{C}(x)\} + [\mathbf{B}]^T[\mathbf{N}]^T\{\varepsilon_t^{(n)}\} + [\mathbf{B}]^T[\mathbf{N}]^T\{\varepsilon_p^{(n)}\})dv$$

As was the case with the $[\mathbf{D}_t]$ matrix in the direct iteration method, $\{\varepsilon_p^{(n)}\}$ need only be determined at the Gauss points if Gaussian integration is employed to determine [**H**].

The solution procedure consists of the following steps (the numbers inside the brackets refer to the load increment, outside the brackets they refer to the iteration):

(1) $[\underline{\mathbf{H}}_0]$ is assembled for the full load level. The system $\{\underline{\phi}_0\} = [\underline{\mathbf{F}}]^{-1}[\underline{\mathbf{H}}_0]$ is solved and the $\{\underline{\sigma}_0\}$, $\{\underline{\varepsilon}_0\}$ arrays are obtained. Each Gauss point is then tested for yield and the load is scaled down to a level which causes first yield.

(2) The load is incremented and $[\underline{\mathbf{H}}] = [\underline{\mathbf{H}}_1]_0$ is assembled ($[\underline{\mathbf{F}}]$ will be unchanged throughout since it is not dependent on the load or the initial strain vector). Next, the stresses $\{\underline{\sigma}_1\}_1$ and strains $\{\underline{\varepsilon}_1\}_1$ are determined.

(3) At each Gauss point, the plastic strain, $\delta\varepsilon_p$, due to the current stress level is calculated and $\{\varepsilon_p^{(1)}\}_1$ is assembled.

(4) $[\underline{\mathbf{H}}_1]_1$ is calculated and the system is solved to give $\{\underline{\sigma}_1\}_2$ and $\{\underline{\varepsilon}_1\}_2$. The process

$$\{\underline{\phi}_1\}_j = [\underline{\mathbf{F}}]^{-1}[\underline{\mathbf{H}}_1]_j$$

is repeated until the difference $\{\underline{\phi}_1\}_{j-1} - \{\underline{\phi}\}_j$ is less than a specified value.

(5) The next load increment is applied and the iterative process repeated.

The difficulty with the initial strain method is that the adhesive stress-strain curve should exhibit a significant amount of strain hardening. If the characteristic is too "flat" beyond initial yield, then $|[D_{ep}]| \approx 0$ and it becomes impossible to determine strain from stress in step (3), since

$$d\{\varepsilon\} = [D_{ep}]^{-1} d\{\sigma\}.$$

This difficulty is circumvented by the initial stress method.

5.2.3 **Initial stress**

The initial stress method has been successfully employed in displacement FEMs (Nayak and Zienkiewicz, 1972) and has been adapted for the present FEM in a manner similar to that suggested by Gallagher and Dhalla (1970).

Rewriting the stress-strain relationship (3.38) to include initial stress $\{\sigma_i\}$, we have

$$\{\sigma\} = [D]\{\varepsilon - \varepsilon_t\} + \{\sigma_i\} \tag{5.20}$$

This leads to the following definitions for the [F] and [H] matrices:

$$[F] = \int \int \frac{1}{2} ([B]^T[N]^T[D]^{-1}[N][B])\, dxdy$$

$$[H] = \int_v -([B]^T[N]^T[D]^{-1}\{C(x)\} + [B]^T[N]^T\{\varepsilon_t\} + [D]^{-1}\{\sigma_i\})dv$$

Where [H] is dependent on the initial stress vector but [F] remains unchanged. The significance of the initial stress vector will become clear once the solution procedure is understood. The procedure is similar to the initial strain case in that the load is applied incrementally, [H] is integrated with Gaussian formulae and [F] remains unchanged throughout.

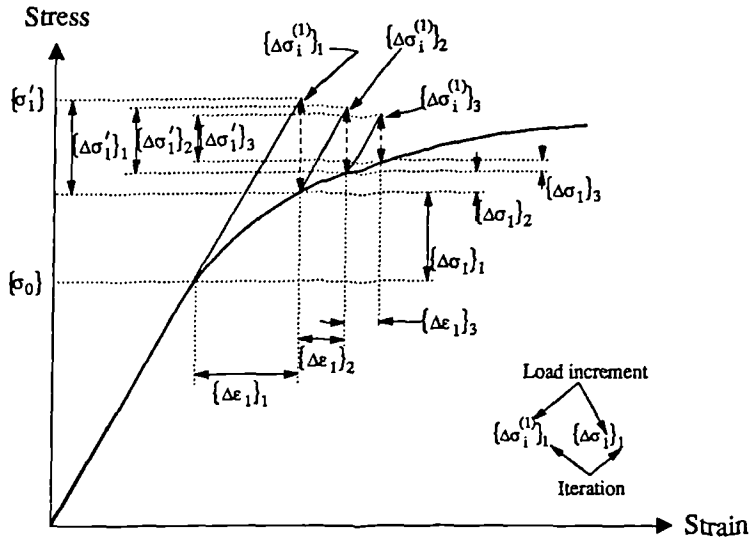

Fig 5.2 *Initial stress solution procedure*

The complete process is as follows (the numbers inside the brackets refer to the load increment, outside the brackets they refer to the iteration):

(1) $[\underline{H}_0]$ is assembled for the full load level. The system $\{\underline{\phi}_0\} = [\underline{F}]^{-1}[\underline{H}_0]$ is solved and the $\{\underline{\sigma}_0\}$, $\{\underline{\varepsilon}_0\}$ arrays are obtained. Each Gauss point is then tested for yield and the load is scaled down to a level which causes first yield.

(2) The load is incremented, $[\underline{H}] = [\underline{H}_1]_0$ is assembled and the system

$$\{\underline{\phi}_1\}_1 = [\underline{F}]^{-1}[\underline{H}_1]_0$$

is solved.

(3) The resulting *changes* in stress $\{\delta\sigma'_1\}_1$ and strain $\{\delta\varepsilon_1\}_1$ are determined.

(4) At each Gauss point, the stress, $\{\delta\sigma_1\}_1$, due to the strain $\{\delta\varepsilon_1\}_1$ is computed in accordance with the plasticity rule (5.11). The current stress strain state is determined (and stored):

$$\{\sigma\} = \{\sigma_0\} + \{\delta\sigma_1\}_1$$

$$\{\varepsilon\} = \{\varepsilon_0\} + \{\delta\varepsilon_1\}_1$$

(5) The difference in stress $\{\delta\sigma'_1\}_1 - \{\delta\sigma_1\}_1$ is treated as an initial stress $\{\sigma_i^{(1)}\}_1$ and used to determine a new [H]. $\{\sigma_i^{(1)}\}$ can be viewed as the stresses required to restore the stress to the correct plastic value (see Fig. 5.2).

(6) The system

$$\{\underline{\phi}_1\}_j = [\underline{F}]^{-1}[\underline{H}_1]_{j-1}$$

is solved and steps 3-5 repeated until the difference $\{\underline{\phi}_1\}_{j-1} - \{\underline{\phi}\}_j$ or the vector $\{\underline{\sigma}_i^{(1)}\}_j$ is less than a specified value.

(7) The next load increment is applied and the iterative process repeated.

5.2.4 **Discussion**

The most efficient method will give an accurate solution while making the least demand on the computer in terms of time and memory. The direct iteration method requires the least number of iterations to achieve convergence since the stiffness matrix is updated in every iteration. This, however, is offset by the amount of time taken to perform each iteration. In Table 5.1 the memory and time requirements made of an IBM PS/2 Model 80 by the three methods are compared. The memory requirements refer to the amount of in core storage required to implement a Modula-2 program with a capacity to handle fifty elements.

METHOD	TIME TO COMPUTE [H] (sec)	TIME TO COMPUTE [F] (sec)	MEMORY REQUIRED (MB)
Elastic	0.05	0.01	0.1
Direct Iteration	45	180	0.45
Initial Strain	0.05	1.0	0.32
Initial Stress	0.05	1.0	0.32

Table 5.1 *Comparison of plastic analysis algorithms*

Clearly, the direct iteration method takes an excessive amount of time to calculate the [F] and [H] matrices. Moreover, it makes the greatest memory demand. Both are a direct result of the fact that sixteen Gauss points are needed, compared with four in the initial strain and stress methods. While the matrix calculation could be speeded up, by determining explicit functions for [F] and [H] at gauss points rather than performing matrix

operations, the memory requirements would remain high. This would present difficulties in extending the method to consider adherend plasticity.

Of the remaining methods initial stress is preferable. There is nothing to choose between them in terms of memory and time requirements. However, as mentioned above, the initial strain method will fail unless the adhesive exhibits a fair degree of strain hardening. Therefore, the initial stress method was adopted.

5.3 PLASTICITY APPLIED TO THE FEM

The FEM program used in the present work, FELDEP, implements plasticity via the initial stress approach. Therefore, the load is applied incrementally, associated strains and stresses are then calculated and iterations performed until the material constitutive law is obeyed. It was mentioned in section 3.1.1 that the program was modified to include the effects of temperature. The complete FEM plastic solution procedure is described by Crocombe (1981) and the modification required to include thermal stresses is given in Appendix Ib.

5.4 COMPARISON OF THE METHODS

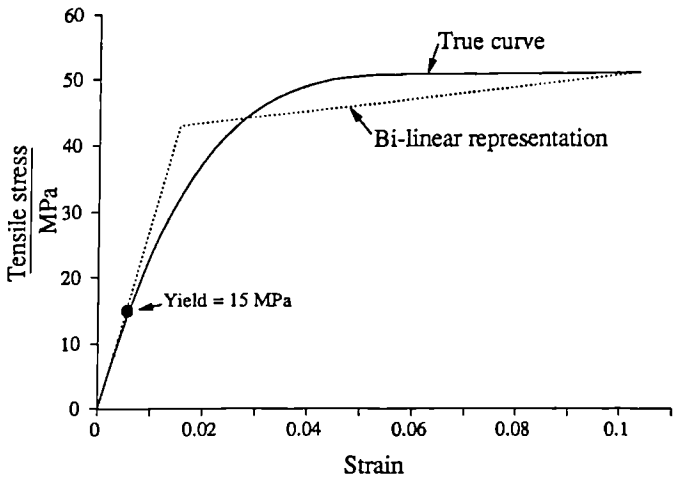

Fig. 5.3 *A theoretical adhesive tensile stress strain curve*

In order to test the accuracy of the present plastic solution, an elasto-plastic analysis of a single lap joint has been performed with a theoretical adhesive stress-strain curve and the results have been compared with FEM.

The adhesive stress-strain curve used, shown in Fig. 5.3, represents a fairly soft adhesive and should provide a good test for the plastic solution.

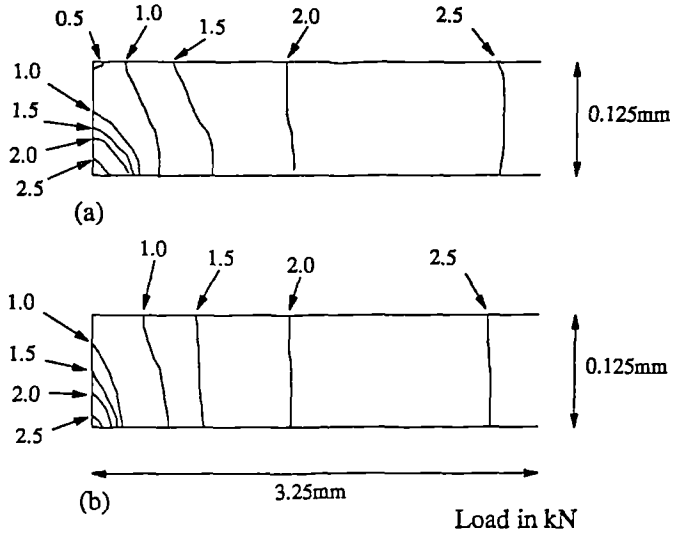

Fig. 5.4 *Spread of the yield zone at the edge of the adhesive layer: (a) FEM and (b) present theory.*

The single lap joint consisted of similar 2mm thick Aluminium adherends with an overlap of 13mm. Fig. 5.4 depicts the predicted spread of the yield surface within the adhesive layer. It can be seen that there is close agreement between the two methods except at the very edge of the overlap. However, as discussed earlier in section 4.1.5, the accuracy of the FEM at the edges could not be matched by the present method even in the elastic case. The maximum principal stresses are also in close agreement as the plot in Fig. 5.5 shows.

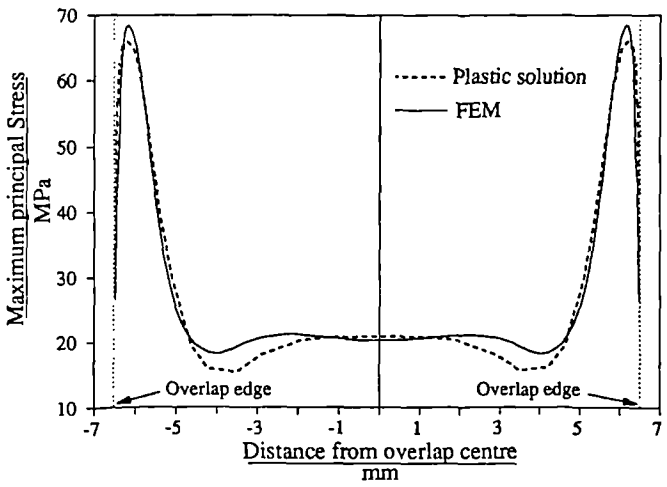

Fig. 5.5 *Maximum average principal stress, due to a load of 8.5kN.*

The main purpose of the present plastic solution is to provide users a simple method of strength estimation. The only difference, as far as the user is concerned, between the elastic and plastic solutions is that a stress versus plastic strain curve is required for the adhesive. This curve can be derived from the true stress strain curve but is a tedious process. The task can be simplified by the use of a simple bi-linear model if this does not significantly compromise the accuracy of the strength predictions. To test whether this is the case, the theoretical adhesive above has been modelled by a bi-linear representation shown in Fig. 5.3. The bi-linear curve is chosen such that its initial slope, failure point and strain energy are equal to the true curve. The finite element maximum principal distributions obtained from the two models are shown in Fig. 5.6. The distributions are in agreement, especially at the peaks, which suggests that a bi-linear representation is acceptable for strength prediction.

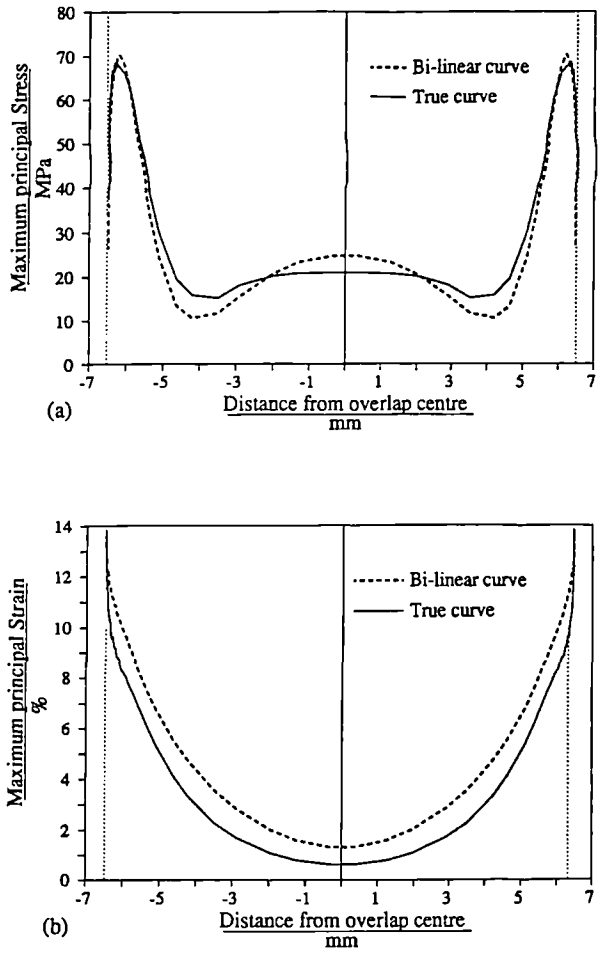

Fig. 5.6 *Averaged principal (a) stress and (b) strain distributions due to a load of 8.5kN.*

Chapter 6

MECHANICAL PROPERTIES OF JOINT MATERIALS

The main purpose of the present stress analysis theory is to provide a basis for strength prediction. Its accuracy is assessed in the next chapter through a comparison with experimental measurements. Single lap joints between aluminium and CFRP adherends have been tested at two temperatures: +20°C and -55°C. This joint is often found in aircraft structures and the temperatures reflect typical operating temperatures. Three types of adhesive, with contrasting mechanical properties, were used. The aim of the work described in this chapter was to generate, for each adherend and adhesive material, the mechanical data required by the analysis. Apart from basic properties such as Young's modulus, Poisson's ratio and the coefficient of expansion, the elasto-plastic stress-strain curve and the failure quantities have been determined.

6.1 MATERIAL TESTING

The traditional method of obtaining properties for *isotropic* materials is to perform a uniaxial tensile test. In this test, difficulties arise in extracting the true stress-strain curve beyond the elastic limit. Necking, which occurs at yield, not only reduces the cross sectional area but can introduce a state of stress other than uniaxial tension. While the latter effect is difficult to compensate, a correction for the reduction in cross-section is possible by assuming constant volume during plastic flow (Appendix IV). In spite of these limitations the tensile test remains in widespread use as no alternative has gained acceptance. It was decided, therefore, to derive material properties through such a test.

For cold tests, specimens were placed inside an environmental chamber which had a fan and a controlled heating element. A cold environment was created by supplying the chamber with liquid nitrogen (-194.7°C) under pressure. The required temperature was maintained by the chamber control system which switched the elements on when necessary. A diagram of the cooling arrangement is shown in Fig. 6.1.

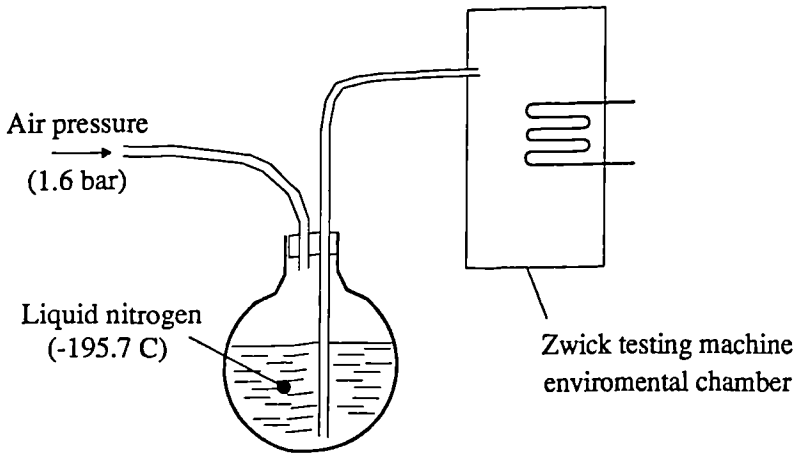

Fig. 6.1 *Cold test rig*

At least six specimens were tested for each possible configuration. The results were then averaged to give the properties reported below. For the adhesive stress strain curves, a bilinear approximation has been determined. As explained in section 5.4, this enables the stress-strain curve of an adhesive to be conveniently described while maintaining the accuracy of the final stress and strain state prediction.

6.2 ADHERENDS

Even though mechanical data for the aluminium and unidirectional CFRP used are available, there can be variations between sheets. Tests were therefore conducted on samples cut from the sheets used for joint manufacture.

The tests were conducted under quasi-static conditions at the two temperatures, -55°C and +20°C, in a 100kN Zwick screw-driven universal testing machine. Load readings were taken directly from the machine load cell which had been calibrated according to BS 1610. To measure strain, a resistance strain gauge was attached to the specimen surface within the gauge length. Technimeasure gauge types FLA-3.23 and CFLA-3.350 were used for the +20°C and -55°C tests respectively. A second specimen, with a gauge attached, was placed close to the active specimen and connected into the bridge circuit to eliminate thermal expansion effects. A bridge amplifier supplied the dc voltage and amplified the output. An x-y plotter fed with the strain and load signals was used to record the results.

Unfortunately, the strain gauges used could only measure strains of up to 3%. Therefore only information up to just beyond the yield point could be recorded in this manner. This was sufficient since the theoretical analysis can only model elastic adherends.

The coefficients of linear expansion due to temperature were determined by placing one specimen inside and the other outside the chamber. Then a temperature differential was created between the two by cooling the chamber.

6.2.1 **Aluminium**

An unclad aluminium alloy conforming to BS L164 has been used. Tensile test specimens were machined to the British Standard BS 18 as shown in Fig. 6.2. The specimen thickness was equal to the sheet (and joint) thickness of 2mm.

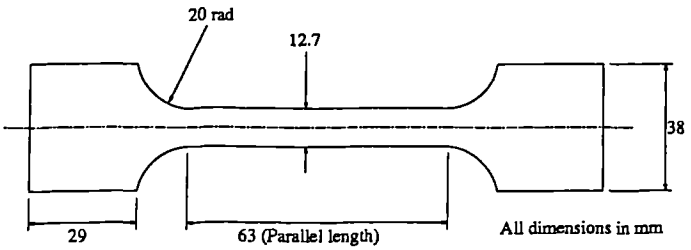

Fig. 6.2 *Aluminium tensile specimen dimensions*

The test results did not indicate any difference in mechanical properties when the Aluminium was cooled to -55°C from room temperature. The material properties are listed in Table 6.1. A Poisson ratio of 0.33, taken from the literature, has been assumed.

Young's Modulus E (GPa)	Shear Modulus G (GPa)	Proof Stress (GPa)	Tensile Strength (GPa)	Expansion Coefficient
75	29	280	560	22×10^{-6}/°C

Table 6.1 *Aluminium mechanical properties*

The coefficient of linear expansion is slightly lower the usual value of 23×10^{-6}/°C. Since the difference is less than 5% it is difficult judge whether it is an intrinsic material property or experimental error.

The tensile test gave a Young's modulus of 78 GPa which suggested a high modulus grade of Aluminium. To check this modulus value, a small free-free beam was vibrated and the first resonant frequency, f, measured. For a beam of length l, density ρ and thickness h, the Young's modulus, E, is given by the relationship

$$E = \frac{f^2 l^2}{kh^2} \rho$$

where k = 1.055 for the first mode of vibration. For the Aluminium beam used, a Young's modulus of 75 GPa was obtained. This value has been used in preference to the tensile test result since the latter test will have been less accurate due to errors in calibration and measurement.

6.2.2 **CFRP**

The unidirectional CFRP sheets were supplied by the Royal Aircraft Establishment (RAE) in Farnborough. The manufacturing details were as follows:

Fibre :	Courtlands XAS
Resin :	Ciba-Geigy 914
Prepreg :	Fibredux 914-CXAS10K-5-34%
Cure :	Ramp rate 7°C/min to 175°C, 340 MPa applied at 80°C, cure 1 h at 175°C, 4 h post cure at 190°C

Standard test specimens, as shown in Fig. 6.3, were manufactured. The unidirectional sheets were tested across as well as along the fibre axis. The intention here was to check results with the available data rather than perform an exhaustive series of tests to determine the various moduli and Poisson ratio.

As with the aluminium there was no difference, beyond that attributable to data scatter, between the values measured at +20°C and -55°C. The measured values of E_x and E_y were found to be within 3% of the RAE data. It was therefore decided that for the remaining properties it would be safe to use the available data. The latter is listed in Table 6.2.

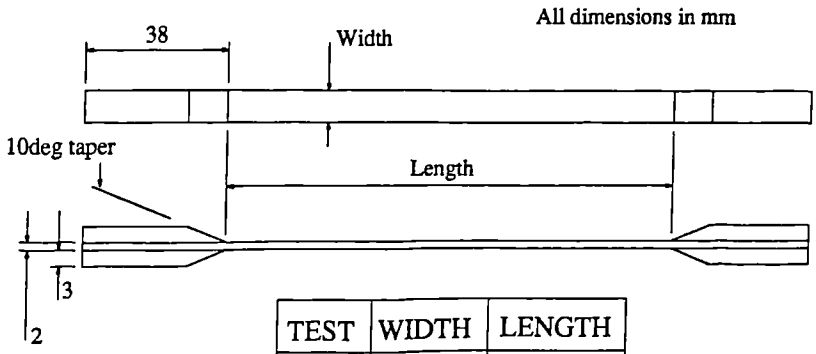

TEST	WIDTH	LENGTH
0	12.7	125
90	25.4	100

Fig. 6.3 *CFRP test specimen*

Long. Modulus E_x (GPa)	Trans. Modulus E_y (GPa)	Shear Modulus G (GPa)	Poisson ratio ν_x, ν_{xy}	Poisson ratio ν_y	Trans. Strength (MPa)
130	8.9	4.7	0.3	0.02	45

Coefficient of linear expansion = 7.5×10^{-6}/°C

Table 6.2 *Unidirectional CFRP mechanical properties*

6.3 ADHESIVES

Conventionally, to derive the mechanical data of a material, it is tested in bulk form. Manufacturing bulk specimen of certain adhesives can be difficult, if not impossible. Furthermore, the fundamental question of whether adhesive properties in thin film are the same as those found in bulk specimen remains unresolved (Adams and Wake, 1984).

On closer examination, the evidence indicates that the ambiguity may be due to the test method rather than any intrinsic material property differences (Adams and Coppendale, 1976, 1979). In order to test an adhesive in thin film form, some sort of joint is required. Examples of this are the thick adherend, butt joint and napkin ring test. The main problem with such methods is that it is difficult to achieve a uniform state of stress in the adhesive since the adherends will deform. Even though there have been efforts to overcome this problem by using thick adherends and measuring deformations with special extensometry (Krieger, 1980), it is not possible

to ensure a uniform stress state. Bulk specimens, on the other hand, do not suffer such problems. Furthermore, the fracture quantity obtained from bulk tests will be purely a property of the material, whereas in joints, fracture may be influenced by interfacial or geometric effects. It was decided, therefore, to endeavour to produce bulk adhesive specimen.

Another difficulty faced when testing adhesives is their loading rate dependant nature. Their behaviour can depend not only on whether the test is load-controlled or strain controlled but also on the actual rate. It is therefore important to simulate the loading conditions that will be exerted on the adhesive in a lap joint. In a thorough investigation, Coppendale (1977) used FEM to simulate a joint tensile test. From the load-time curve, he determined the stress-time and strain-time relationships within the joint using stress controlled and strain controlled adhesive curves respectively. He found that the rates of strain increase were far from linear whereas the rate of stress increase was constant. It was therefore concluded that the adhesive behaviour in a joint was best described by a curve obtained under stress (or load) controlled conditions. Consequently, adhesives have been tested here under load control.

The three adhesives tested were chosen for their contrasting mechanical properties. The intention was to test the analysis for different types of stress-strain curves. Araldite MY 750/HY 956 was chosen to represent a strong brittle adhesive while Araldite 2005 represented a moderately strong, ductile system. The third adhesive, Permabond VOX 501, was chosen for its low modulus and high ductility.

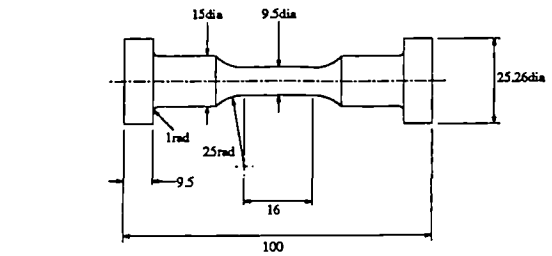

(a) Uniaxial tensile test specimen

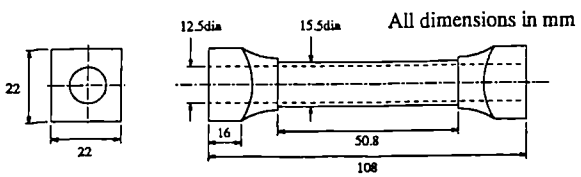

(b) Annular torsion test specimen

Fig. 6.4 *Adhesive tensile test specimen for (a) tensile and (b) torsion tests.*

The tensile tests were conducted on specimen of the type illustrated in Fig. 6.4a. These were produced by machining cylindrical casts of bulk adhesive. For comparison with tensile data, shear stress-strain data was also produced. This was achieved by testing an annular specimen (Fig. 6.4b) in torsion. The calculation of shear stress from the measured torque was based on the assumption that the shear stress varied linearly across the specimen wall thickness. The twist along the gauge length was measured with a potentiometer and converted to give values of shear strain.

The load controlled tensile tests were performed on a Dartec hydraulic universal testing machine at its lowest possible rate of 25N/s. Unfortunately, there was no arrangement available for a load controlled torsion test. Instead, a screw driven torsion rig, originally designed by Professor J.L.M. Morrison, has been used.

6.3.1 **Araldite MY750/HY 956**

This system consists of Araldite MY 750, an unmodified liquid epoxy resin and a hardener HY 956 (hydroxyalkylated polyamine), a liquid of moderately low viscosity. These were mixed in the manufacturer's recommended ratio of 100:25 by weight. Attempts to produce void free casts by degasing the mixture proved unsuccessful due to the relatively quick exothermic reaction of the system even at room temperature. Instead a procedure was followed whereby the materials were poured carefully and then mixed with a submerged paddle to minimise the formation of air bubbles. The mixture was then cured at 60°C for four hours. This was deemed sufficient to allow post curing and stabilisation of material properties. Otherwise, age hardening might occur causing the mechanical behaviour to be age dependent (Coppendale, 1977).

At room temperature (20°C), the extension was measured by two LVDT extensometers which were mounted on either side of the specimen. The ouput signals were averaged to reduce the error due to bending and recorded, along with the load cell output, on an x-y chart recorder.

Since the LVDTs were not designed to work at -55°C, a system of strain gauges was used. Gauges were mounted on either side of the specimen, again to reduce errors due to bending, and a second specimen was also connected into the bridge to reduce temperature effects.

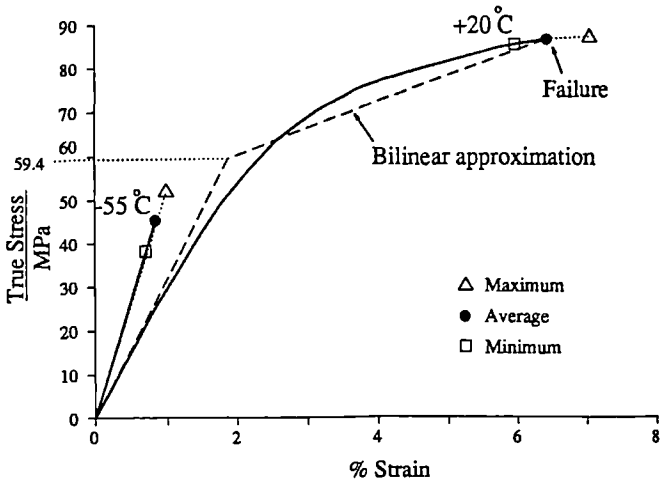

Fig. 6.5 *MY 750/HY 956 tensile stress strain curve*

The true stress strain curves derived from the tests are plotted in Fig. 6.5. At +20°C the material behaves in a linearly elastic manner until a stress of approximately 12 MPa and then exhibits non-linearity until a strain of 9%. Surprisingly, none of the specimen showed a significant amount of necking which suggested that the final strains were not entirely plastic. On unloading the specimen it was found that the material could sustain upto 4% strain without suffering permanent deformation.

This type of anelastic behaviour is common in polymers and the yield point is often difficult to determine. Usually, the yield stress is defined as the point where permanent deformation first begins. However many polymers yield at the point of maximum stress (Bowden, 1962 and Coppendale, 1977). Such behaviour is difficult to model and is not incorporated in the present theory. To overcome this problem, Raghava *et al* (1957) proposed a definition of the yield stress as the point where a line parallel to the initial curve but offset at a strain of 0.003 intersects the stress-strain curve.

At -55°C, MY 750/HY 956 is stiffer than at +20°C and behaves linearly before failing. Furthermore, the failure stress is almost halved. It should be noted that this is the average value. The failure stresses in fact ranged from 40 MPa up to 70 MPa.

Table 6.3 lists the failure quantities along with other properties including Young's modulus which was measured with the aid of strain gauges. The value reported for the shear modulus was determined from the shear-stress strain curve (Fig. 6.6).

Temperature (°C)	Young's Modulus E (GPa)	Shear Modulus G (GPa)	Maximum Stress (MPa)	Maximum Strain (%)	Maximum Plastic Strain (%)
+20	3.18	1.15	86.2	6.4	3.8
-50	5.62	2.0	45.2	0.85	-

Coefficient of expansion = 56.7×10^{-6}/°C

Table 6.3 *MY 750/HY 956 properties*

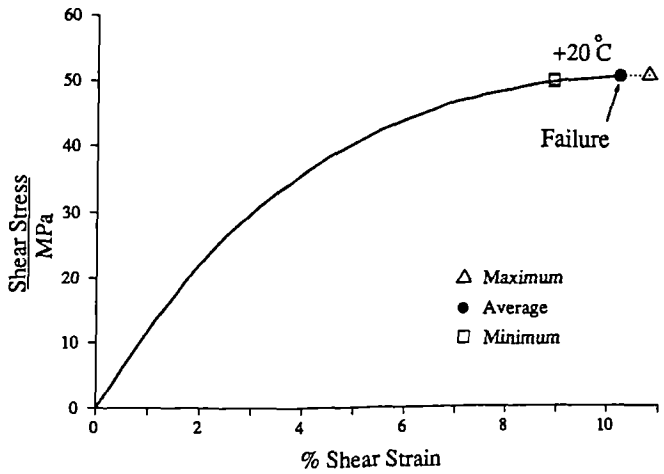

Fig. 6.6 *MY 750/HY 956 shear stress strain curve.*

The two moduli give a Poisson's ratio of 0.37 which is typical of epoxies. At 56.7×10^{-6}/°C, the expansion coefficient is within 1% of the literature values of 60×10^{-6}/°C.

6.3.2 Araldite 2005

This is a toughened epoxy consisting of Araldite 2005A, which is a modified epoxy paste, and hardener 2005B mixed in the ratio 100:50 by weight. It was intended to produce and test specimens in a manner identical to that outlined above for the MY 750/HY 956 adhesive. Unfortunately, it proved impossible to produce

acceptable void free castings. On the manufacturer's suggestion, this problem was overcome by substituting Araldite MY 750 for the 2005A epoxy.

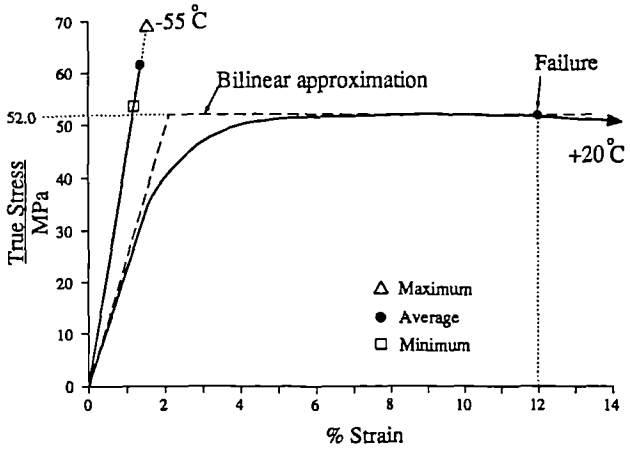

Fig. 6.7 *Araldite 2005 stress strain curve*

Fig 6.7 shows the stress strain curves for Araldite 2005 or rather, MY 750/2005B. The material behaviour at +20°C can be described as elastic, perfectly plastic. However, there is a disturbing drop in stress as the strain increases. This is disturbing because this is a load controlled test and therefore the load should not decrease. The suggestion is that the material plastic flow is too sudden for the testing machine to follow even though it was capable of moving the cross head at 2m/sec. It would therefore be plausible to conclude that failure occurred at the point where true stress begins to decrease. On this basis the average failure strain was found to be just under 12% as shown in Fig. 6.7.

Like the MY 750/HY 956 adhesive above, the behaviour at -55°C is brittle. Here, however, the final stress is higher than that observed at room temperature; this, and the other fracture quantities are given in Table 6.4.

Temperature (°C)	Young's Modulus E (GPa)	Shear Modulus G (GPa)	Maximum Stress (MPa)	Maximum Strain (%)	Maximum Plastic Strain (%)
+20	2.48	0.92	52.0	12.0	9.9
-50	4.6	1.68	62.4	1.3	-

Coefficient of expansion = 54.6×10^{-6}/°C

Table 6.4 *Araldite 2005 elastic properties*

The shear stress strain curve (Fig. 6.8) gives a shear modulus of 0.7 GPa. This value, when combined with the Young's modulus derived from the tensile test, 2.48 GPa, gives a Poisson's ratio of 0.77! Clearly one of the moduli is wrong. The evidence indicates that the torsion test result is unreliable because this gives a much lower strain energy to failure than the tensile test. Furthermore, buckling was noticed in the specimen during the test which suggests that the material was too soft to be tested in annular form.

Therefore, the shear modulus given in Table 6.4 has been extrapolated from the tensile test results. For this purpose, the Poisson's ratio was assumed to be 0.35. This is typical of the values used for the 2005 Adhesive (Harwell, 1986).

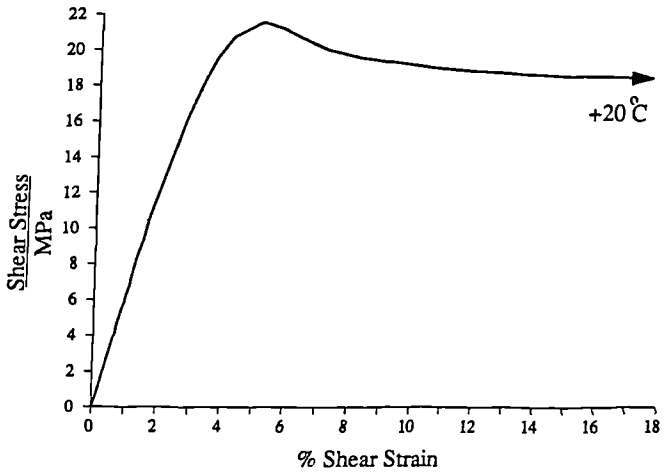

Fig. 6.8 *Araldite 2005 shear stress strain curve.*

6.3.3 **Permabond VOX 501**

Permabond VOX 501 is a viscous, two-part adhesive composed of a modified oxirane and various acrylic monomers. It is supplied in a cartridge which, when operated by a dispensing gun releases the components into a mixing nozzle.

The high viscosity leads to difficulties in producing void free bulk specimen of the size required. Instead, flat tension specimen were produced (see Fig 6.9). Therefore only tensile tests on the bulk adhesive were possible.

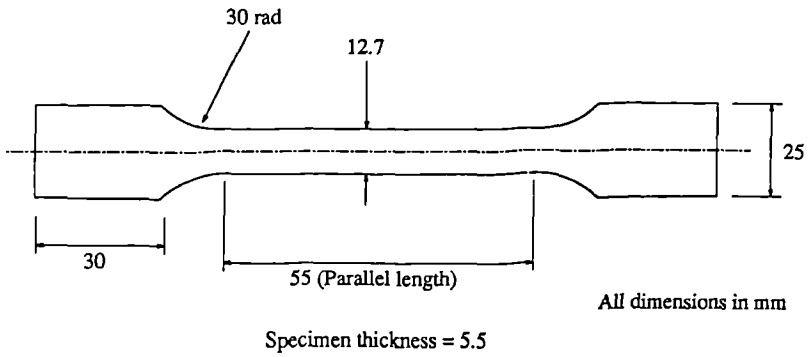

Fig 6.9 *Permabond VOX 501 specimen*

The flat specimens could only be tested in the Zwick testing machine and were therefore strain controlled. The tests were conducted at 3mm/min, which is a similar rate to that at which the joints were tested. Strains were measure by Techni-measure type YL-10 gauges. These could measure strains of up to 20%. Strains beyond 20% were determined from the cross head displacement.

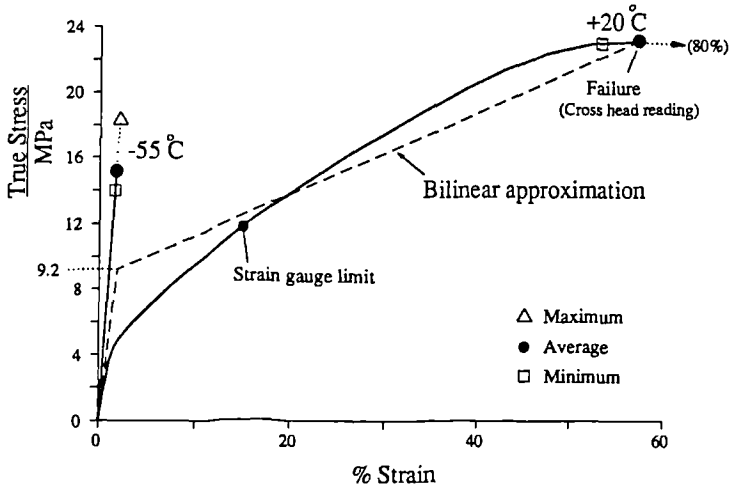

Fig. 6.10 *Permabond VOX 501 stress strain curve*

As the room temperature true stress-strain curve shows (Fig. 6.10) the material is extremely ductile, exhibiting almost 60% strain before failure. It is suspected that the true value might be higher since the specimen invariably failed at a void. The stress, on the other hand, appears to be at a peak.

In direct contrast, the material is very brittle at -55°C and hardly deforms before failure. Moreover, the stress at failure is lower than at room temperature (Table 6.5). This result is probably due to the presence of voids which would be more critical at low temperatures due to the brittle nature of the material.

It was not possible to produce bulk VOX 501 for shear testing. The shear modulus given in Table 6.5 has been calculated from the tensile modulus by assuming a value of 0.37 for the Poisson's ratio.

Temperature (°C)	Young's Modulus E (GPa)	Shear Modulus G (GPa)	Maximum Stress (MPa)	Maximum Strain (%)	Maximum Plastic Strain (%)
+20	0.49	0.18	23.1	57	52.3
-50	0.9	0.33	15	1.1	-

Coefficient of expansion = 60.0×10^{-6}/°C

Table 6.5 *Permabond VOX 501 elastic properties*

6.4 DISCUSSION

As stated above, at least six specimen were tested for each configuration. In each test it was found that while every specimen followed an almost identical stress-strain curve, the point of failure varied considerably. This was particularly true of the cold tests. The logical explanation is that the specimen contained defects, such as voids, thus causing the observed scatter. Such defects would exacerbate the situation in cold tests where the material is extremely brittle and highly susceptible to fracture at a flaw.

Whatever the cause of the scatter may be, a failure quantity is required from the tests. In choosing the average value, the presumption here is that similar defects will arise in joints. Nonetheless it must be recognised that there is a greater chance of having voids in bulk specimens than in the thin glue line.

For the room temperature curves, the scatter is unlikely significantly to alter the failure criterion. For example, the MY 750/HY 956 adhesive failed, on average, at a strain of 6.4%. The maximum observed deviation from this was a value of 7.0% which is within 10% of the average. In the cold tests however, values were found to deviate by up to 40% from the average. The suggestion is that a uniaxial tensile test can give most of the stress-strain curve but not the failure point. Some sort of fracture test (and specimen) might be more

appropriate for this purpose. Unfortunately, fracture tests can at best give an indication of stress to failure but not strain.

Chapter 7

FAILURE ANALYSIS OF SINGLE LAP CFRP/ALUMINIUM JOINTS

The accuracy of the present stress analysis was judged earlier (in Chapters 4 & 5) by correlating results with the FEM. This chapter attempts a more thorough validation by comparing predicted joint strength with experimental measurements. To this end, single lap joints between CFRP/Aluminium adherends, bonded by three mechanically contrasting adhesives, have been tested to failure at two temperatures, +20°C and -55°C. As mentioned in the previous chapter, the joint and temperatures are typical for aircraft structures.

The present theory predicts stresses and strains, not joint strengths. A failure criterion is necessary to interpret these distributions for strength prediction. Unfortunately, there is no universal criterion which is applicable to all possible modes of failure. Instead, there exist several criteria; those which can be applied to the present theory are described in the next section. Strengths are then predicted according to each criterion and the results compared with measured values. From this study conclusions are drawn regarding the accuracy of the method in predicting the various modes of failure.

7.1 FAILURE CRITERIA

There are, generally speaking, two approaches to predicting failure in a structure. One method assumes that the material contains some inherent flaws or cracks and that failure occurs when they propagate. Such methods make use of fracture mechanics (FM) to predict crack initiation and thus failure.

There are two serious drawbacks in applying FM to joints. First, FM was initially developed to predict failure in brittle materials and later extended by Hutchinson (1968) and by Rice and Rosengren (1968) to elasto-plastic materials. In joints, the crack is considered to be at or near the adhesive-adherend interface. For brittle (and elastic) adhesives it is possible to apply FM to calculate the stress intensity (or energy) at the crack due to a load and then to relate this to a material fracture quantity. However, when the adhesive is elasto-plastic, the basic assumption of FM is undermined since the plastic region in front of the crack is not in a continuum but it is at or very close to a bi-material interface. Therefore, it is not *rigourously* possible to relate the work done by

a given load to crack propagation. However, the adherend is often more than 20 times as stiff as the adhesive, so that much of the plastic deformation will be in the adhesive. This would explain the success Chen (1985) and Groth (1987) among other have had in predicting joint failure for elasto-plastic materials using FM.

The other drawback of FM, of greater concern here, is the need to consider a crack in the stress analysis. Since there is no such provision in the present model, an alternative approach is sought. In any case, the adhesive layer is usually an uncracked continuum. Continuum failure criteria, which are failure surfaces in three-dimensional stress or strain space, are an alternative.

7.1.1 **Failure Criteria in uncracked continuum**

In an adhesive joint there are three distinct types of failure mode. Failure may occur at the interface (adhesive failure) or within the adhesive layer (cohesive failure). Alternatively the adherend itself may fail. However, if surfaces are properly prepared then adhesive failure will be seldom (Adams, 1986). Adherend failure is also rare unless the material is a laminate, in which case transverse failure is possible. Therefore, in the present work, cohesive failure and laminate failure criteria are considered.

The purpose of a failure criterion is to predict from the behaviour of materials in a *simple tensile (or shear test)* when failure will occur under any condition of applied stress. By far the most debatable quantity obtained from the tensile test is failure. While maximum values of stress, strain or energy determined from the test give a good indication for brittle materials, there is a lack of understanding as to what these values mean in ductile materials. Some of the difficulty is due to a lack of knowledge of stress distribution in front of cracks and inclusions within the material. For this reason, there exist a number of failure criteria. The following criteria have been applied to the present theory:

(a) **Stress** - The three dimensional state of stress at a point can be resolved not only to give the maximum principal or shear stress but also the strain energy or distortion energy. When considering yield (section 5.1), the modified von Mises criterion was used. This has been extended to give the following failure criterion:

$$\sigma_{max} = \sqrt{(3J_2)} \tag{7.1}$$

where σ_{max} is the maximum stress given by the uniaxial test.

$$J_2 = {}^1/_2[(\sigma_x - J_1/3)^2 + (\sigma_y - J_1/3)^2 + (\sigma_z - J_1/3)^2 + (\tau_{xy})^2]$$

$$J_1 = \sigma_x + \sigma_y + \sigma_z$$

(b) **Strain** - Strain too can be resolved to give either maximum vectorial values or energy at a point. Since the von Mises criterion already gives an indication of the energy, it was decided to use a maximum principal tensile strain criterion:

$$\varepsilon_{max} = (\varepsilon_x + \varepsilon_y)/2 + \sqrt{[(\varepsilon_x - \varepsilon_y)^2/4 + \gamma^2/4]} \tag{7.2}$$

where ε_{max} is the maximum strain as determined from the uniaxial test.

(c) **Plastic strain** or **work** - In the incremental initial stress method employed here for elasto-plastic analysis, uniaxial plastic strain and work vectors are calculated (eqn (5.10) in 5.3). These may be related to the maximum uniaxial plastic strain and the area under the stress versus plastic strain curve respectively. These quantities are illustrated graphically in Fig. 7.1.

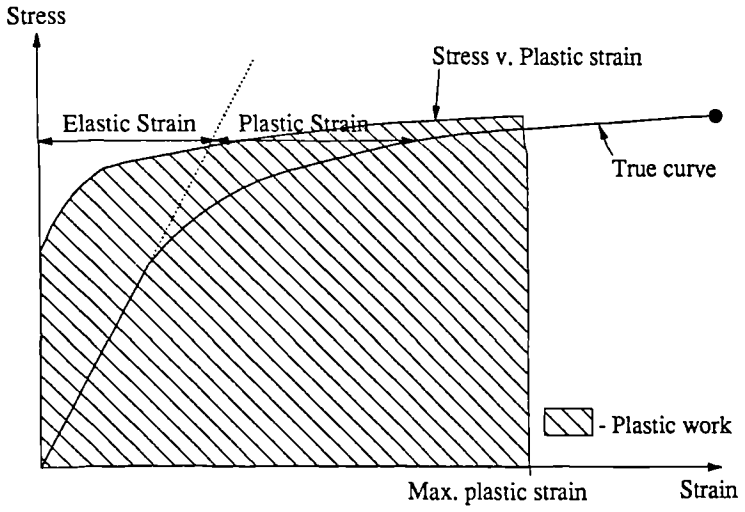

Fig. 7.1 *Derivation of the stress versus plastic strain curve from a uniaxial tensile stress-strain curve.*

There should be no difference between these two criteria since a value of plastic strain corresponds to a unique amount of plastic work. Any disparity indicates an error in the numerical solution, probably caused by taking too large an increment of load.

(d) **Peel Stress** - Experimental observations suggest that failure in unidirectional CFRP adherends is due to transverse stress. It was therefore decided to relate the peel stresses at the interface, where they are a maximum, to the CFRP transverse strength.

7.1.2 Effective Modulus method

For their elasto-plastic solutions, Hart-Smith (1973b) and Grant and Taig (1976) suggest a shear strain to failure criterion. As Hart-Smith states, this is, in fact a maximum shear strain energy criterion. Other yield (and failure) criteria, such as the von Mises, are also based on shear, or distortion, energy. If a maximum shear energy failure criterion is valid, then it is now shown that it is possible to estimate the strength of joints, even for those with elasto-plastic adhesives, by simple closed form solutions.

First, it is necessary to make a few definitions. In a three-dimensional principal stress system, the total strain energy, U, and shear strain energy, U^*, are defined as:

$$U = [\sigma_1^2 + \sigma_2^2 + \sigma_3^2 - 2\nu(\sigma_1\sigma_2 + \sigma_2\sigma_3 + \sigma_3\sigma_1)]/2E$$

$$U^* = [\sigma_1^2 + \sigma_2^2 + \sigma_3^2 - \nu(\sigma_1\sigma_2 + \sigma_2\sigma_3 + \sigma_3\sigma_1)]/6G$$

In a uniaxial test, $\sigma_1 = \sigma$, $\sigma_2 = 0$, $\sigma_3 = 0$, so

$$U = \frac{\sigma^2}{2E} \tag{7.5}$$

$$U^* = \frac{\sigma^2}{6G} \tag{7.6}$$

Eliminating σ from eqns (7.5) and (7.6) we have the following relationship between the two energies in a tensile test:

$$U^* = U\,\frac{2(1+\nu)}{3} \tag{7.7}$$

The total strain energy U in a tensile test is simply the area under the stress strain curve. It should be noted that eqn (7.7) is only approximate since the Poisson's ratio, assumed constant here, will vary when the material is plastic.

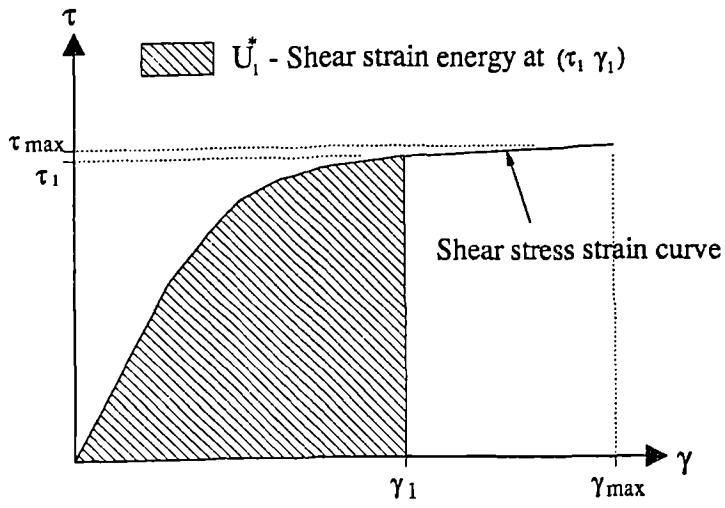

Fig. 7.2 *A shear stress strain curve.*

Consider now the behaviour of a material in shear (Fig. 7.2). Then, for a given shear strain γ_1, there can only be one corresponding value of shear stress, τ_1. But γ_1 also describes a unique shear strain energy, U^*_1. Thus, the maximum value of shear strain, γ_{max}, directly corresponds to the maximum value of shear energy.

The problem now reduces to one of predicting the shear strain within the adhesive accurately. If the material is ductile, then an elasto-plastic analysis is usually necessary. However elastic solutions can, by suitable modification, be used to estimate the shear strains, even when the adhesive is plastic.

This is possible because the *shape* of the shear strain distributions in a lap joint is the same whether the adhesive stress-strain curve is elastic or elasto-plastic. Fig. 7.3a shows three theoretical adhesive tensile stress-strain curves which describe an equal shear strain energy to failure. The shear stress and strain distributions, obtained from a finite element analysis of an Aluminium-Aluminium single lap joint, are shown in Fig. 7.3.

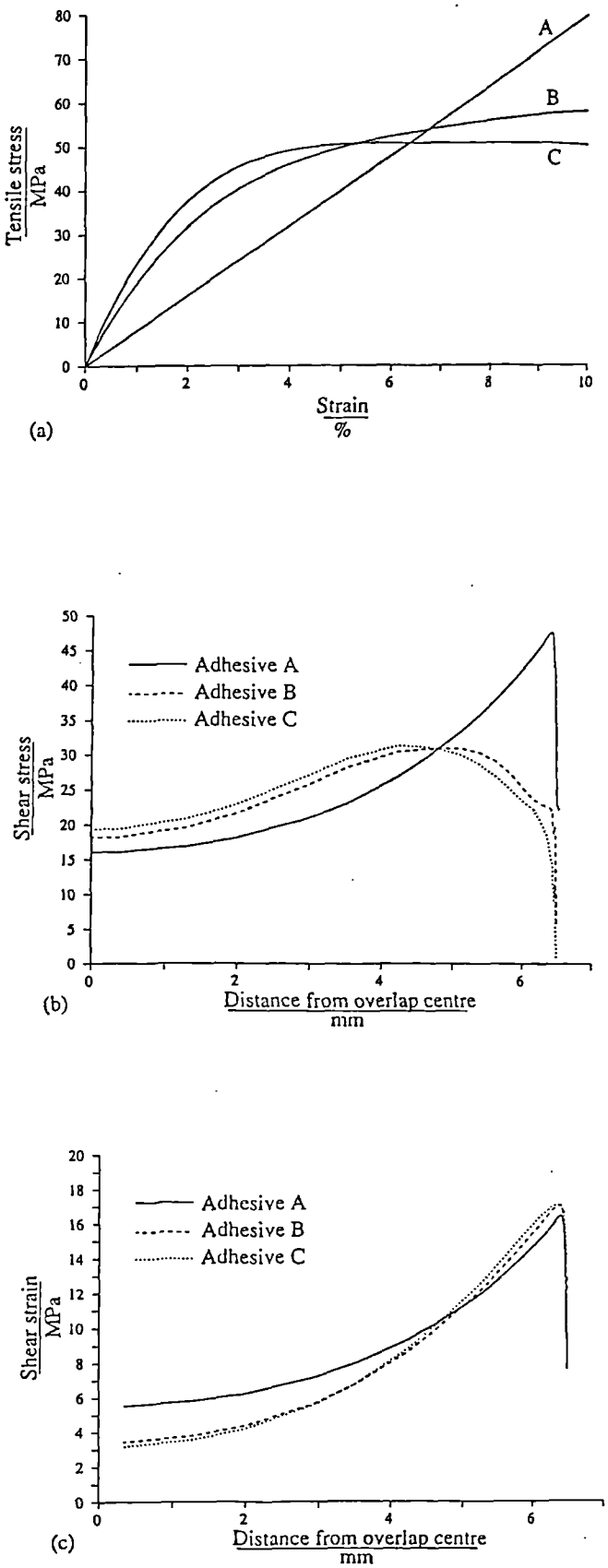

Fig. 7.3 *(a) Theoretical adhesives curves and the resulting single lap joint shear (a) stress and (b) strain distributions for a load of 8.5kN.*

It can be seen that while the maximum shear stress is dependent on the curve used, the *maximum* shear strains are all within 5% of each other. This result suggests that the maximum shear strain in a joint is dependent, not on the shape of the stress-strain curve, but on the total shear strain energy described. Significantly, one of the adhesive stress-strain curves, A (Fig. 7.3), is linear. Therefore maximum shear strains can be estimated with an *elastic* analysis by using a linear curve which describes the same shear strain energy to failure, U^*, as the true tensile stress-strain curve.

The gradient of this linear curve, termed the Effective Young's Modulus (E_{eff}), is given by the expression (see Fig. 7.4):

$$E_{eff} = \frac{2U^*}{\varepsilon^2_{max}} \tag{7.8}$$

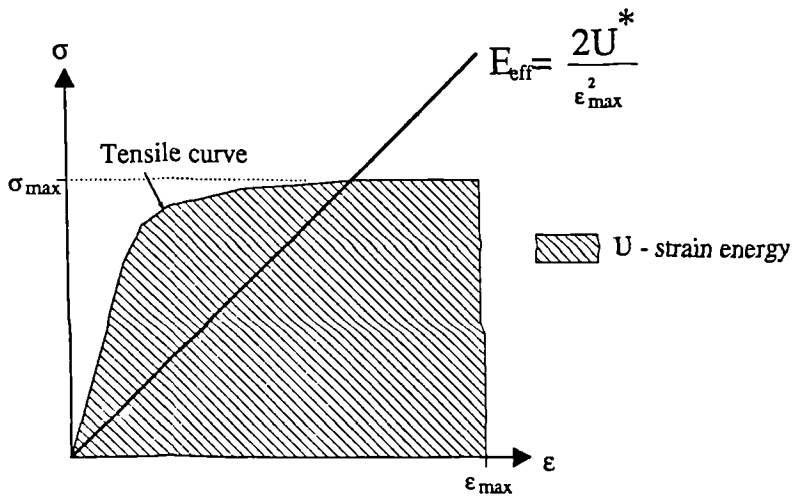

Fig. 7.4 *Definition of the Effective Young's Modulus.*

The Effective Shear Modulus (G_{eff}) is given by the usual relationship:

$$G_{eff} = \frac{E_{eff}}{2(1+\nu)} \tag{7.9}$$

When employing the Effective Modulus Method (EMM), γ_{max}, the value of the maximum shear strain to be used as a failure criterion, must be chosen with care. If γ_{max} is to correspond to the maximum shear strain energy, U^*, then

$$\gamma^2_{max} = \frac{2U^*}{E_{eff}} \tag{7.10}$$

Substituting eqn (7.8) into eqn (7.10) implies the following relationship between maximum snear and tensile strains:

$$\gamma_{max} = \varepsilon_{max}\sqrt{[2(1+\nu)]} \tag{7.11}$$

Thus, for typical adhesives ($\nu \approx 0.3$ to 0.4) maximum shear strains should be 60% to 70% greater than tensile strains. Experimental evidence (Harris, 1983) suggests that shear strains are even larger than this simple equation predicts. As stated earlier, one source of error may be the assumption of a constant Poisson's ratio even when the adhesive is plastic.

In any case, if the EMM is to work for lap joints, then elastic theories ought to predict values of shear strains that are close to those obtained by the more powerful non-linear FEM. In order to judge whether this is the case, results from FEM have been compared with the EMM (applied to Allman) for two theoretical adhesive curves which represent extremes of adhesive behaviour.

Curve A (Fig. 7.5a) represents a stiff low strain to failure material, whereas curve B represents a material with low modulus and a high strain to failure. The FEA was conducted with a large displacement solution. The results are presented in Figs. 7.5b,c. The peak strains are in close agreement, in fact within 3% for adhesive A and 5% for adhesive B. The success of this approach for strength prediction has been demonstrated by Mallick and Adams for balanced double (1987) and single (1989) lap joints. It remains to be seen whether the EMM is applicable to the unbalanced CFRP/Aluminium joint considered here.

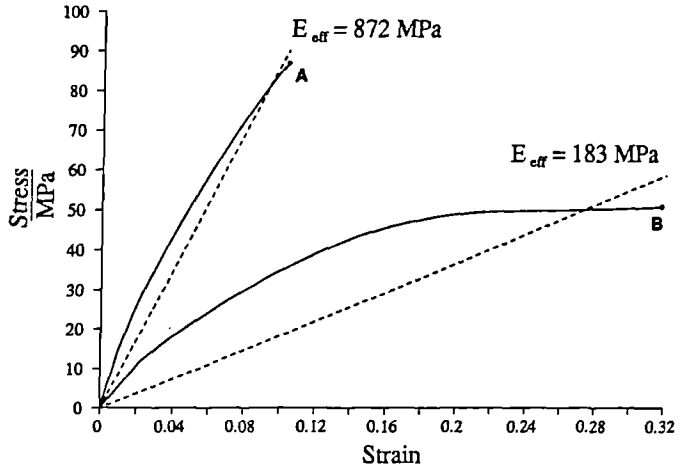

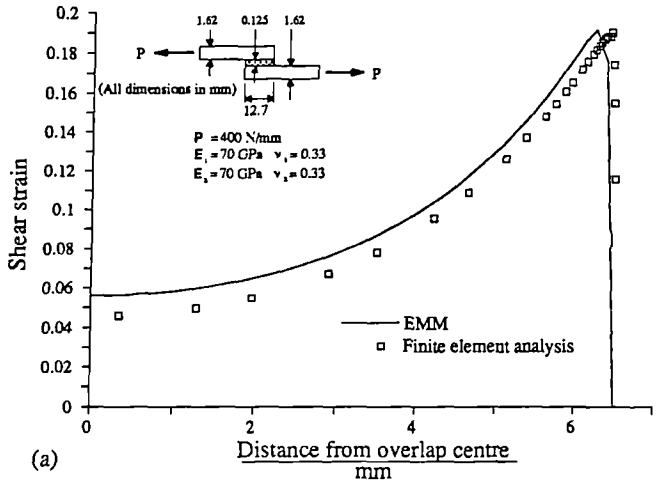

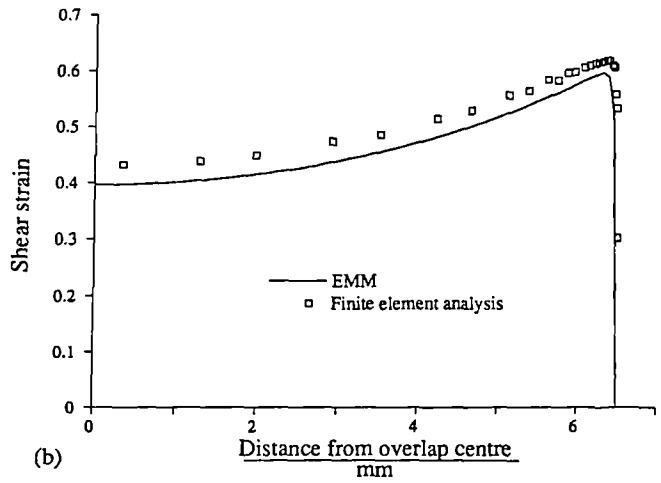

Fig. 7.5 *(a) Stress-strain curves for theoretical adhesives A and B and resulting joint shear strains: (b) adhesive A and (c) adhesive B.*

7.2 FAILURE ANALYSIS

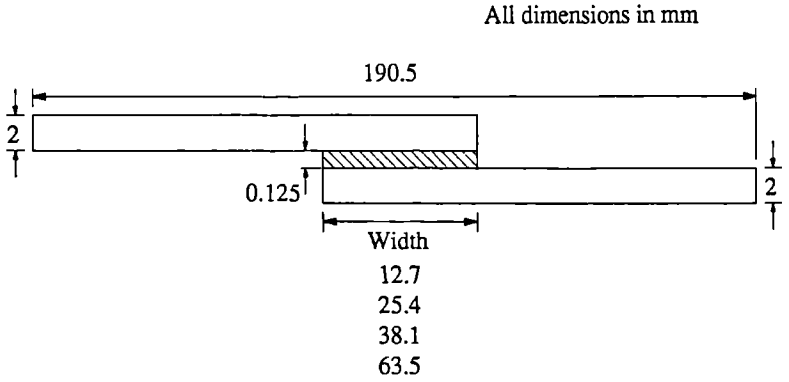

Fig. 7.6 *Geometry of the single lap joints tested*

Single lap joints between aluminium and CFRP adherends (Fig. 7.6) were tested to failure in a Zwick screw-driven universal testing machine. Joints were tested at various overlap lengths and for three mechanically contrasting adhesives cured at +60°C. In addition, tests were conducted at room (+20°C) and low (-55°C) temperatures using the rig described in section 6.1. The adherend and adhesive material properties at these temperatures are given in the previous chapter. In the analysis, thermal stresses were considered by setting ΔT = Cure(°C) - Operating(°C). This gave ΔT = -40°C and ΔT = -115°C for the room and low temperature cases respectively. For strength prediction, a bilinear approximation (see section 5.4) to the adhesive elasto-plastic behaviour was used. The failure criteria were applied at every Gauss point in the adhesive except for the composite failure, in which case the peel stress at the interface was calculated.

7.2.1 MY 750/HY 956

The predicted and measured strengths for joints with the MY 750/HY 956 adhesive at room temperature are compared graphically in Fig. 7.7.

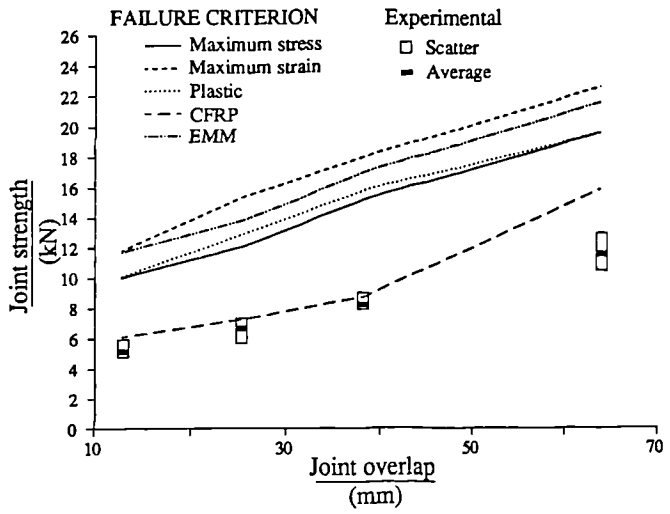

Fig. 7.7 *Predicted and experimental mean strength for joints with MY 750/HY 956 at +20 ℃*

One noticeable feature is that the strain criterion predicts slightly higher strengths than the maximum stress. The suggestion that points of maximum stress are not necessarily at maximum strain can be partly explained by the fact that the joint contains thermal strains. While the strains alone are not harmful, they give rise to stresses which are. Therefore, the stress criterion will generally predict lower strengths.

The predictions suggest that the composite is more likely to fail before the adhesive. Examples of adherend surfaces after joint failure are shown in Plate 7.1a. In the case of the MY 750/HY 956 joint at room temperature, the Aluminium is covered by composite suggesting that failure might indeed have occurred in the composite.

The accuracy of the composite failure predictions is good except at the largest overlap. This is not surprising since, at large overlaps, the adherends will be slightly bent due to the thermal mismatch. Compounding this with the fact that the overlap can no longer be treated as rigid will undermine the basis of the edge bending moment calculations (section 4.1.3). In ignoring these detrimental effects, the theory overestimates the joint strength.

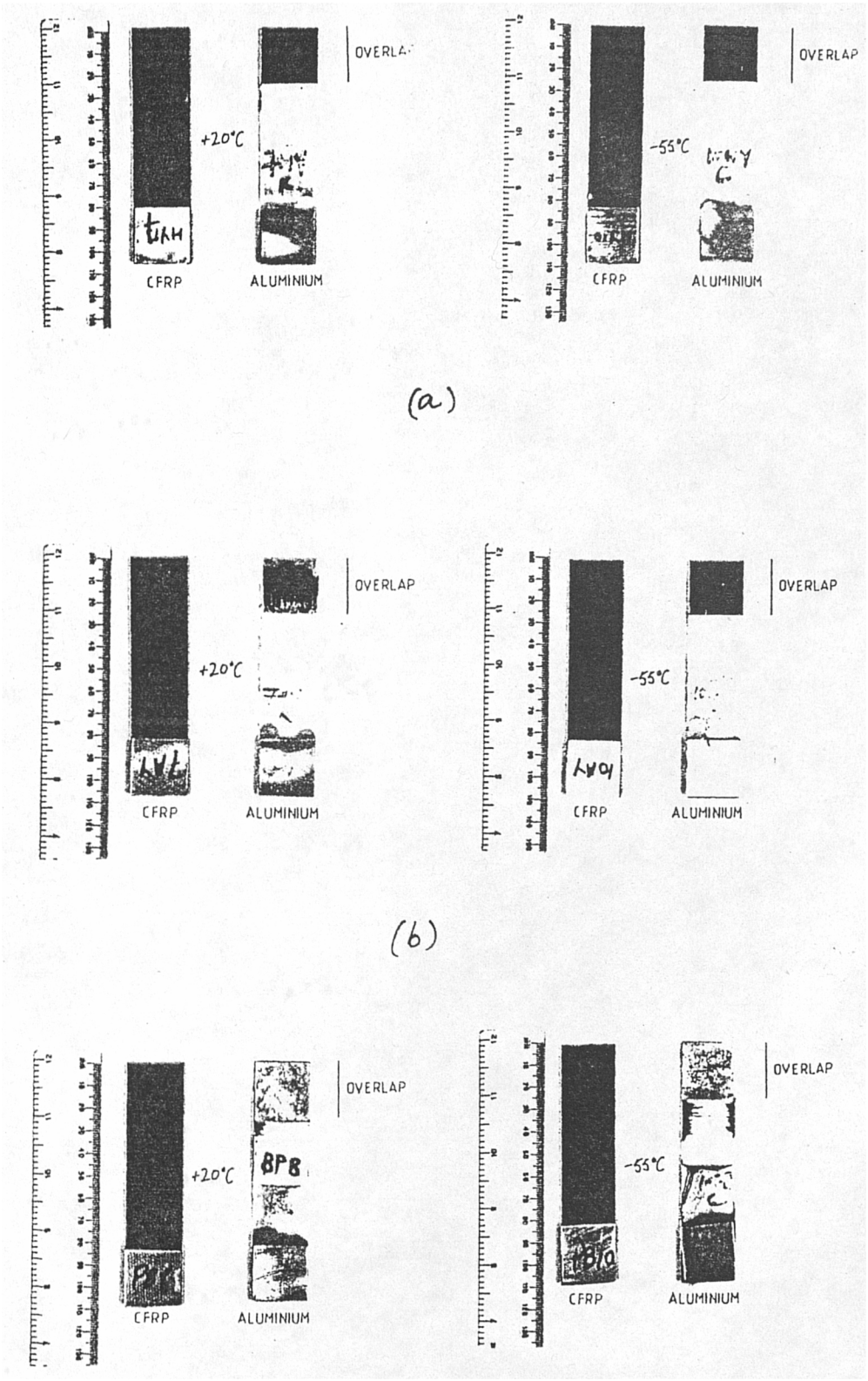

Plate 7.1 *Examples of adherend surfaces after joint failure: Joints with (a) MY 750/HY 956 (b) MY 750/2005B and (c) VOX 501.*

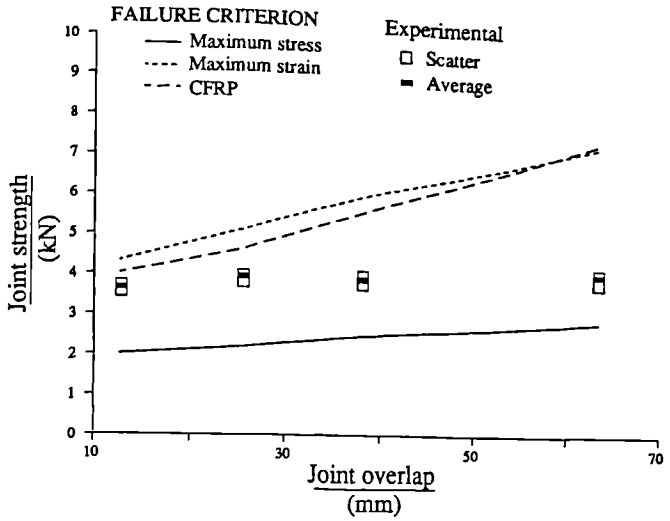

Fig. 7.8 *Predicted and experimental mean strength for joints with MY 750/HY 956 at -55 ℃*

At the low temperature, the adhesive behaves in an elastic, brittle manner (section 6.3.1). Theoretical predictions were therefore based on an elastic analysis and are compared with experiment in Fig. 7.8. The theory predicts failure will occur in the adhesive whereas the observed mode appeared to be composite failure (Plate 7.1a). However, it is difficult to be certain of the failure mode from a study of the adherend surfaces since failure may have begun in the adhesive and progressed along the composite.

If it is assumed that failure occurs in the composite, then predicted strengths are too high. Therefore, the present analysis, in conjunction with the data available, is unable to provide a conclusive explanation of MY 750/HY 956 joint failures at low temperatures.

7.2.2 **MY 750/2005B**

At room temperature, MY 750/2005B behaves in an elastic perfectly plastic manner and can withstand a stress of 52 MPa. This is similar to the transverse strength of the composite (45 MPa). Therefore, failure in either the adhesive or composite can be expected without resorting to an analysis.

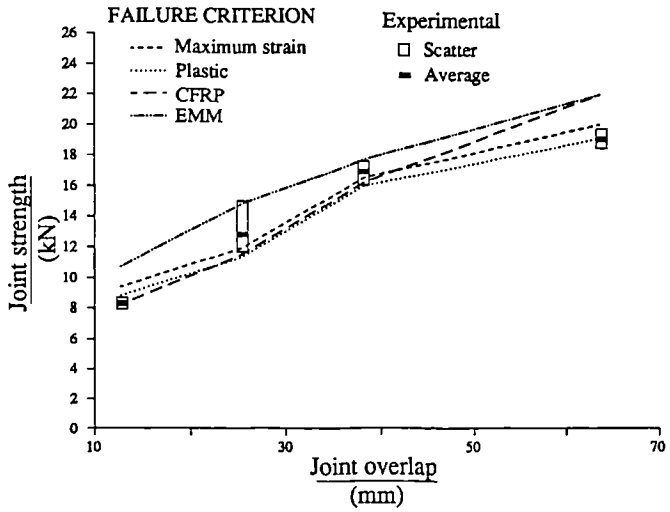

Fig. 7.9 *Predicted and experimental mean strength for joints with MY 750/2005B at +20 °C*

The theoretical and experimental predictions are compared in Fig. 7.9. A maximum stress criterion is not included since the adhesive is perfectly plastic. As with MY 750/HY 956, the maximum strain criterion overestimates the strength slightly. The plastic field appears to be a better guide to adhesive failure since the predictions are very close to the experimental values. At most overlaps, however, there is little difference in the predictions between composite and adhesive failure. A typical failure surface is shown in Plate 7.1b. It is difficult to establish the mode of failure from this since there are traces of both composite and adhesive on the Aluminium surface.

Since the failure may have been in the adhesive, strength predictions based on the EMM are included in Fig. 7.9. The predictions are within 15% which suggests that the method can be used to estimate strength for this type of joint.

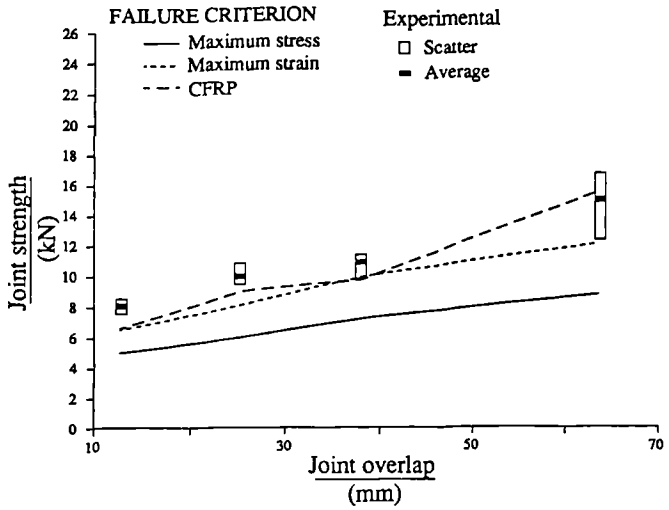

Fig. 7.10 *Predicted and experimental mean strength for joints with MY 750/2005B at -55 ℃*

The strengths at -55°C are compared in Fig 7.10. From the failure surfaces (Plate 7.1b), it was not possible to establish where failure began. The theory predicts failure in the adhesive, but at lower loads than were observed. This discrepancy probably arises from using the failure quantity measured in the bulk specimen. If composite failure is assumed, then the theoretical results are in better agreement with experiment. Even so, the predictions are underestimates, suggesting the theoretical stresses are too large. This can easily occur at singularity points in a linear analysis such as this since the stress relieving mechanism of plastic deformation is not allowed to occur.

7.2.3 **VOX 501**

The room temperature predicted and measured strengths are given in Fig. 7.11. The theoretical stresses at the interface were too low to predict composite failure even at high loads. This is not surprising considering the fact that the maximum stress that VOX 501 can sustain (23MPa) is much lower than the composite transverse strength (45MPa). Therefore, a composite failure criterion is not included in Fig. 7.11.

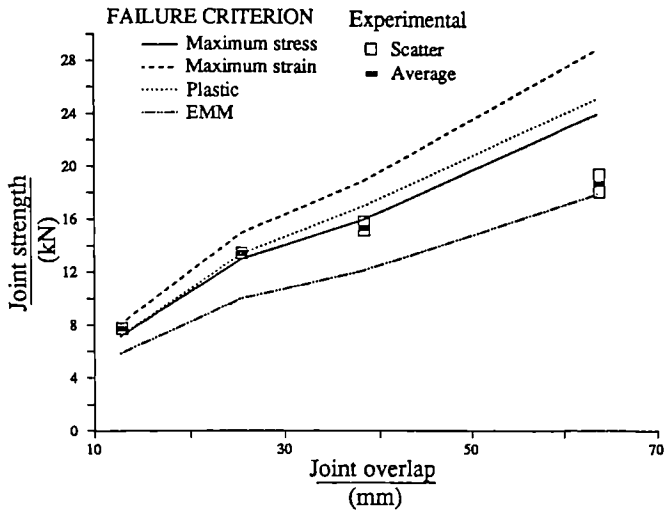

Fig. 7.11 *Predicted and experimental mean strength for joints with VOX 501 at 20 ℃*

Adhesive failure based on maximum strain is once again found to be an overestimate. The remaining criteria, maximum stress and plastic strain/work give very similar strengths. These compare very well with experiment except at the large overlap. This is very encouraging since it shows that the theory is able to predict strength even when the adhesive exhibits an excessive amount of plasticity. Less accurate is the EMM which underestimates strength by upto 25%. Nevertheless it does provide an estimate even for this extremely ductile adhesive.

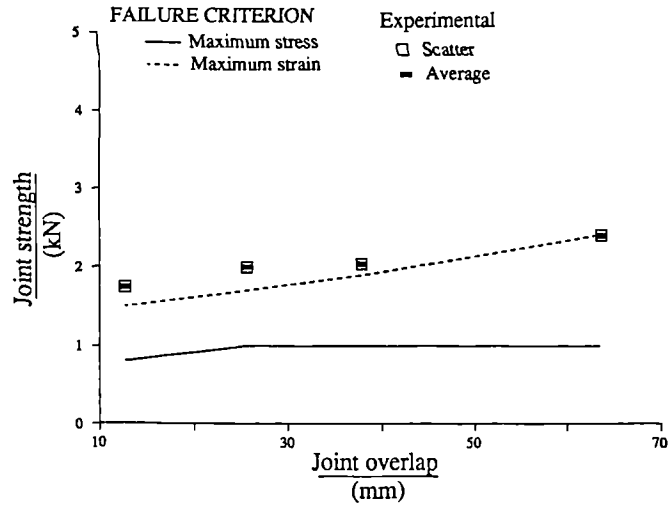

Fig. 7.12 *Predicted and experimental mean strength for joints with VOX 501 at -55 ℃*

At -55°C, the theoretical strengths, based on maximum stress, are lower than those observed, as shown in Fig. 7.12, whereas the predictions based on the maximum strain criterion agree well with experiment.

VOX 501 is an excellent example of the beneficial effect of ductility. At +20°C it is able to withstand large amounts of deformation which results in high joint strengths. At -55°C, however, the material supports a similar stress but hardly deforms before failure (Fig. 6.10). The resulting joint strength is significantly lower.

7.3 DISCUSSION AND CONCLUSIONS

Clearly, the present method can successfully predict strengths for elasto-plastic adhesives at room temperature, despite the neglecting plasticity in the aluminium adherend. For most cases, predictions are within 5% of the experimental values. The main exception is the 63.5mm overlap which appears to be at the edge of the range of validity for the theory.

It is not possible to identify one criterion for all the modes of failure. At room temperature, the plastic work and the maximum stress criteria seem appropriate. However, at -55°C, the material is brittle, thus the plastic criterion is invalid, while the maximum stress criterion is less accurate than maximum strain.

Through the use of a few simple continuum failure criteria, it has been found that the present theory is capable of accurate joint strength prediction for elasto-plastic adhesives. When material behaviour is brittle the predictions are less accurate. However, it has not been possible to establish whether this is due to a deficiency in the method. It is suspected that this is due to the unsatisfactory mechanical property data. As mentioned in the last chapter, the percentage deviation of the fracture quantities at +20°C was far less than at -55°C.

Finally, it was shown that adoption of a new approach, the Effective Modulus Method, enables joint strength to be estimated through a linear analysis even when the adhesive behaviour is non-linear.

Chapter 8

GENERAL DISCUSSION AND CONCLUSIONS

The lap shear joint is not only the most commonly occurring adhesive joint, but also the basis of a popular adhesive test. Knowledge of the stresses and strains in such a joint is important since it leads to an understanding of joint strength, thus enabling selection of design criteria and desirable adhesive properties. If the benefits of adhesive joints are to be enjoyed, then such knowledge should be accessible by the widest possible audience.

A review of the current lap joint stress analysis methods revealed that these were based either on simple, easy-to-use, closed form methods, or on numerical techniques such as the finite element method (FEM) which require specialist knowledge. The accuracy of the closed form solutions is limited by their inability to model the spew fillet, material plasticity and variations of stress through the adhesive thickness. Furthermore, the in-plane stresses in the adhesive are often ignored. These stresses are not insignificant and can influence adhesive plastic and thermal response. The use of FEM enables all of these effects to be considered. In addition, if large displacement FEM is used then the effect of joint rotation is more accurately analysed. The drawback with FEM is that it demands expensive computing power and requires specialist knowledge in the preparation of data and interpretation of results. It is therefore not generally accessible. It was concluded that there existed a need for an analysis which was as easy to use as the closed form solutions but approached the accuracy of FEM.

Such an analysis has been developed. It is in essence an equilibrium finite element method. The finite element is a adherend-adhesive-adherend sandwich with stress as the basic variable. With the numerical nature of the method a computer implementation of the solution is necessary. There is no disadvantage in this respect by comparison with the more useful closed form solutions which also require some form of computing power. The analysis improves on closed form methods by considering adhesive plasticity, in-plane stress and variation of stress through the adhesive thickness. The present method is capable of analysing a general joint consisting

of dissimilar adherends of unequal thickness. In addition, thermal deformation of both adherend and adhesive is incorporated.

The accuracy of the predicted distributions was established by means of a comparison with FEM results. The predictions were in close agreement except at points close to the overlap edges where mathematical singularities exist. At these points, the FEM stresses were always higher and it was concluded that the present method could not predict singular stresses. But it was felt that in a real joint singular stresses would be eliminated by the presence of a spew fillet or local plastic flow.

The thermal component of stress within a loaded lap joint is often neglected. Using the present method and FEM to study the nature of such stresses revealed that the stresses arising from a thermal mismatch between adherends are much greater than those due to adhesive thermal deformation. However, if the adhesive is very stiff, then adhesive deformation can give rise to significant stress.

Many modern adhesives exhibit a large degree of plastic deformation before failure. Therefore, if the present method is to be of use in strength prediction then such behaviour must be accommodated within the solution. This was achieved by incorporating Prandtl-Reuss plasticity through an initial stress approach. This study has been limited to consideration of plasticity in the adhesive layer. Theoretically, there is no difficulty in considering adherend plasticity. The only restriction is the available computing memory.

To measure the accuracy of the solution obtained, strengths were predicted for lap joints and compared with experiments for three mechanically contrasting adhesives. A single lap CFRP to Aluminium joint was used for the purpose. This joint, common in the aerospace industry, provided a particularly good test for the present theory since it consists of adherends dissimilar in terms of both mechanical and thermal properties. To test the thermal predictions, the joints were tested at room and low temperatures.

By the application of appropriate failure criterion, reasonable predictions of joint strength have been achieved at room temperature. At low temperatures, the predictions were less accurate. However, it was felt that the material data, rather than the analysis was to blame. The data was generated through conventional bulk specimen tensile tests. It was felt that these might be inappropriate since the fracture was brittle. Specimen

failure will therefore have been influenced by any voids present and by surface irregularities caused by the attached strain gauges . A need for an alternative test was identified.

To summarise: shortcomings in current methods of stress analysis have been identified. An alternative method has been proposed and implemented. The accuracy of the solution has been verified by a comparison with FEM predictions and experimental measurements.

Appendix I

IMPLEMENTATION OF THERMAL ANALYSIS IN FELDEP

A ELASTIC SOLUTION

In section 3.1 the FEM system equation was shown to be:

$$\{f\} = [K]\{\delta\}.$$

when thermal stresses are introduced this becomes (section 3.1.1):

$$\{f\} - \int_V [B]^T\{\sigma_0\}\, dv = [K]\{\delta\}$$

The difference can be viewed as subracting from the nodal load vector {f} an equivalent "*thermal load vector*":

$$\int_V [B]^T\{\sigma_0\}\, dv \qquad (A1.1)$$

To achieve this in FELDEP, a new subroutine. ELTHERM, was written. The routine calculates eqn (A1.1) at each gauss point for any given element and updates the global nodal load array. Since $\{\sigma_0\}=[D]^{-1}\{\varepsilon_t\}$, the thermal strain vector, $\{\varepsilon_t\}$, is required. This is held in a new array, ELDTSN(), which is calculated in PRELIM for each element.

The only other change required is at the stress calculation stage. At the end of a solution FELDEP stores the displacements in array $\{\delta\}$. From $\{\delta\}$, the strain, $\{\varepsilon\}$, is determined according to eqn (3.1). The stresses, when thermal strains are present, must be calculated according to eqn (3.9), repeated here for clarity:

$$\{\sigma\} = [D]^{-1}\{\varepsilon - \varepsilon_t\}.$$

It can be seen that the thermal strains $\{\varepsilon_t\}$ must be "removed" from the strain vector $\{\varepsilon\}$. Moreover, if a plain strain solution is sought then the σ_z stress component must be calculated according to the relation:

$$\sigma_z = \nu(\sigma_x + \sigma_y) - E\alpha\Delta T$$

In FELDEP these changes have been achieved by modifying the stress calculation routine ELSTR.

B PLASTIC CASE

In a plastic solution, FELDEP applies the load incrementally and then iterates within each increment until convergence. Thermal stresses are considered in exactly the same manner as described above except for one very important difference. The thermal load vector is applied at *only the first iteration* of any increment and the thermal strains are "removed" for stress calculation at the end of the *first iteration only*.

Appendix II

SHAPE FUNCTION ARRAY

A shape funtion array [**B**] is required such that it relates the stress fuctions throughout an element [Φ] to the nodal values [ϕ] (see section 3.4.3). To ensure equilibrium of stresses throughout the joint, the shape functions and their first derivative should display continuity inside and at the edge of each element. Element shape functions with this class of continuity are obtained when the stress functions are interpolated by cubic Hermitian polynomials between their nodal values. For the typical element of length 2l with end nodes numbered (i) and (i+1) (see Fig. 3.9) the expression for any of the stress functions ϕ_i (i = 1,2,3 or 4) is

$$\begin{aligned}\phi_i = {} & \frac{1}{2}\left[1 - \frac{3x}{2l} + \frac{x^3}{2l^3}\right]\phi_i^{(i)} \\ & + \frac{1}{4}\left[1 - \frac{x}{l} - \frac{x^2}{l^2} + \frac{x^3}{l^3}\right]\frac{d\phi_i^{(i)}}{dx} \\ & + \frac{1}{2}\left[1 + \frac{3x}{2l} + \frac{x^3}{2l^3}\right]\phi_i^{(i+1)} \\ & + \frac{1}{4}\left[-1 - \frac{x}{l} + \frac{x^2}{l^2} + \frac{x^3}{l^3}\right]\frac{d\phi_i^{(i+1)}}{dx}\end{aligned} \qquad \text{(A2.1)}$$

Now, $\{\Phi\} = [\mathbf{B}]\{\phi\}$, where

$\{\Phi\}_{12\times1} = \{\phi_1\ \phi_1'\ \phi_1''\ \phi_2\ \phi_2'\ \phi_2''\ \phi_3\ \phi_3'\ \phi_3''\ \phi_4\ \phi_4'\ \phi_4''\}^T$

$\{\phi\}_{16\times1} = \{\phi_1^{(i)}\ \phi_1'^{(i)}\ \phi_2^{(i)}\ \phi_2'^{(i)} \ldots\ldots \phi_4^{(i+1)}\ \phi_4'^{(i+1)}\}^T$

Substituting the shape function (A2.1) into this equation it is found that the matrix $[\mathbf{B}]_{12x16}$ is zero except at the points defined below:

$$B(1,1) = \frac{1}{2}\left[1 - \frac{3x}{2l} + \frac{x^3}{2l^3}\right]$$

$$B(2,1) = \frac{dB(1,1)}{dx}$$

$$B(3,1) = \frac{dB(2,1)}{dx}$$

$$B(1,2) = \frac{l}{4}\left[1 - \frac{x}{l} - \frac{x^2}{l^2} + \frac{x^3}{l^3}\right]$$

$$B(2,2) = \frac{dB(1,2)}{dx}$$

$$B(3,2) = \frac{dB(2,2)}{dx}$$

$$B(1,9) = + \frac{1}{2}\left[1 + \frac{3x}{2l} + \frac{x^3}{2l^3}\right]$$

$$B(2,9) = \frac{dB(1,9)}{dx}$$

$$B(3,9) = \frac{dB(2,9)}{dx}$$

$$B(1,10) = \frac{l}{4}\left[-1 - \frac{x}{l} + \frac{x^2}{l^2} + \frac{x^3}{l^3}\right]$$

$$B(2,10) = \frac{dB(1,10)}{dx}$$

$$B(3,10) = \frac{dB(2,10)}{dx}$$

$$B(i,j) = B(i-2,j-3)$$

for i = 4,5,6 j = 3,4,11,12
i = 7,8,9 j = 5,6,13,14
i = 10,11,12 j = 7,8,15,16

Appendix III

FORMULATION MATRICES

MODULUS MATRIX [D]

The formulation matrix [**D**] is a [9×9] matrix and is the elastic plain strain modulus array for the whole element. It is assembled from the individual adherend and adhesive modulus matrices. Therefore

$$[D] = \begin{bmatrix} [D_1] & & \\ & [D_a] & \\ & & [D_2] \end{bmatrix}$$

where

$$[D_a] = \frac{1}{E}\begin{bmatrix} (1-\nu^2) & -2(1+\nu)\nu & 0 \\ -2(1+\nu)\nu & (1-\nu^2) & 0 \\ 0 & 0 & 2(1+\nu) \end{bmatrix}$$

$$[D_i] = \begin{bmatrix} \dfrac{(1-\nu_{xyi}\nu_{yxi})}{E_{xi}} & -(1+\nu_{yzi})\dfrac{(E_{xi}\nu_{yxi}+E_{yi}\nu_{xyi})}{E_{xi}E_{yi}} & 0 \\ -(1+\nu_{yzi})\dfrac{(E_{xi}\nu_{yxi}+E_{yi}\nu_{xyi})}{E_{xi}E_{yi}} & \dfrac{(1-\nu^2_{xyi})}{E_{xi}} & 0 \\ 0 & 0 & \dfrac{1}{G_i} \end{bmatrix} \quad \text{for } i=1,2$$

ELEMENTAL MATRICES [F], [H]

If the joint is assumed to have unit width, then for each element

$$[F] = \int\int \frac{1}{2}([B]^T[N]^T[D]^{-1}[N][B])\,dxdy$$

$$[H] = \int\int -([B]^T[N]^T[D]^{-1}\{C(x)\} + [B]^T[N]^T\{\varepsilon_t\})\,dxdy$$

Here [**B**] is the shape function array given in Appendix II and [**D**] is the joint modulus array defined above. The arrays [**N**] {**C(x)**} depend on whether the joint is a single or double lap joint. Therefore [**F**] and [**H**] are

different for single and double lap joints and are listed explicitly below. In the case of the [F] array only the inner product, $[N]^T[D]^{-1}[N]$, is given since the full array can be calculated in core.

Single lap joint

The elements of the inner product of the [F] matrix, $[F']_{12\times12}$, are given below. Since the matrix is symmetric, only the diagonal and upper half are listed:

$F'(1,1) = 4h_1^2D(4,4)/t+6h_1^3D(4,4)/t^2+3h_1 4D(4,4)/t^3+h_1D(1,1),$

$F'(1,2) = 0,$

$F'(1,3) = (-2)h_1^2D(4,2)t/15+(-3)h_1^4D(4,2)/(10t)+(-3)h_1^3D(4,2)/5+h_1^3D(1,2)/6,$

$F'(1,4) = 4h_1^2D(4,4)/t+7h_1^3D(4,4)/t^2+4h_1^4D(4,4)/t^3+h_1D(1,1),$

$F'(1,5) = 0,$

$F'(1,6) = -h_1^2D(4,2)t/15-h_1^4D(4,2)/t/5+(-47)h_1^3D(4,2)/120+h_1^3D(1,2)/80,$

$F'(1,7) = -4h_1h2D(4,4)/t-6h_1h_2^2D(4,4)/t^2-6h_1^2h_2D(4,4)/t^2-6h_1^2h_2^2D(4,4)/t^3,$

$F'(1,8) = 0,$

$F'(1,9) = -h_1h_2D(4,2)t/30+3h_1^2h_2^2D(4,2)/(10t)+h_1h_2^2D(4,2)/20+h_1^2h_2D(4,2)/20,$

$F'(1,10) = 2h_1h_2D(4,4)/t+4h_1h_2^2D(4,4)/^2+3h_1^2h_2D(4,4)/t^2+4h_1^2h_2^2D(4,4)/t^3,$

$F'(1,11) = 0,$

$F'(1,12) = h_1h_2D(4,2)t/60-h_1^2h_2^2D(4,2)/t/5-h_1h_2^2D(4,2)/30-h_1^2h_2D(4,2)/40,$

$F'(2,2) = 2h_1^2D(6,6)t/15+3h_1^4D(6,6)/(10t)+h_1^3D(6,6)/10+h_1^3D(3,3)/3,$

$F'(2,3) = 0,$

$F'(2,4) = 0,$

$F'(2,5) = 2h_1^2D(6,6)t/15+2h_1^4D(6,6)/(5t)+7h_1^3D(6,6)/60+5h_1^3D(3,3)/12,$

$F'(2,6) = 0,$

$F'(2,7) = 0,$

$F'(2,8) = h_1h_2D(6,6)t/15+(-3)h_1^2h_2^2D(6,6)/(5t)-h_1h_2^2D(6,6)/10-h_1^2h_2D(6,6)/10,$

$F'(2,9) = 0,$

$F'(2,10) = 0,$

$F'(2,11) = -h_1h_2D(6,6)t/30+2h_1^2h_2^2D(6,6)/(5t)+h_1h_2^2D(6,6)/15+h_1^2h_2D(6,6)/20,$

$F'(2,12) = 0,$

$F'(3,3) = h_1^2D(4,4)^3/105+11h_1^3D(4,4)t^2/210+13h_1^4D(4,4)t/140+h_1^5D(2,2)/20,$

$F'(3,4) = -h_1^2D(4,2)t/15-h_1^4D(4,2)/t/5+(-37)h_1^3D(4,2)/120+h_1^3D(1,2)/24,$

$F'(3,5) = 0,$

$F'(3,6) = h_1^2D(4,4)^3/105+11h_1^3D(4,4)t^2/180+13h_1^4D(4,4)t/105+13h_1^5D(2,2)/180,$

$F'(3,7) = h_1h_2D(4,2)t/30+3h_1^2h_2^2D(4,2)/(10t)+h_1h_2^2D(4,2)/20+h_1^2h_2D(4,2)/20,$

$F'(3,8) = 0,$

$F'(3,9) = h_1h_2D(4,4)^3/70+13h_1h_2^2D(4,4)t^2/420+13h_1^2h_2D(4,4)t^2/420+9h_1^2h_2^2D(4,4)t/140,$

$F'(3,10) = h_1h_2D(4,2)t/60-h_1^2h_2^2D(4,2)/t/5-h_1h_2^2D(4,2)/30-h_1^2h_2D(4,2)/40,$

$F'(3,11) = 0,$

$F'(3,12) = -h_1h_2D(4,4)t^3/140+(-13)h_1h_2^2D(4,4)t^2/630+(-13)h_1^2h_2D(4,4)t^2/840+(-3)h_1^2h_2^2D(4,4)t/70,$

$F'(4,4) = h_1^2D(4,4)/t+2h_1^3D(4,4)/t^2+4h_1^4D(4,4)/(3t^3)+h_1D(1,1)/3,$

$F'(4,5) = 0,$

$F'(4,6) = -h_1^2D(4,2)t/30+(-2)h_1^4D(4,2)/(15t)-h_1^3D(4,2)/5+h_1^3D(1,2)/30,$

$F'(4,7) = -2h_1h_2D(4,4)/t-3h_1h_2^2D(4,4)/t^2-4h_1^2h_2D(4,4)/t^2-4h_1^2h_2^2D(4,4)/t^3,$

$F'(4,8) = 0,$

$F'(4,9) = -h_1h_2D(4,2)t/60+h_1^2h_2^2D(4,2)/t/5+h_1h_2^2D(4,2)/40+h_1^2h_2D(4,2)/30,$

$F'(4,10) = h_1h_2D(4,4)/t+2h_1h_2^2D(4,4)/t^2+2h_1^2h_2D(4,4)/t^2+8h_1^2h_2^2D(4,4)/(3t^3),$

$F'(4,11) = 0,$

$F'(4,12) = h_1h_2D(4,2)t/120+(-2)h_1^2h_2^2D(4,2)/(15t)-h_1h_2^2D(4,2)/60-h_1^2h_2D(4,2)/60,$

$F'(5,5) = h_1^2D(6,6)t/30+2h_1^4D(6,6)/(15t)+h_1^3D(6,6)/30+2h_1^3D(3,3)/15,$

$F'(5,6) = 0,$

$F'(5,7) = 0,$

$F'(5,8) = h_1h_2D(6,6)t/30+(-2)h_1^2h_2^2D(6,6)/(5t)-h_1h_2^2D(6,6)/20-h_1^2h_2D(6,6)/15,$

$F'(5,9) = 0,$

$F'(5,10) = 0,$

$F'(5,11) = -h_1h_2D(6,6)t/60+4h_1^2h_2^2D(6,6)/(15t)+h_1h_2^2D(6,6)/30+h_1^2h_2D(6,6)/30,$

$F'(5,12) = 0,$

$$F'(6,6) = h_1^2D(4,4)t^3/420+11h_1^3D(4,4)^2/630+13h_1^4D(4,4)t/315+11h_1^5D(2,2)/420,$$

$$F'(6,7) = -h_1h_2D(4,2)t/60+h_1^2h_2^2D(4,2)/t/5+h_1h_2^2D(4,2)/40+h_1^2h_2D(4,2)/30,$$

$$F'(6,8) = 0,$$

$$F'(6,9) = h_1h_2D(4,4)t^3/140+13h_1h_2^2D(4,4)t^2/840+13h_1^2h_2D(4,4)^2/630+3h_1^2h_2^2D(4,4)t/70,$$

$$F'(6,10) = h_1h_2D(4,2)t/120+(-2)h_1^2h_2^2D(4,2)/(15t)-h_1h_2^2D(4,2)/60-h_1^2h_2D(4,2)/60,$$

$$F'(6,11) = 0,$$

$$F'(6,12) = -h_1h_2D(4,4)t^3/280+(-13)h_1h_2^2D(4,4)t^2/1260+(-13)h_1^2h_2D(4,4)t^2/1260-h_1^2h_2^2D(4,4)t/35,$$

$$F'(7,7) = 4h_2^2D(4,4)/t+6h_2^3D(4,4)/t^2+3h_2^4D(4,4)/t^3+h_2D(7,7),$$

$$F'(7,8) = 0,$$

$$F'(7,9) = (-2)h_2^2D(4,2)t/15+(-3)h_2^4D(4,2)/(10t)+(-3)h_2^3D(4,2)/5+h_2^3D(7,2)/6,$$

$$F'(7,10) = -4h_2^2D(4,4)/t-7h_2^3D(4,4)/t^2-4h_2^4D(4,4)/t^3-h_2D(7,7),$$

$$F'(7,11) = 0,$$

$$F'(7,12) = h_2^2D(4,2)t/15+h_2^4D(4,2)/t/5+47h_2^3D(4,2)/120-h_2^3D(7,2)/8,$$

$$F'(8,8) = 2h_2^2D(6,6)t/15+3h_2^4D(6,6)/(10t)+h_2^3D(6,6)/10+h_2^3D(9,9)/3,$$

$$F'(8,9) = 0,$$

$$F'(8,10) = 0,$$

$$F'(8,11) = (-2)h_2^2D(6,6)t/15+(-2)h_2^4D(6,6)/(5t)+(-7)h_2^3D(6,6)/60+(-5)h_2^3D(9,9)/12,$$

$$F'(8,12) = 0,$$

$F'(9,9) = h_2^2D(4,4)t^3/105+11h_2^3D(4,4)t^2/210+13h_2^4D(4,4)t/140+h_2^5D(8,8)/20,$

$F'(9,10) = h_2^2D(4,2)t/15+h_2^4D(4,2)/t/5+37h_2^3D(4,2)/120-h_2^3D(7,2)/24,$

$F'(9,11) = 0,$

$F'(9,12) = -h_2^2D(4,4)t^3/105+(-11)h_2^3D(4,4)t^2/180+(-13)h_2^4D(4,4)t/105+(-13)h_2^5D(8,8)/180,$

$F'(10,10) = h_2^2D(4,4)/t+2h_2^3D(4,4)/t^2+4h_2^4D(4,4)/(3t^3)+h_2D(7,7)/3,$

$F'(10,11) = 0,$

$F'(10,12) = -h_2^2D(4,2)t/30+(-2)h_2^4D(4,2)/(15t)-h_2^3D(4,2)/5+h_2^3D(7,2)/30,$

$F'(11,11) = h_2^2D(6,6)t/30+2h_2^4D(6,6)/(15t)+h_2^3D(6,6)/30+2h_2^3D(9,9)/15,$

$F'(11,12) = 0,$

$F'(12,12) = h_2^2D(4,4)^3/420+11h_2^3D(4,4)t^2/630+13h_2^4D(4,4)t/315+11h_2^5D(8,8)/420.$

The elements of the [H] vector are:

$H(1) = v(3)-4v(1)l/5-u(2)+u(1)l,$

$H(2) = v(3)l-2v(2)l/3-3v(1)l/15-u(3)+2u(1)l/3,$

$H(3) = v(6)-4v(4)l/5-u(5)+u(4)l,$

$H(4) = v(6)l-2v(5)l/3-3v(4)l/15-u(6)+2u(4)l/3,$

$H(5) = v(9)-4v(7)l/5-u(8)+u(7)l,$

$H(6) = v(9)l-2v(8)l/3-3v(7)l/15-u(9)+2u(7)l/3,$

$H(7) = v(12)-4v(10)l/5-u(11)+u(10)l,$

H(8) = v(12)l-2v(11)l/3-3v(10)l/15-u(12)+2u(10)l/3,

H(9) = -v(3)+4v(1)l/5+u(2)+u(1)l,

H(10) = v(3)l+2v(2)l/3-3v(1)l/15+u(3)-2u(1)l/3,

H(11) = -v(6)+4v(4)l/5+u(5)+u(4)l,

H(12) = v(6)l+2v(5)l/3-3v(4)l/15+u(6)-2u(4)l/3,

H(13 = -v(9)+4v(7)l/5+u(8)+u(7)l,

H(14) = v(9)l+2v(8)l/3-3v(7)l/15+u(9)-2u(7)l/3,

H(15) = -v(12)+4v(10)l/5+u(11)+u(10)l,

H(16) = v(12)l+2v(11)l/3-3v(10)l/15+u(12)-2u(10)l/3,

where l is the element semi-length and the arrays u, v and w are defined as follows:

v(1) = $12h_1QD(4,4)/t^2+12h_1^2QD(4,4)/t^3$,

v(2) = 0,

v(3) = $-3h_1^2QD(4,5)/(5t)-h_1QD(4,5)/10$,

v(4) = $6h_1QD(4,4)/t^2+8h_1^2QD(4,4)/t^3$,

v(5) = 0,

v(6) = $-2h_1^2QD(4,5)/(5t)-h_1QD(4,5)/20$,

v(7) = $-12h_2QD(4,4)/t^2-12h_2^2QD(4,4)/t^3$,

v(8) = 0,

$v(9) = 3h_2^2QD(4,5)/(5t)+h_2QD(4,5)/10,$

$v(10) = 6h_2QD(4,4)/t^2+8h_2^2QD(4,4)/t^3,$

$v(12) = 0,$

$v(12) = -2h_2^2QD(4,5)/(5t)-h_2QD(4,5)/20$

$u(i) = w(i) + v(i)x$ for i=1,12 where x is the distance between the element centre and overlap centre and the w array is:

$w(1) = -8h_1PD(4,4)/t-12h_1D(4,4)p/t^2-6h_1^2PD(4,4)/t^2-12h_1^2D(4,4)p/t^3+2h_1\alpha_1\Delta T(1+\nu_{xy1}E_{y1}/E_{x1})-2h_1\alpha_a\Delta T(1+\nu_a),$

$w(2) = 6h_1^2QD(6,6)/(5t)+h_1QD(6,6)/5,$

$w(3) = 2h_1PD(4,5)t/15+3h_1^2D(4,5)p/(5t)+h_1D(4,5)p/10+11h_1^2PD(4,5)/20+h_1\alpha_a\Delta T(1+\nu_a)t^2/6+h_1^2\alpha_a\Delta T(1+\nu_a)t/2+h_1^3\alpha_1\Delta T(1+\nu_{yz1})/3,$

$w(4) = -4h_1PD(4,4)/t-6h_1D(4,4)p/t^2-4h_1^2PD(4,4)/t^2-8h_1^2D(4,4)p/t^3+h_1a_1\Delta T(1+\nu_{xy1}E_{y1}/E_{x1})-h_1\alpha_a\Delta T(1+\nu_a),$

$w(5) = 4h_1^2QD(6,6)/(5t)+h_1QD(6,6)/10,$

$w(6) = h_1PD(4,5)t/15+2h_1^2D(4,5)p/(5t)+h_1D(4,5)p/20+11h_1^2PD(4,5)/30+h_1\alpha_a\Delta T(1+\nu_a)t^2/12+h_1^2\alpha_a\Delta T(1+\nu_a)t/3+h_1^3\alpha_1\Delta T(1+\nu_{yz1})/4,$

$w(7) = 4h_2PD(4,4)/t+12h_2D(4,4)p/t^2+6h_2^2PD(4,4)/t^2+12h_2^2D(4,4)p/t^3+2h_2a_2\Delta T(1+\nu_{xy2}E_{y2}/E_{x2})-2h_2\alpha_a\Delta T(1+\nu_a),$

$w(8) = -6h_2^2QD(6,6)/(5t)-h_2QD(6,6)/5,$

$w(9) = h_2PD(4,5)t/30+(-3)h_2^2D(4,5)p/(5t)-h_2D(4,5)p/10-h_2^2PD(4,5)/20+h_2\alpha_a\Delta T(1+\nu_a)t^2/6+h_2^2\alpha_a\Delta T(1+\nu_a)t/2+h_2^3\alpha_2\Delta T(1+\nu_{yz2})/3,$

$w(10) = -2h_2PD(4,4)/t-6h_2D(4,4)p/t^2-4h_2^2PD(4,4)/t^2-8h_2^2D(4,4)p/t^3+h_2-h_2\alpha_2\Delta T(1+\nu_{xy2}E_{y2}/E_{x2})$,

$w(11) = 4h_2^2QD(6,6)/(5t)+h_2QD(6,6)/10$,

$w(12) = -h_2PD(4,5)t/60+2h_2^2D(4,5)p/(5t)+h_2D(4,5)p/20+h_2^2PD(4,5)/30-h_2\alpha_a\Delta T(1+\nu_a)t^2/12-h_2^2\alpha_a\Delta T(1+\nu_a)t/3-h_2^3\alpha_2\Delta T(1+\nu_{yz2})/4$,

Double lap joint

The elements of the inner product of the [F] matrix, $[F']_{12\times12}$, are given below. Since the matrix is symmetric, only the diagonal and upper half are listed:

$F'(1,1) = h_1^2D(7,7)/h_2+h_1D(1,1)$,

$F'(1,2) = 0$,

$F'(1,3) = -h_1^2D(7,8)t/2-h_1^2h_2D(7,8)/6-h_1^3D(7,8)/4+h_1^3D(1,2)/12$,

$F'(1,4) = h_1^2D(7,7)/h_2/2+h_1D(1,1)/2$,

$F'(1,5) = 0$,

$F'(1,6) = -h_1^2D(7,8)t/4-h_1^2h_2D(7,8)/12-h_1^3D(7,8)/6+h_1^3D(1,2)/16$,

$F'(1,7) = h_1D(7,7)t/h_2$,

$F'(1,8) = 0$,

$F'(1,9) = -h_1D(7,8)t^2/4-h_1h_2D(7,8)t/6$,

$F'(1,10) = h_1D(7,7)t/h_2/2$,

$F'(1,11) = 0$,

$F'(1,12) = -h_1D(7,8)t^2/6-h_1h_2D(7,8)t/12$,

$F'(2,2) = h_1^2D(6,6)t+h_1^2h_2D(9,9)/3+h_1^3D(3,3)/3,$

$F'(2,3) = 0,$

$F'(2,4) = 0,$

$F'(2,5) = h_1^2D(6,6)t/2+h_1^2h_2D(9,9)/6+5h_1^3D(3,3)/24,$

$F'(2,6) = 0,$

$F'(2,7) = 0,$

$F'(2,8) = h_1D(6,6)t^2/2+h_1h_2D(9,9)t/3,$

$F'(2,9) = 0,$

$F'(2,10) = 0,$

$F'(2,11) = h_1D(6,6)t^2/3+h_1h_2D(9,9)t/6,$

$F'(2,12) = 0,$

$F'(3,3) = h_1^2D(4,4)t^3/3+h_1^3D(4,4)t^2/2+h_1^2h_2D(8,8)t^2+h_1^4D(4,4)t/4+2h_1^2h_2^2D(8,8)t/3+h_1^3h_2D(8,8)t+2h_1^2h_2^3D(8,8)/15+h_1^3h_2^2D(8,8)/3+h_1^4h_2D(8,8)/4+h_1^5D(2,2)/20,$

$F'(3,4) = -h_1^2D(7,8)t/4-h_1^2h_2D(7,8)/12-h_1^3D(7,8)/8+h_1^3D(1,2)/48,$

$F'(3,5) = 0,$

$F'(3,6) = h_1^2D(4,4)t^3/6+7h_1^3D(4,4)t^2/24+h_1^2h_2D(8,8)t^2/2+h_1^4D(4,4)t/6+h_1^2h_2^2D(8,8)t/3+7h_1^3h_2D(8,8)t/12+h_1^2h_2^3D(8,8)/15+7h_1^3h_2^2D(8,8)/36+h_1^4h_2D(8,8)/6+13h_1^5D(2,2)/360,$

$F'(3,7) = h_1D(4,5)t^2/4-h_1D(7,8)t^2/2+h_1^2D(4,5)t/4-h_1h_2D(7,8)t/6-h_1^2D(7,8)t/4,$

$F'(3,8) = 0,$

$F'(3,9) = h_1D(4,4)t^4/8+h_1^2D(4,4)t^3/12+h_1h_2D(8,8)t^3/2+h_1h_2^2D(8,8)t^2/2+h_1^2h_2D(8,8)t^2/4+2h_1h_2^3D(8,8)t/15+h_1^2h_2^2D(8,8)t/6,$

$F'(3,10) = h_1D(4,5)t^2/12-h_1D(7,8)t^2/4+h_1^2D(4,5)t/8-h_1h_2D(7,8)t/12-h_1^2D(7,8)t/8,$

$F'(3,11) = 0,$

$F'(3,12) = 11h_1D(4,4)t^4/120+h_1^2D(4,4)t^3/16+h_1h_2D(8,8)t^3/3+5h_1h_2^2D(8,8)t^2/18+h_1^2h_2D(8,8)t^2/6+h_1h_2^3D(8,8)t/15+h_1^2h_2^2D(8,8)t/12,$

$F'(4,4) = h_1^2D(7,7)/h_2/4+h_1D(1,1)/3,$

$F'(4,5) = 0,$

$F'(4,6) = -h_1^2D(7,8)t/8-h_1^2h_2D(7,8)/24-h_1^3D(7,8)/12+h_1^3D(1,2)/60,$

$F'(4,7) = h_1D(7,7)t/h_2/2,$

$F'(4,8) = 0,$

$F'(4,9) = -h_1D(7,8)t^2/8-h_1h_2D(7,8)t/12,$

$F'(4,10) = h_1D(7,7)t/h_2/4,$

$F'(4,11) = 0,$

$F'(4,12) = -h_1D(7,8)t^2/12-h_1h_2D(7,8)t/24,$

$F'(5,5) = h_1^2D(6,6)t/4+h_1^2h_2D(9,9)/12+2h_1^3D(3,3)/15,$

$F'(5,6) = 0,$

$F'(5,7) = 0,$

$F'(5,8) = h_1D(6,6)t^2/4+h_1h_2D(9,9)t/6,$

$F'(5,9) = 0,$

$F'(5,10) = 0,$

$F'(5,11) = h_1D(6,6)t^2/6+h_1h_2D(9,9)t/12,$

$F'(5,12) = 0,$

$F'(6,6) = h_1^2D(4,4)t^3/12+h_1^3D(4,4)t^2/6+h_1^2h_2D(8,8)t^2/4+h_1^4D(4,4)t/9+h_1^2h_2^2D(8,8)t/6+h_1^3h_2D(8,8)t/3+h_1^2h_2^3D(8,8)/30+h_1^3h_2^2D(8,8)/9+h_1^4h_2D(8,8)/9+11h_1^5D(2,2)/420,$

$F'(6,7) = h_1D(4,5)t^2/8-h_1D(7,8)t^2/4+h_1^2D(4,5)t/6-h_1h_2D(7,8)t/12-h_1^2D(7,8)t/6,$

$F'(6,8) = 0,$

$F'(6,9) = h_1D(4,4)t^4/16+h_1^2D(4,4)t^3/18+h_1h_2D(8,8)t^3/4+h_1h_2^2D(8,8)t^2/4+h_1^2h_2D(8,8)t^2/6+h_1h_2^3D(8,8)t/15+h_1^2h_2^2D(8,8)t/9,$

$F'(6,10) = h_1D(4,5)t^2/24-h_1D(7,8)t^2/8+h_1^2D(4,5)t/12-h_1h_2D(7,8)t/24-h_1^2D(7,8)t/12,$

$F'(6,11) = 0,$

$F'(6,12) = 11h_1D(4,4)t^4/240+h_1^2D(4,4)^3/24+h_1h_2D(8,8)^3/6+5h_1h_2^2D(8,8)^2/36+h_1^2h_2D(8,8)t^2/9+h_1h_2^3D(8,8)t/30+h_1^2h_2^2D(8,8)t/18,$

$F'(7,7) = D(7,7)t^2/h_2+D(4,4)t,$

$F'(7,8) = 0,$

$F'(7,9) = D(4,5)t^3/12-D(7,8)t^3/4-h_2D(7,8)t^2/6,$

$F'(7,10) = D(7,7)t^2/h_2/2+D(4,4)t/2,$

$F'(7,11) = 0,$

$F'(7,12) = D(4,5)t^3/16-D(7,8)t^3/6-h_2D(7,8)t^2/12,$

$F'(8,8) = D(6,6)t^3/3+h_2D(9,9)t^2/3,$

$F'(8,9) = 0,$

$F'(8,10) = 0,$

$F'(8,11) = 5D(6,6)t^3/24+h_2D(9,9)t^2/6,$

$F'(8,12) = 0,$

$F'(9,9) = D(4,4)t^5/20+h_2D(8,8)t^4/4+h_2^2D(8,8)t^3/3+2h_2^3D(8,8)t^2/15,$

$F'(9,10) = D(4,5)t^3/48-D(7,8)t^3/8-h_2D(7,8)t^2/12,$

$F'(9,11) = 0,$

$F'(9,12) = 13D(4,4)^5/360+h_2D(8,8)t^4/6+7h_2^2D(8,8)t^3/36+h_2^3D(8,8)t^2/15,$

$F'(10,10) = D(7,7)t^2/h_2/4+D(4,4)t/3,$

$F'(10,11) = 0,$

$F'(10,12) = D(4,5)t^3/60-D(7,8)t^3/12-h_2D(7,8)t^2/24,$

$F'(11,11) = 2D(6,6)t^3/15+h_2D(9,9)t^2/12,$

$F'(11,12) = 0,$

$F'(12,12) = 11D(4,4)t^5/420+h_2D(8,8)t^4/9+h_2^2D(8,8)t^3/9+h_2^3D(8,8)t^2/30,$

The elements of the (**H**) array are:

$H(1,1) = -u(2)+u(1)l,$

H(1,2) = -u(3)+2u(1)l/3,

H(1,3) = -u(5)+u(4)l,

H(1,4) = -u(6)+2u(4)l/3,

H(1,5) = -u(8)+u(7)l,

H(1,6) = -u(9)+2u(7)l/3,

H(1,7) = -u(11)+u(10)l,

H(1,8) = -u(12)+2u(10)l/3,

H(1,9) = u(2)+u(1)l,

H(1,10) = u(3)-2ul(1)/3,

H(1,11) = u(5)+u(4)l,

H(1,12) = u(6)-2u(4)l/3,

H(1,13) = u(8)+u(7)l,

H(1,14) = u(9)-2u(7)l/3,

H(1,15) = u(11)+u(10)l,

H(1,16) = u(12)-2u(10)l/3,

where u is the following array:

$u(1) = h_1PD(4,4)/h_2-h_1\alpha_1\Delta T(1+\nu_{xy1}E_{y1}/E_{x1})+h_1\alpha_2\Delta T(1+\nu_{xy2}E_{y2}/E_{x2})$,

u(2) = 0,

$$u(3) = -h_1PD(7,8)t/2-h_1h_2PD(7,8)/6-h_1^2PD(7,8)/4-h_1\alpha_a\Delta T(1+\nu_a)t^2/2-h_1^2\alpha_a\Delta T(1+\nu_a)5t/2-h_1h_2\alpha_2\Delta T(1+\nu_{yz2})t-h_1h_2^2m26/3-h_1^2h_2\alpha_2\Delta T(1+\nu_{yz2})/2-h_1^3\alpha_1\Delta T(1+\nu_{yz1})/6,$$

$$u(4) = h_1PD(4,4)/h_2/2-h_1a_1\Delta T(1+\nu_{xy1}E_{y1}/E_{x1})/2+h_1a_2\Delta T(1+\nu_{xy2}E_{y2}/E_{x2})/2,$$

$$u(5) = 0,$$

$$u(6) = -h_1PD(7,8)t/4-h_1h_2PD(7,8)/12-h_1^2PD(7,8)/6-h_1\alpha_a\Delta T(1+\nu_a)t^2/4-h_1^2\alpha_a\Delta T(1+\nu_a)t/3-h_1h_2\alpha_2\Delta T(1+\nu_{yz2})t/2-h_1h_2^2\alpha_2\Delta T(1+\nu_{yz2})/6-h_1^2h_2\alpha_2\Delta T(1+\nu_{yz2})/3-h_1^3\alpha_1\Delta T(1+\nu_{yz1})/8,$$

$$u(7) = PD(4,4)t/h_2-\alpha_a\Delta T(1+\nu_a)t+a_2\Delta T(1+\nu_{xy2}E_{y2}/E_{x2})t,$$

$$u(8) = 0,$$

$$u(9) = -PD(7,8)t^2/4-h_2PD(7,8)t/6-\alpha_a\Delta T(1+\nu_a)t^3/6-h_2\alpha_2\Delta T(1+\nu_{yz2})t^2/2-h_2^2\alpha_2\Delta T(1+\nu_{yz2})t/3,$$

$$u(10) = PD(4,4)t/h_2/2-\alpha_a\Delta T(1+\nu_a)t/2+a_2\Delta T(1+\nu_{xy2}E_{y2}/E_{x2})/2,$$

$$u(11) = 0,$$

$$u(12) = -PD(7,8)t^2/6-h_2PD(7,8)t/12-\alpha_a\Delta T(1+\nu_a)t^3/8-h_2\alpha_2\Delta T(1+\nu_{yz2})t^2/3-h_2^2\alpha_2\Delta T(1+\nu_{yz2})t/6.$$

Appendix IV

DERIVATION OF TRUE STRESS STRAIN CURVE FROM A TENSILE TEST

In a uniaxial tensile test, difficulties arise in extracting the true stress-strain curve beyond the elastic limit. Necking, which occurs at yield, not only reduces the cross sectional area but can introduce a state of stress other than uniaxial tension. While the latter effect is difficult to compensate, a correction for the reduction in cross-section is possible by assuming constant volume during plastic flow.

True stress is defined as

$$\frac{P}{A} \qquad \text{(AIV.1)}$$

where A is the instantaneous cross sectional area. If the original cross-sectional area is A_0, then at a strain, ε, the instantaneous cross section is $A_0(1-\nu\varepsilon)^2$. Thus

$$A = A_0(1-2\nu\varepsilon+\nu^2\varepsilon^2) \qquad \text{(AIV.2)}$$

When the material is plastic, the volume remains constant and $\nu = 0.5$. Substituting this value into eqn (AIV.2) and assuming that the ε^2 term is small gives

$$A = A_0(1-\varepsilon) \qquad \text{(AIV.3)}$$

Substituting eqn (AIV.3) into eqn (AIV.1) we get the following definition for true stress:

$$\frac{P}{A_0(1-\varepsilon)} \qquad \text{(AIV.1)}$$

If l_1 is the extended length and l_0 is the original length then true strain, ε, is defined by

$$\varepsilon = \int_{l}^{l} \frac{dl}{l} = \ln(l/l_0)$$

REFERENCES

ADAMS, R.D., **CHAMBERS**, S.H., **del STROTHER**, P.J.A. and **PEPPIAT**, N.A. *Rubber model for adhesive lap joints*, J. Strain Analysis, 8, 52-57, (1973)

ADAMS, R.D., and **COPPENDALE**, J., *Measurement of the elastic moduli of structural adhesives by a resonant bar technique*, J. Mech. Eng. Science, 18 No 3, (1976)

ADAMS, R.D., and **COPPENDALE**, J., *The Stress-Strain behaviour of Axially-Loaded Butt Joints*, J. Mech. Eng. Science, 18 No 3, (1976)

ADAMS, R.D., and **HARRIS**, J.A., *Strength prediction of bonded single lap joints by non-linear finite element methods*, Int. J. Adhesion and Adhesives, 4 No. 2, (1984)

ADAMS, R.D. and **PEPPIAT**, N.A., *Effect of Poisson's ratio strain in adherends on stresses of an idealized lap joint*, J. Strain Analysis, 8, 134-139, (1973)

ADAMS, R.D. and **PEPPIAT**, N.A., *Stress analysis of Adhesive-bonded Lap Joints*, J. Strain Analysis, 9, 185-196, (1974)

ADAMS, R.D. and **WAKE**, W.C., *Structural Adhesive Joints in Engineering*, Elsevier Applied Science Publishers, (1984)

ALLMAN, D.J., *A theory for the elastic stresses in adhesive bonded lap joints*, Quart. J. of Mech. and Appl. Maths., XXX Part 4, 415-436, (1977)

BATHE, K-J. and **WILSON**, E.L., *Numerical methods in finite element analysis*, Prentice-Hall, (1976)

BIGWOOD, D., Unpublished Ph.D. thesis, Surrey University, (1989)

BOOKER, M.J., *The stress distribution in adhesively bonded lap joints*, M.Sc. Thesis, Imp. College of Science and Tech., (1980)

CHEN, D. and **CHENG**, S., *Thermal stresses in laminated beams*, J. Therm. Stress, 5, 67-84, (1982)

CHEN, D. and **CHENG**, S., *An analysis of adhesive bonded single lap joints*, ASME J. Appl. Mech., 50, 109-115, (1983)

CHEN, Z., *GMESH - A Novel Finite Element Mesh Generating Program*, Internal Report, Dept. of Mech. Eng., University of Bristol, (1982)

CHEN, Z., *The Failure and Fracture analysis of adhesive bonds*, Ph. D. thesis, University of Bristol, (1985)

CHEN, W.T. and **NELSON**, C.W., *Thermal stresses in bonded joints*, IBM J. R & D, 23, 179-, (1979)

COOPER, P. and **SAWYER**, J.W., *A critical Examination of Stresses in an Elastic Single Lap joint*, NASA TP 1507, (1979)

COPPENDALE, J., *The stress and failure analysis of structural adhesive joints*, Ph.D. Thesis, University of Bristol, (1977)

CROCOMBE, A.D., *The non-linear stress and failure analysis of adhesive tests*, Ph.D thesis, University of Bristol, (1981)

CROCOMBE, A.D. and **ADAMS**, R.D., *Influence of the Spew Fillet and other Parameters on the Stress Distribution in the Single Lap Joint*, J. Adhesion, 13, 141-155, (1981)

CROCOMBE, A.D. and **EVANS**, I.E., *The influence of cladding and other thickness effects on adhesive joint strength*, Proc. Adhesion '87, PRI Publications, (1987)

DELALE, F., **ERDOGEN**, F. and **AYDINOGLU**, M.N., *Stresses in adhesively bonded joints - A closed form solution*, J. Composite Mat., 15, 249-271, (1981)

Engineering Sciences Data Item Number 79016, *Inelastic shear stresses and strains in the adhesives bonding lap joints loaded in tension or shear (computer program)*, Engineering Sciences Data Unit, (1979)

Engineering Sciences Data Item Number 80039, *Elastic adhesive stresses in multistep lap joints loaded in tension (computer program)*, Engineering Sciences Data Unit, (1979)

GALLAGHER, R.H. and **DHALL**, A.K., *Direct flexibility finite element elastoplastic analysis*, Proc. 1st Int. Conf. Structural Mech., 6 Part, 443-462, (1971)

GOLAND, M. and **REISSNER**, E., *The stresses in cemented joints*, J. Appl. Mechs., Trans. Am. Soc. Mech. Engs., 66, A17-A27, (1944)

GRANT, P., **SANDERS**, R.C.and **WARD**, A.P., *Developments in Bonded Joint Analyses*, BAC report No. SOR(P) 137, (1983)

GRANT, P. and **TAIG**, I.C., *Strength and stress analysis of bonded joints*, BAC report No. SOR(P) 109, (1976)

GROTH, H.L, *Analysis of Adhesive Joints*, Report No 87-17, Royal Inst. of Tech., Stockholm, Sweden, (1987)

HARRIS, J.A., *Non-linear analysis and testing of adhesive joints under impact and Quasi-static loading*, Ph.D. thesis, University of Bristol, (1983)

HART-SMITH, L.J., *Adhesive-bonded scarf and stepped-lap joints*, NASA Report CR-112237, Langley Research Centre, (1973a)

HART-SMITH, L.J., *Adhesive-bonded single lap joints*, NASA Report CR-112236, Langley Research Centre, (1973b)

HARWELL Report AERE G 4115, *A computer program for the non-linear stress analysis of adhesively bonded single lap joints*, (1986)

HINTON, E., and **OWEN**, D.R., *Finite elements in plasticity*, Academic Press, (1978)

HUTCHINSON, J.W., J. Mechanics and Physics of Solids, 16, 1968

JOHNSONS, W. and **MELLOR**, P.B., *Engineering Plasticity*, Van Nostrand Rheinhold Co., (1973)

KINLOCH, A.J., *The science of adhesion, Part 1 Surface and interfacial aspects*, J. Mat. Sci., 15, 2141-2166, (1980)

KINLOCH, A.J., *A fracture mechanics approach to the failure of structural joints*, Developments in Adhesives-2, ed. KINLOCH, A.J., 83-124, (1981)

KINLOCH, A.J., *The science of adhesion, Part 2 Mechanics and mechanisms of failure*, J. Mat. Sci., 17, 617-651, (1982)

KLINE, R.A., *Stress Analysis of Adhesively Bonded Joints*, Adhesive Joints, ed. MITTAL, K.L., 587-610, (1982)

KUTSCHA, D., *Mechanics of Adhesive Bonded Lap-Type Joints - Survey and Review*, MLTDR-64-298, (1964)

LEFEBVRE, D.R., **DILLARD**, D.A.,and **BRINSON**, H.F., *A model for the Diffusion of Moisture in Adhesive joints. Part II: Experimental*, J. Adhesion, 27 No. 1, (1989b)

LEFEBVRE, D.R., **DILLARD**, D.A.,and **WARD**, T.C., *A model for the Diffusion of Moisture in Adhesive joints. Part I: Equations Governing Diffusion*, J. Adhesion, 27 No. 1, (1989a)

LEICHTI, K., **JOHNSON**, W.S. and **DILLARD**, D.A., *Experimentally Determined Strength of Adhesively Bonded Joints*, Joining Fibre-Reinforced Plastics, ed. MATHEWS, F.L., 105-183, (1987)

LUBKIN, J.L. and **REISSNER**, E., *Stress distributions and design data for adhesive lap joints between circular tubes*, Trans. ASME, 78, 1213-1221, (1956)

MALLICK, V. and **ADAMS**, R.D., *The stresses and strain in bonded joints between metal and composite materials*, Proc. Adhesion '87, PRI Publications, (1987)

MALLICK, V. and **ADAMS**, R.D., *Strength prediction of lap joints with elasto-plastic adhesives using linear closed form methods*, Proc. Structural Adhesives in Engineering II '89, Butterworth, (1989)

McLAREN, A.S. and **MacINNES**, I., *The Influence of the stress distribution in an adhesive lap joint of bending and adhering sheets*, British J. Appl. Phy., 9, 72-77, (1958)

NAYAK, G.C. and **ZIENKIEWICZ**, O.C., *Elasto-Plastic stress analysis. A generalization for various constitutive relations including strain softening*, J. Num. Methods in Eng., 5, 113-135, (1972)

PEPPIAT, N.A., *Stress analysis of Adhesive joints*, Ph.D. thesis, Univeristy of Bristol, (1974)

PIAN, T.H.H., *Hybrid elements in Numerical and Computer methods in structural mechanics*, Eds. FENVES, S.J., PERRONE, N., ROBINSON, A.R. and SCHNOBRICH, W.C., Acad. Press, New York, (1973)

RAGHAVA, R.S. and **CADELL**, R.M, *The macroscopic yield behaviour of polymers*, J. Mat. Sci., 8, 225-232, (1973)

REDDY, M.N. and **SINHA**, P.K., *Stresses in adhesive bonded joints for composites*, Fibre Sc. Tech., 8, 33-, (1975)

RENTON, W.J. and **VINSON**, J.R., *Analysis of adhesively bonded joints between panels of composite materials*, J. Appl. Mech., Trans. ASME, 101-106, (1977)

RICE, J.R. and **ROSENGREN**, G.F., J. Mechanics and Physics of Solids, 16, 1968

ROY, S., **LEFEBVRE**, D.R., **DILLARD**, D.A.,and **REDDY**, J.N., *A model for the Diffusion of Moisture in Adhesive joints. Part III: Numerical Simulation*, J. Adhesion, 27 No. 1, (1989)

RYBICKI, E.F. and **SCHMIT**, L.A. Jr., *An Incremental Complementary Energy Method of Nonlinear Stress Analysis*, J. AIAA, 8 No 10, 1805-1812, (1970)

SHANLEY, F.R., *Strength of Materials*, McGraw-Hill, (1957)

SINHA, P.K. and **REDDY**, M.N., *Thermal analysis of composite bonded joints*, Fibre Sc. Tech., 9, 153-, (1976)

SNEDDON, I., Adhesion, ed. ELEY, D., Chapter 9, Oxford University Press, (1961)

SRINIVAS, S., *Analysis of bonded joints*, NASA TN D7846/D7860, (1975)

TAUCHERT, T.R., *Energy Principles in Structural Mechanics*, McGraw-Hill, (1974)

VOLKERSEN, O., *Die Nietkraftverteilung in zugbeanspruchten Nietverbindungen mit Konstanten Laschenquerschnitten*, Luftfarhtforschung, 15, 41-47, (1938)

VOLKERSEN, O., *Recherches sur la theorie des assemblages colles*, Construction Metallique, 4, 3-13, (1965)

WAH, T., *Stress distribution in a bonded anisotropic lap joint*, Trans. ASME Series H, 95, 174-, (1973)

WASHIZU, K., *Variational Methods in Elasticity and Plasticity*, Pergamon Press, (1982)

WEITSMAN, Y., *An investigation of non-linear visco-elastic effects on load transfer in a symmetric double lap joint*, J. Adhesion, 11, 279-, (1981)

WEITSMAN, Y., *Residual thermal stresses in a symmetric double lap joint*, J. Thermal Stresses, 3, 521-, (1980)

WEITSMAN, Y., *Stresses in adhesive joints due to moisture and temperature* , J. Comp. Mat., 11, 378-394, (1977)

ZHAO, X., *A new method for the determination of bending moments for single lap joints*, Unpublished report, Bristol, (1989).

ZIENKIEWICZ, O.C. and **TAYLOR** R.L., *The Finite Element Method*, 1, McGraw-Hill, (1989)